INFORMATION TO USERS

This manuscript has been reproduced from the microfilm master. UMI films the text directly from the original or copy submitted. Thus, some thesis and dissertation copies are in typewriter face, while others may be from any type of computer printer.

The quality of this reproduction is dependent upon the quality of the copy submitted. Broken or indistinct print, colored or poor quality illustrations and photographs, print bleedthrough, substandard margins, and improper alignment can adversely affect reproduction.

In the unlikely event that the author did not send UMI a complete manuscript and there are missing pages, these will be noted. Also, if unauthorized copyright material had to be removed, a note will indicate the deletion.

Oversize materials (e.g., maps, drawings, charts) are reproduced by sectioning the original, beginning at the upper left-hand corner and continuing from left to right in equal sections with small overlaps.

Photographs included in the original manuscript have been reproduced xerographically in this copy. Higher quality 6" x 9" black and white photographic prints are available for any photographs or illustrations appearing in this copy for an additional charge. Contact UMI directly to order.

Bell & Howell Information and Learning
300 North Zeeb Road, Ann Arbor, MI 48106-1346 USA
800-521-0600

CALCULATION OF TRANSPORT PROPERTIES OF LIQUID METALS AND THEIR ALLOYS VIA MOLECULAR DYNAMICS

by

Frank Joseph Cherne III

A Dissertation Submitted to the Faculty of the

DEPARTMENT OF MATERIALS SCIENCE AND ENGINEERING

In Partial Fulfillment of the Requirements
For the Degree of

DOCTOR OF PHILOSOPHY

In the Graduate College

THE UNIVERSITY OF ARIZONA

2000

UMI Number: 9992138

UMI®

UMI Microform 9992138

Copyright 2001 by Bell & Howell Information and Learning Company.
All rights reserved. This microform edition is protected against
unauthorized copying under Title 17, United States Code.

Bell & Howell Information and Learning Company
300 North Zeeb Road
P.O. Box 1346
Ann Arbor, MI 48106-1346

THE UNIVERSITY OF ARIZONA ®
GRADUATE COLLEGE

As members of the Final Examination Committee, we certify that we have read the dissertation prepared by Frank Joseph Cherne III entitled Calculation of Transport Properties of Liquid Metals and Their Alloys via Molecular Dynamics

and recommend that it be accepted as fulfilling the dissertation requirement for the Degree of Doctor of Philosophy

Joseph H. Simmons	11/7/00 Date
Pierre A. Deymier	Nov 7 2000 Date
David R. Poirier	Nov. 7, 2000 Date
Michael Barfield	11/07/00 Date
Stephen Kukolich	Nov 7, 2000 Date

Final approval and acceptance of this dissertation is contingent upon the candidate's submission of the final copy of the dissertation to the Graduate College.

I hereby certify that I have read this dissertation prepared under my direction and recommend that it be accepted as fulfilling the dissertation requirement.

~~Dissertation~~ Director Pierre A. Deymier	Nov 7, 2000 Date

STATEMENT BY AUTHOR

This dissertation has been submitted in partial fulfillment of requirements for an advanced degree at The University of Arizona and is deposited in the University Library to be made available to borrowers under rules of the Library.

Brief quotations from this dissertation are allowable without special permission, provided that accurate acknowledgment of source is made. Requests for permission for extended quotation from or reproduction of this manuscript in whole or in part may be granted by the head of the major department or the Dean of the Graduate College when in his or her judgment the proposed use of the material is in the interests of scholarship. In all other instances, however, permission must be obtained from the author.

SIGNED: Frank J. Chesa III

ACKNOWLEDGEMENTS

In consideration of all the people who touch one's life, I find it is necessary to acknowledge many people who have had a profound impact on encouraging me to pursue this higher degree. Those people who comprise my inner workings shall be mentioned first. Each of these people hold a special place in their own way. I would like to express my deepest gratitude to my family members that struggled with me through this pursuit. These include my wife Stephanie, my two lovely daughters Amanda and Andrea, my father Frank J. Cherne, and my mother Paulann White. My wife has had the patience of the saints with me in this long-term pursuit. My daughters explored (not always on their terms) the building blocks of matter: electrons, atoms, and crystal structures. My father kept me focused on the task at hand while my mother marveled and gloried in my experience. I would like to also express my deepest gratitude to Elizabeth Shaw whose editorial expertise helped polish my grammatical blunders. There are other people who have touched my life in their own unique way and encouraged me along the way that I would like to acknowledge as well, namely, Nick Franks, Jim Wulliman, and Orville Nance.

At this time, I would also like to express my gratitude to several past teachers and professors who helped me complete in a direct and indirect way. The making of an individual comes through his growth and development and therefore I would like to take this time to remember those in a semi-chronological order these teachers who promoted growth and development in my life. John Mooy who shared a piece of his curiosity and inventiveness with me during my young age. Robert and Betty Bearg stimulated my mental faculties in the subjects of mathematics and physics. Dr. Roy Campbell of Southwestern Adventist University tolerated me as a religion student out-performing physics majors in the upper division physics classes. Dr. Herbert Roth showed me technical writing is possible despite my fear of the blank page.

I would like to express my gratitude to a couple of faculty members who went beyond the encouragement level and directed my mind toward the pursuit of this scientific degree, namely, Pierre Deymier and Dr. Poirier. Dissertations would not come to fruition without a dissertation advisor; Pierre acted as my dissertation advisor. Pierre not only shared with me his wealth of knowledge on the art of molecular dynamics, he transcended the realm of a dissertation advisor by sharing with me friendship. Dr. Poirier provided many helpful insights and directed me to many worthwhile papers within the topic area of liquid metal transport properties. Dr. Poirier's breadth of knowledge was invaluable.

DEDICATION

I would like to dedicate this dissertation to five individuals in my life who are and who were part of my life. The first three individuals I would like to dedicate this dissertation to are my deceased grandparents, Betty Ross, Paul Ross and Frank Cherne. Paul Ross scrambled three puzzles together to watch me reassemble them. Somehow he must have known that I was destined to solve life's great mysteries. Betty Ross reminded me of these early childhood experiences as a reaffirmation of my analytical abilities. Frank Cherne, my grandfather, showed me through his varied life experiences that there are more mountains to climb and pathways to follow.

The final two individuals I would like to whom I dedicate this dissertation are my lovely daughters, Amanda and Andrea. They have taught me to examine life with the curiosity of a child. It is my prayer and desire that Amanda and Andrea utilize their God given talents to their fullest.

TABLE OF CONTENTS

TABLE OF CONTENTS - *Continued*

LIST OF ILLUSTRATIONS

LIST OF ILLUSTRATIONS – *continued*

LIST OF ILLUSTRATIONS – *continued*

LIST OF ILLUSTRATIONS – *continued*

LIST OF TABLES

ABSTRACT

The advanced casting modeler requires accurate viscosity and diffusivity data of liquid metals and their alloys. The present work discusses the use of equilibrium and non-equilibrium molecular dynamics techniques to obtain such data without having to rely on oversimplified phenomenological expressions or difficult and expensive experiments. Utilizing the embedded atom method (EAM), the viscosities and diffusivities for a series of equilibrium and non-equilibrium molecular dynamics simulations of nickel, aluminum, and nickel-aluminum alloys are presented. A critical comparison between the equilibrium and non-equilibrium methods is presented. Besides the transport properties, structural data for the liquids are also evaluated. EAM does a poor job of describing the transport properties of nickel-aluminum alloys, particularly near the equiatomic concentration. It has been suggested that charge transfer between nickel and aluminum atoms is responsible for the discrepancy between numerical calculations and available experimental data. A modified electronic distribution function has been developed to simulate the charge transfer associated with compound formation. The effects of such a "charge transfer" modification to the embedded atom method are evaluated. The results of these simulations indicate that the embedded atom method combined with molecular dynamics may be used as a method to predict reasonably the transport properties.

CHAPTER 1

INTRODUCTION

In an effort to minimize research and development time, the casting industry is turning toward a system of computer-aided analysis and prototyping[1]. These advanced casters utilize thermophysical properties such as viscosity and diffusion coefficients. The modern casting engineer utilizes these properties in solving numerically the conservation equations for mass, momentum, energy, and solutal concentration of each alloy element. The viscosity data for metals and metallic alloys, however, are sparse. Furthermore, the experimental diffusion data are almost non-existent. Therefore, the casting engineer has to rely on either theoretical and correlation models or phenomenological models for their values. Sometimes the engineer will do sensitivity studies to study the effect of a range of values. These studies give an idea of the effects one variable may have upon the modeled solidification process.

When examining the available viscosity data for pure liquid nickel, Figure 1.1, it is observed that at 1750 K the measured viscosity from a variety of authors ranges from 4.4 mPa s to approximately 6.2 mPa s that represents a 25-30 percent deviation between the experiments[2]. The line indicated by **p** was an experimental work performed by Petrushevskii[3]. This set of experimental data was obtained using an oscillating vessel with Shvidkovskii solution for calculating viscosity. According to Iida and Guthrie[2], the Shvidkovskii equations tend to overestimate the viscosity near the melting point.

One may assume that for liquid aluminum the discrepancies in the experimental viscosities should be fewer on account of its lower melting point and potentially less

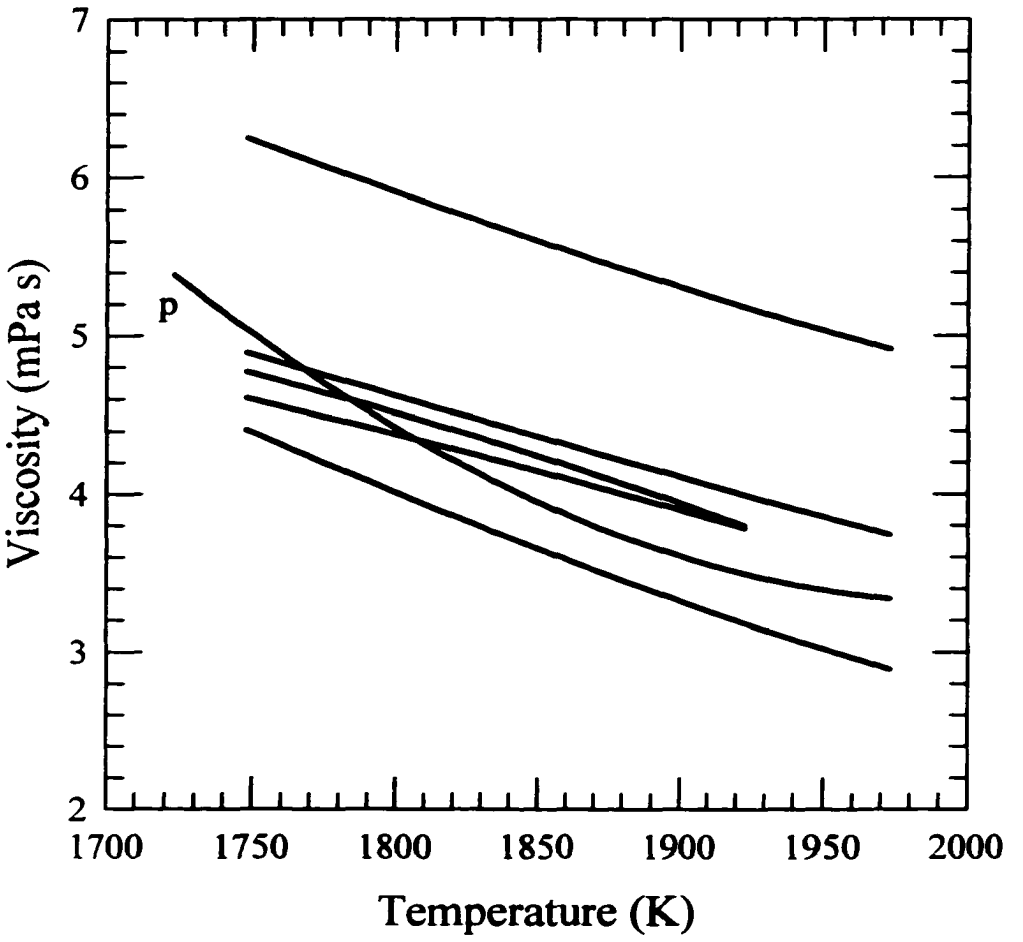

Figure 1.1. Experimental viscosities of liquid nickel as reported by Iida and Guthrie [2] and Petrushevskii[3].

convection errors, etc. However this is not observed. Figure 1.2 shows the experimental results from a variety of authors referenced in Iida and Guthrie[2]. These results come from the 1950s and the 1960s. The lower curve at 950 K reports a value of 1.2 mPa s, and the upper curve at the same temperature reports 4.15 mPa s. The higher value is almost four times greater than the lower value. In consideration of these large discrepancies in the experimental viscosity data, a re-examination of the data is in order.

As a result of the discrepancies in viscosity, the casting modeler often looks at empirical relations to estimate the value of the viscosity, which provide only rough estimates. Thus, the modeler can do no more than predict trends by his calculations.

When presenting the availability of pure liquid metal diffusivities, the literature reports such self-diffusivities. In addition, the complexity of obtaining accurate measurements for liquid alloys limits the availability of diffusion data for many compositions. This paucity in the diffusion data requires the modeler to use empirical relations between the viscosity and diffusion coefficient, such as the Stokes-Einstein or the Sutherland-Einstein models. With the disparity already shown in the viscosity data, the applicability of these relations should be questioned.

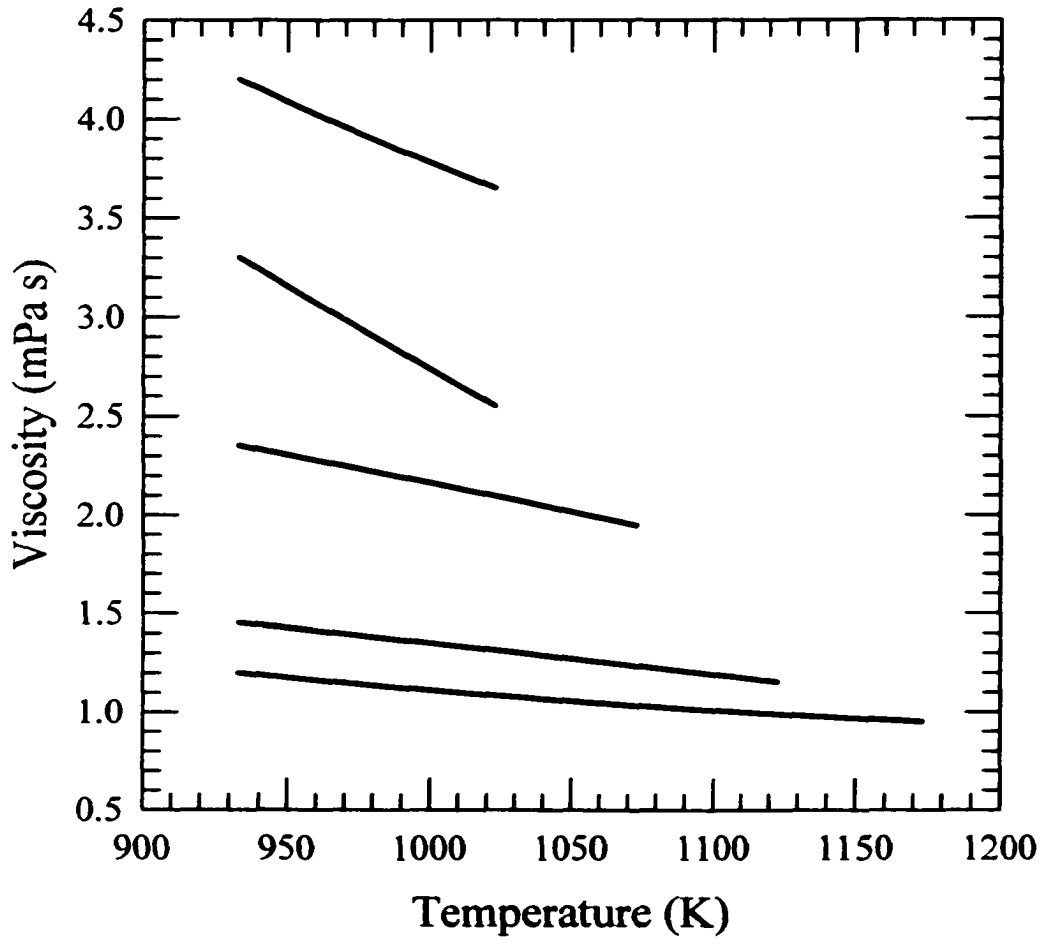

Figure 1.2. Aluminum viscosity as a function of temperature from reference [2].

The following statement found in Iida and Guthrie [2] on page 168 suggests that there is a better way to obtain transport data; it states:

> In the theory of liquids, the space and time dependent correlation functions are the most fundamental properties. A complete knowledge of these functions at different densities and temperatures is sufficient to calculate all thermodynamic and transport properties of classical liquids. Unfortunately, there is, at the present time, no practical theory, other than the machine solution of Newton's equation of motion for each atom, for computing time-dependent correlation functions for liquids from first principles.

This statement implies that atomistic simulations are required to calculate such time-dependent quantities as viscosity and diffusivity. In the following chapters, viscosity and diffusivity will be evaluated for the nickel-aluminum system, utilizing the atomistic simulation techniques of equilibrium and non-equilibrium molecular dynamics techniques.

The machine solution of Newton's equations of motion requires selection of a potential. We chose to utilize the formalism of the embedded-atom method (EAM) initially proposed by Daw and Baskes [4] because of its applicability to transition metals. Within the aluminum and nickel system there are many different EAM potentials; however many utilize highly parameterized spline-fit functions. We selected the EAM potential suggested by Cai and Ye [5] for its analytical form.

In Chapter 2 the experimental methods used in obtaining both viscosity and diffusivity data are examined. In addition, the existing theories and correlation functions are discussed. Chapter 3 studies the EAM potential. Chapter 4 explains the atomistic techniques of non-equilibrium and equilibrium molecular dynamics. In Chapters 5 and 6,

the results of the calculations are presented, and finally, in Chapter 7 conclusions and future directions are given.

CHAPTER 2

TRANSPORT PROPERTIES

This chapter examines experimental techniques, theoretical models, and correlation methods used in obtaining the transport coefficients of diffusivity and viscosity.

2.1. Viscosity

Viscosity is defined as the fluid's resistance to an applied shearing force, assuming the fluid is incompressible. Rayleigh [6] describes viscosity in the following manner:

> let us conceive of a fluid divided into parallel strata in such a manner that while each stratum moves in its own plane with uniform velocity, a change of velocity occurs in passing from one stratum to another. The simplest supposition we can make is that the velocities of all the strata are in the same direction but increase uniformly in magnitude as we pass along a line perpendicular to the planes of stratification. Under these circumstances a tangential force between contiguous strata is called into play, in the direction of the relative motion, and of magnitude proportional to the rate at which the velocity changes and to a coefficient of viscosity...[6]

Rayleigh goes on to say that the origin of the tangential force belongs to molecular science. Iida and Guthrie [2] describe viscosity from an atomic view by saying that, "the motions of the atoms through a liquid are impeded by frictional forces set up by their nearest neighbors." Therefore, from an atomistic view, viscosity is the measure of the friction between the atoms.

The frictional force called viscosity plays an important role in the quantitative solutions of problems in fluid flow behavior. Sir Isaac Newton used the following equation to describe this stress:

$$\tau = \eta \frac{\partial v_x}{\partial z} \tag{2.1}$$

where τ is the shear stress and $\frac{\partial v_x}{\partial z}$ is the velocity gradient, v_x is the velocity in the x direction, z is the direction perpendicular to the flow, and η is the viscosity of the fluid between the parallel plates.

Viscosity is sometimes reported as kinematic viscosity, ν, which is defined as the value of the fluid viscosity divided by the fluid mass density. In other words,

$$\nu = \frac{\eta}{\rho}. \tag{2.2}$$

Another term for kinematic viscosity is momentum diffusivity. Kinematic viscosity in SI units is measured in m^2s^{-1}.

2.1.1. Methods of Viscosity Measurement

There are several methods for measuring viscosity. Only a few of these are applicable to liquid metals, because of their low kinematic viscosity, relatively high melting points, and chemical reactivity. According to Iida and Guthrie[2] the suitable methods include (a) capillary, (b) rotational, (c) oscillating plate, and (d) oscillating vessel. The following summary of these techniques discusses the advantages and disadvantages of each technique. For more information, we refer the reader to reference [2].

2.1.1.1. Capillary method

The capillary method consists of a thin capillary tube in between a reservoir bulb and a measuring bulb. This method requires the fluid to be forced or sucked through the

capillary tube. The time it takes to fill the measuring bulb relates to the viscosity of the liquid metal. This method is rather simple in its experimental approach. It provides, however, only relative and not absolute values for the viscosity.

Very fine tubes (inner diameter less than 0.15-0.2 mm) with a long bore (greater than 70-80 mm) are required for viscosity measurement of metallic liquids with the capillary method. These requirements are imposed by the need for a low Reynolds numbers, which are associated with laminar flow. Typical capillary tubes are made from heat-resistant or quartz glass. The method, therefore, is only appropriate for low melting-point liquids where the melting-point of the metal is less than 1400-1500K.

Concerns with this method are possible contamination issues and blockages by minute non-metallic inclusions and bubbles within the thin tube. Any such concerns could have an adverse effect upon efflux times (times to fill the bulb). As a result, it is imperative that the liquid metal be free from impurities.

2.1.1.2. Rotational Method

The rotational method consists of two coaxial cylinders that rotate. When the outer cylinder rotates with a constant angular velocity, the inner cylinder, although attached to a fiber, is affected by the force imposed on it by the viscous liquid. The torque to the inner cylinder is indicated by angular displacement of the fiber, which is related to the viscosity of the liquid.

The simplicity of the mathematics makes this method attractive. The low-viscosity of the metallic liquids, however, requires that the two concentric cylinders have

a small clearance or a thin layer of fluid between them. With such thin fluid layers, it is difficult to maintain coaxial configuration.

2.1.1.3. Oscillating Plate Method

To obtain viscosities using the oscillating plate method, a flat plate is submerged in the viscous liquid. This plate then oscillates vertically in the liquid with a constant driving force. Measurements of the oscillating amplitude of the plate in air or in a vacuum are related to the oscillations of the plate in the liquid sample. The product of the viscosity and the density of the liquid are related to the amplitudes. This product can be constantly measured or monitored.

Again the apparatus is relatively simple to construct and operate. Although this method is applicable for some metals, this method is unsuitable for measurements of low-viscosity liquid metals. The reason lies in the fact that a thin oscillating plate of large surface area must be moved so slowly within the liquid that data become difficult to obtain.

2.1.1.4. Oscillating Vessel Method

Finally, the method most commonly utilized in the viscosity measurement of metallic fluids is the oscillating vessel method (examples for nickel alloy systems include references [3] and [7]). Figure 2.1 illustrates the apparatus for this method. Essentially, the vessel is set into an oscillating motion about a vertical axis. Upon establishing the oscillating motion, the stepping motor is turned off and a gradual decay of the oscillations results, which is attributed to the frictional forces, associated within the

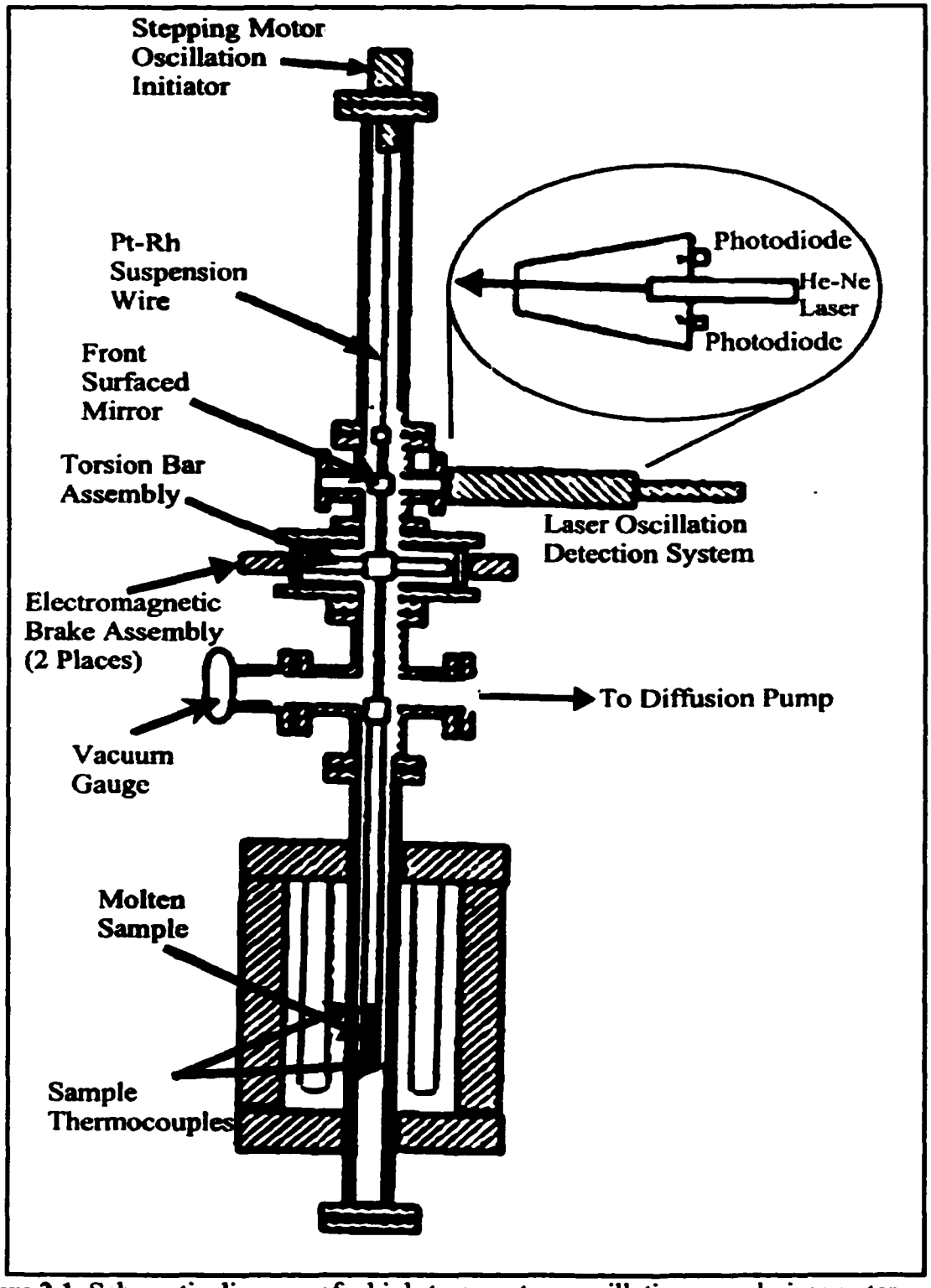

Figure 2.1. Schematic diagram of a high-temperature oscillating vessel viscometer.

liquid. The laser detection system detects the rate of decay in the oscillations. This rate is then related to the viscosity through several approximations and equations.

The primary advantage of this method is that the apparatus is simple. The periodic time of the oscillations can be measured with a high degree of accuracy by use of a laser assembly. Probably the most important factor is that the vessel height does not have to be excessive, which implies that temperature can be maintained uniformly in the measurement region. Its principle disadvantages, however, are the complexity of the mathematics associated with the dampening oscillations and the solutions utilized in solving these oscillations. The following statement made by Iida and Guthrie[2] concerning the oscillating vessel method describes this fundamental problem:

> Unfortunately, the calculation of the viscosity of a liquid from the observed logarithmic decrement and period of the oscillations is extremely complicated. A major reason for large discrepancies among experimental viscosity data is the result of approximations in the working formulae used to connect the observed damping of oscillations and dimensions of the apparatus with the viscosity of the liquid.

Individual researchers may report viscosity values within 1-5 percent; yet another approach to the solution of the viscosity may yield a discrepancy as large as 30-50 percent. In other words, there are several different equations used to obtain the viscosity from the data of dampening oscillations. Those most commonly used are Knappwost's equation, Roscoe's equation, and Shvidkovskii's equations. According to Iida and Guthrie[2], Shvidkovskii's equations yield higher viscosities close to the melting point of the substance. Depending upon which equation is used, one can arrive at differing results. Iida *et al.* [8] performed a detailed experimental investigation into the problem relating to the solutions. Figure 2.2 shows how the viscosity of liquid bismuth can vary,

depending upon the formula used with the same set of measurements. Therefore, a more reliable approach in determining viscosities is needed.

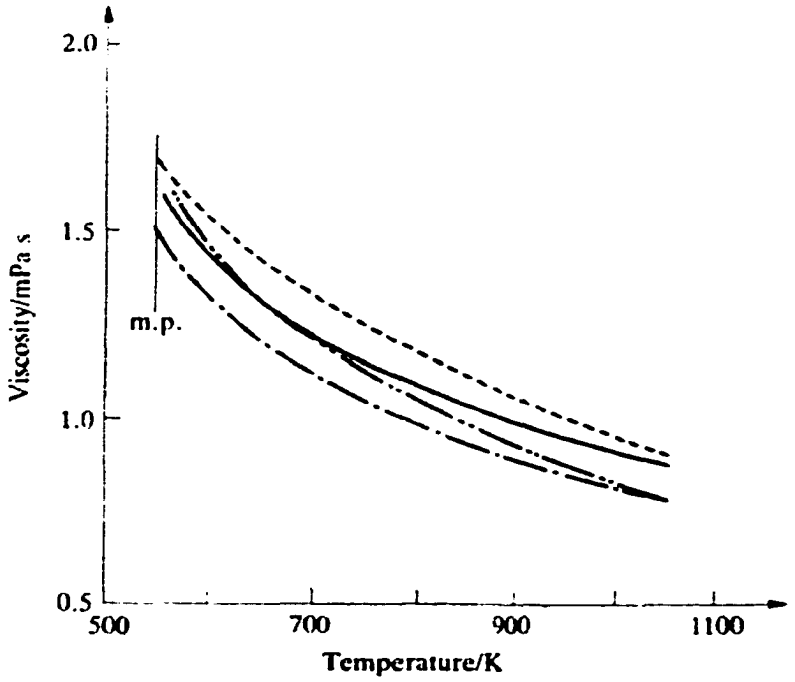

Figure 2.2. Oscillating vessel solutions used in the determination of the viscosity of liquid bismuth.[2] The solid line represents the viscosity measured by a capillary viscometer and the dashed lines represent the solutions to the viscosity utilizing Knappwost's formula, Roscoe's formula, Shvidkovskii's formula.

2.1.2. Theoretical or Phenomenological Models of Viscosity for Pure Metallic Liquids

There is a variety of models used to predict the viscosity of metals. Some of these models arise from the statistical mechanical theory of liquids, others from empirical relations. The following subsections outline and describe the most significant approaches. For the other approaches, as well as, more detailed descriptions the reader is referred to Iida and Guthrie[2].

2.1.2.1. Born-Green Approach to Viscosity

This method could be described as a pair distribution function method based on kinetic theory. Born and Green[9] derived the following expression in terms of a pair distribution function $g(r)$ and a pair interatomic potential $\varphi(r)$. Within this model, the viscosity is

$$\eta = \frac{2\pi}{15}\left(\frac{m}{kT}\right)^{1/2} n_0 \int_0^\infty g(r)\frac{\partial\varphi(r)}{\partial r} r^4 dr \tag{2.3}$$

where m is the mass of the atoms or molecules, k is Boltzmann's constant, T is temperature, and n_0 is the average number density of the liquid. Assuming that one knows the pair distribution function and the pair interatomic potential this expression can be solved. However, the validity of equation (2.3) depends upon the pair potential chosen, which is generally unknown.

2.1.2.2. Hard Sphere Theory (Enskog Theory)

Originally this theory or solution was proposed by Enskog[10]. This method solves the reduced Liouiville equation in a similar approach as is used in the solution of Boltzmann's equation for gases of moderate density. Enskog's approach then uses a series of approximations to obtain an expression for viscosity. The resulting equation is as follows:

$$\eta = \eta_G\left\{\frac{1}{g(r)} + 0.8\left(\frac{b}{v}\right) + 0.761\left(\frac{b}{v}\right)^2 g(r)\right\} \tag{2.4}$$

where $b = \frac{2\pi\sigma^3}{3}$, σ is the diameter of the atom treated as a hard sphere, v is the volume of the atomic sphere, $g(r)$ is the equilibrium pair correlation function, and η_G is an expression for the viscosity of dilute hard sphere gases as defined by the following:

$$\eta_G = \frac{5}{16}\left(\frac{mk_BT}{\pi}\right)^{1/2}\frac{1}{\sigma^2}. \tag{2.5}$$

m is the mass of the sphere and T is the temperature. Note, these expressions were derived through the use of many correction factors and they neglect successive collisions and many-body interactions. The usefulness of this expression is again limited by the knowledge of $g(r)$.

2.1.2.3. Chapman Equation

Chapman[11] analyzed a series of viscosity data for liquid metals in the light of the theory presented by Born-Green[9] and Kirkwood [12]. Chapman "arrived at a generalized model for the viscosity of liquid metals which involves no assumptions of the structure other than that the atoms are spherical and that the potential between atoms can be expressed by some function $\varphi(r)$ of the distance between atoms and an energy parameter [13] ." The fundamental equation that Chapman obtained for the reduced viscosity η^* is:

$$\eta^*\left(V^*\right)^2 = f\left(T^*\right) \tag{2.6}$$

where V^* is the reduced volume and T^* is the reduced temperature. The reduced quantities are as follows:

$$\eta^* = \frac{\eta\delta^2 N_0}{\sqrt{MRT}} \tag{2.7}$$

$$T^* = \frac{k_b T}{\varepsilon} \tag{2.8}$$

and

$$V^* = \frac{1}{n\delta^3}. \tag{2.9}$$

The variables found in equations 2.7 through 2.9 are:

δ = interatomic distance for the close-packed crystal at 0 K, Å

ε = energy parameter from a Lennard-Jones potential for the metal

N_0 = Avogadro's number,

M = atomic weight,

R = gas constant,

T = absolute temperature, K,

k_b = Boltzmann's constant, and

n = number of atoms per unit volume.

Chapman assumed that all metals obey a simple Lennard-Jones pair potential. Based upon this assumption he then fit the data of the liquid sodium and potassium to an empirical equation (2.6). The resulting correlation function could then be applied to other metals.

The correlation function that Chapman developed gives rough estimates of the viscosity of liquid metals. Although the simple Lennard-Jones pair potential can be

applied to the simple metals, it neglects the many-body interactions associated with transition metals.

2.1.2.4. Andrade's Equation

Andrade's equation[14] is of notable interest in that it has been applied to both pure metals and binary liquid metals with reasonable success[15]. Originally it was proposed for simple monatomic liquids. Andrade's expression is

$$\eta v^{1/3} = A e^{\left(\frac{C}{vT}\right)} \tag{2.10}$$

where v is the specific volume, T is the temperature, while A and C are empirical constants. The difficulty with Andrade's equation is that it cannot be used to predict the viscosity without a series of data points to get a good statistical average for the constants A and C. Furthermore, there is no rigorous theoretical explanation for the relation given in equation (2.10).

Comparing the prior mentioned models, the Born-Green theory[9] with its foundation in statistical mechanical theory provides an exact expression for the viscosity; however, its usefulness in predicting viscosity may be hindered by requiring a knowledge of the pair potential, $\varphi(r)$, and the pair distribution function $g(r)$. The Enskog theory[10] reduces the complexity, yet it requires also a knowledge of the pair distribution function $g(r)$. The empirical form of Chapman's and Andrade's equation may be helpful in giving rough estimates of viscosity, which assume the adjustable parameters have been fitted to sufficient experimental data. As a result of these significant complications, a more

predictive model or another approach in obtaining monoatomic viscosities should be developed.

2.1.3. Binary Models of Viscosity

2.1.3.1. Revised Enskog Theory

The Revised Enskog Theory (RET) is an application of the hard-sphere theory described in the prior section to binary mixtures of hard spheres. It was first extended to deal with binary [16] and then multicomponent fluid mixtures [17]. The theory was further refined by van Beijeren and Ernst [18]. The refinement that Beijeren and Ernst proposed dealt with including an exact local equilibrium pair-distribution function term. However, as Castillo and Casteñada [19] stated: "The main difficulty in applying the RET to transport coefficient expressions to real fluids lies in relating the contact values of the hard-sphere radial distribution function and the hard-sphere diameters appearing in the theory to quantities associated with the real system." In other words, the usefulness of this theory is limited by knowledge of the pair-distribution functions for a variety of number densities and for the set of hard sphere diameters.

2.1.3.2. Kucharski's Model for Binary Liquids

Kucharski[20] proposed the following empirical function based on rate theory to predict the shear viscosity in binary alloys.

$$\eta = \sum_{i=1}^{2} X_i \left(\frac{V_i}{V}\right)\left(\frac{\beta}{\beta_i}\right)^2 \gamma_i^{\alpha} \eta_i \qquad (2.11)$$

where V_i is the molar volume of species i, V is the molar volume of the alloy, γ_i is the activity coefficient, η_i is the viscosity of the species, X_i is the mole fraction of the ith component, $\beta=X_A V_A^{1/3}+X_B V_B^{1/3}$, α is a constant, and

$$\beta_i = X_i V_i^{1/3} + \frac{X_j V_j^{4/3}}{V_i}. \tag{2.12}$$

Kucharski successfully applied these equations to several binary mixtures and found that the constant α had some temperature dependence. However, Ganesan *et al.* [15] applied Kucharski's equations to an aluminum-copper alloy and found the constant α varied, not only with temperature, but also with composition, suggesting that these predictive equations must be used with care.

2.1.3.3. Viscosity for Binary via Gibbs Energies of Mixing

Seetharaman and Du Sichen[21] proposed a phenomenological correlation for the viscosity of metallic alloys based on the Gibbs energy of mixing. The basic correlation for viscosity looks like an Arrhenius equation,

$$\eta = Ae^{\left(\frac{\Delta G^*}{RT}\right)} \tag{2.13}$$

with

$$A = \frac{hN_A\rho}{M} \tag{2.14}$$

where ρ is the mass density of the melt, h is planck's constant, N_A is Avagadro's number, M is the molecular weight of the mixture, and ΔG^* is activation energy of mixing. In

their paper, they derive a way of determining the ΔG^* from known thermodynamic values for the Gibbs energy of mixing. Their conclusion was that

$$\Delta G^* = \sum X_i \Delta G_i^* + \Delta^m G_{mix} + 3RTX_1X_2 \qquad (2.15)$$

where $\Delta^m G_{mix}$ is the Gibbs energy of mixing and ΔG_i^* is the Gibbs energy for the pure component. Their predictions work well for those substances of which the thermodynamic quantities are known. Their approach predicts the viscosity for the Ag-Au system quite accurately. But again, the lack of thermodynamic data for many alloys renders this approach not so attractive.

2.1.3.4. Phenomenological Method of Iida *et al.*

This method of predicting the viscosity of binary melts is based on a phenomenological point of view. It attempts to evaluate the viscosity in terms of known physical quantities. Iida *et al.*[2] arrived at the following expression:

$$\eta = (X_1\eta_1 + X_2\eta_2)\left\{-\frac{5X_1X_2(d_1-d_2)^2}{X_1d_1^2 + X_2d_2^2} + 2\left[\left(1+\frac{X_1X_2(m_1^{1/2}-m_2^{1/2})^2}{X_1m_1^{1/2}+X_2m_2^{1/2}}\right)^{1/2} - 1\right] - \frac{0.12X_1X_2\Delta u}{kT}\right\} \qquad (2.16)$$

where d_i is the diameter of the atom from the ionic radius of Pauling, m_i is the mass of an atom, X_i is the fraction of each species, and Δu is the interchange energy which is related to the enthalpy of mixing. This model predicts the viscosity fairly well. However, as Iida and Guthrie point out, this model does not predict the viscosity of the melt when the phase diagram exhibits an intermetallic compound.

To conclude this section on viscosity measurements and theories to predict them, most if not all of these methods of predicting viscosity have flaws. It is apparent that the best approach to determine and predict viscosities of liquids is from an atomistic point of view. That is the approach we have undertaken in this research, and the following chapters detail just such a method.

2.2. Diffusion

Having looked at the problems associated with experimental and theoretical determination of viscosity, we now examine diffusivity. Diffusion occurs as the result of a concentration gradient or a density gradient. This quantity corresponds to the motion of the atoms in a liquid. The units on the diffusion coefficient are the same as kinematic viscosity. The flux of atoms can be expressed in terms of Fick's First Law:

$$J = -D\nabla c \tag{2.17}$$

where c is the concentration of the atoms, ∇c is the concentration gradient, and D is the diffusion coefficient or diffusivity. For liquid metals the diffusion coefficient is on the order of 10^{-9} m^2 s^{-1}.

Knowledge of the diffusion coefficient is vital to the metallurgical modeler because this property helps predict the structure of the alloys formed during solidification.

2.2.1. Measurement Techniques

Unlike the section on measuring viscosity, this section will simply refer the reader to Iida and Guthrie[2] for the details of each method. The methods for the measurement of diffusivity in liquid metals consist of capillary-reservoir, diffusion couple, shear cell,

plane source, electro-chemical concentration cell, slow neutron scattering, and nuclear magnetic resonance. To obtain the self-diffusivity of a pure liquid metal, most techniques require a radioactive isotope. Therefore, many self-diffusivities are unavailable. Furthermore, the available data for both pure and binary liquids may not have taken effects such as convection and sampling technique[13].

In view of the scarcity of diffusion data, the engineer or researcher sometimes employs a variety of empirical relationships between viscosity and diffusivity. Each of the empirical relationships arises out of some concept or viewpoint of the liquid structure or the mechanisms of diffusion. As we have already explored, the accuracy of viscosity data is questionable and its availability is sparse. The following subsections briefly address the common models or theories utilized by the researcher or engineer. For more detailed information the reader is referred to Poirier and Geiger[13], or Iida and Guthrie[2]. Note that the theories addressed are only a few of the prominent ones, namely the Hydrodynamic Theory, Eyring's Theory, Fluctuation Theory, and the Universal Scaling Law.

2.2.2. Hydrodynamic Theory

Hydrodynamic theory describes a system of atoms or molecules as unreacting spherical particles moving through a medium. The medium has a uniform frictional force, namely viscosity, that acts upon the particle. The resulting expression, called the Stokes-Einstein Equation relates the diffusion coefficient to the viscosity of the liquid. The relationship is as follows:

$$D = \frac{kT}{6\pi R\eta} \tag{2.18}$$

where R is the radius of the spherical particles. Sutherland [22] proposed a correction to the Stokes-Einstein relation, namely:

$$D = \frac{kT}{6\pi R\eta}\frac{\left(1+\frac{3\eta}{B_s R}\right)}{\left(1+\frac{2\eta}{B_s R}\right)} \tag{2.19}$$

where B_s is the coefficient of sliding friction between the diffusion particles and the medium. The atoms which impede the diffusing atoms constitute the medium. At the extreme case of $B_s=\infty$, the equation reduces to the Stokes-Einstein equation. While at the other extreme $B_s=0$ we obtain the Sutherland-Einstein equation,

$$D = \frac{kT}{4\pi R\eta} \tag{2.20}$$

The relative size of the particles diffusing to the size of the particles constituting the medium determine which equation is more appropriate[13]. The Stokes-Einstein equation is more appropriate when the radius is large compared to the host. The Sutherland-Einstein equation is more appropriate in the case of the diffusing particles being approximately equal in size to the particles constituting the medium. The principle shortcoming of this model is that it essentially neglects the interactions between the particles. However, these relations have been helpful in predicting the self diffusion coefficient of several metallic fluids and often used with molten glasses.

2.2.3. Eyring's Theory

Eyring's theory[23] is considered the activated state theory of diffusion. This theory describes an atom making a series of small discrete jumps from empty space in the liquid to another empty space or hole to hole. The results of this theory is an expression for the self-diffusion coefficient, namely:

$$D = \frac{kT}{2R\eta} \tag{2.21}$$

where the variables are the same as those defined in the Stokes-Einstein relationship. As can be seen, this equation predicts diffusion coefficients of approximately six to nine times greater than either of the expressions from hydrodynamical theory. When one analyzes the viscosity and diffusion data of metals with accurate data, this model is unsuitable.

2.2.4. Fluctuation Theory

This theory is attributed to Cohen and Turnbull [24] and later developed by Swalin [25] and Reynik [26]. It is based on processes involving fluctuations in the volume of atoms expanding and contracting. When the local area "opens" up, a diffusing atom moves through the volume. Reynik predicts a linear temperature dependence of the diffusivity; of course this is at odds with the concept that diffusion is a thermally activated process that obeys an Arhenius relationship. Furthermore, Swalin[25] suggests that this theory calculates better relative values for diffusivity rather than absolute values.

2.2.5. Universal Scaling Law

Recently, Dzugutov proposed an empirical scaling law that relates the diffusion coefficient to the radial distribution function and the entropy of the system[27]. The dimensionless diffusion coefficient $D^{\dagger}$ behaves as

$$D^{\dagger} = 0.049e^{S_2} \tag{2.22}$$

where S_2 is the excess entropy and is defined as

$$S_2 = -2\pi\rho\int_0^{\infty}\{g(r)\ln(g(r)) - (g(r)-1)\}r^2 dr \tag{2.23}$$

where ρ is the atomic density, r is the radial position, and $g(r)$ is the radial distribution function. A complete knowledge of the radial distribution function allows one to calculate the value for the pair approximation for the excess entropy S_2. The dimensionless diffusion coefficient calculated with equation 2.22 is related to the actual diffusion coefficient by the following relationship:

$$D = D^{\dagger}\Gamma_E\sigma^2 \tag{2.24}$$

where Γ_E is the collision frequency determined from Enskog's theory and σ is the hard-sphere diameter. σ can be interpreted as the position of the first maximum of the radial distribution function $g(r)$. The value for Γ_E is calculated from Enskog's theory as:

$$\Gamma_E = 4\sigma^2 g(\sigma)\rho\sqrt{\frac{\pi k_B T}{m}} \tag{2.25}$$

where m is the atomic mass, T is the temperature of the system, $g(\sigma)$ is the value of the radial distribution function at σ, and k_B is Boltzmann's constant. This model or scaling

law was successfully applied to a variety of pure liquids and solids. Dzugutov [26] performed a variety of molecular dynamics simulations to deduce that equation 2.22 was valid for a variety of systems where $-S_2$ is greater than 1.5 k_b. However, upon examining one of the Figures found in Dzugutov's paper (Figure 2.3), it appears that equation 2.22 may be only valid for values of $-S_2$ greater than 2 k_b. Yet in the lower limit of the graph where $-S_2$ is between 1.5 k_b and 2 k_b, the actual $D^\dagger$ appears to be exceeding the value predicted from equation 2.22. Thus, because of the underestimation of $D^\dagger$ for this range, one must be cautious, and apply equation 2.22 with great care.

2.2.6. Other Models of Diffusion

Of the models we have discussed for diffusion, we chose here to examine our data in the light of hydrodynamic theory and the universal scaling law. There are other models of diffusion in liquids that describe the diffusivity reasonably well. Turkdogan[28] describes a rigid sphere model for the self-diffusivity in liquid metals. Cahoon[29] proposed a model for solute impurity diffusion in liquid metals by including Engel-Brewer valences within an activation energy term. Cahoon found that his modified "hole" theory worked well for almost all solute impurities in Al, Ga, and Ag solvents.

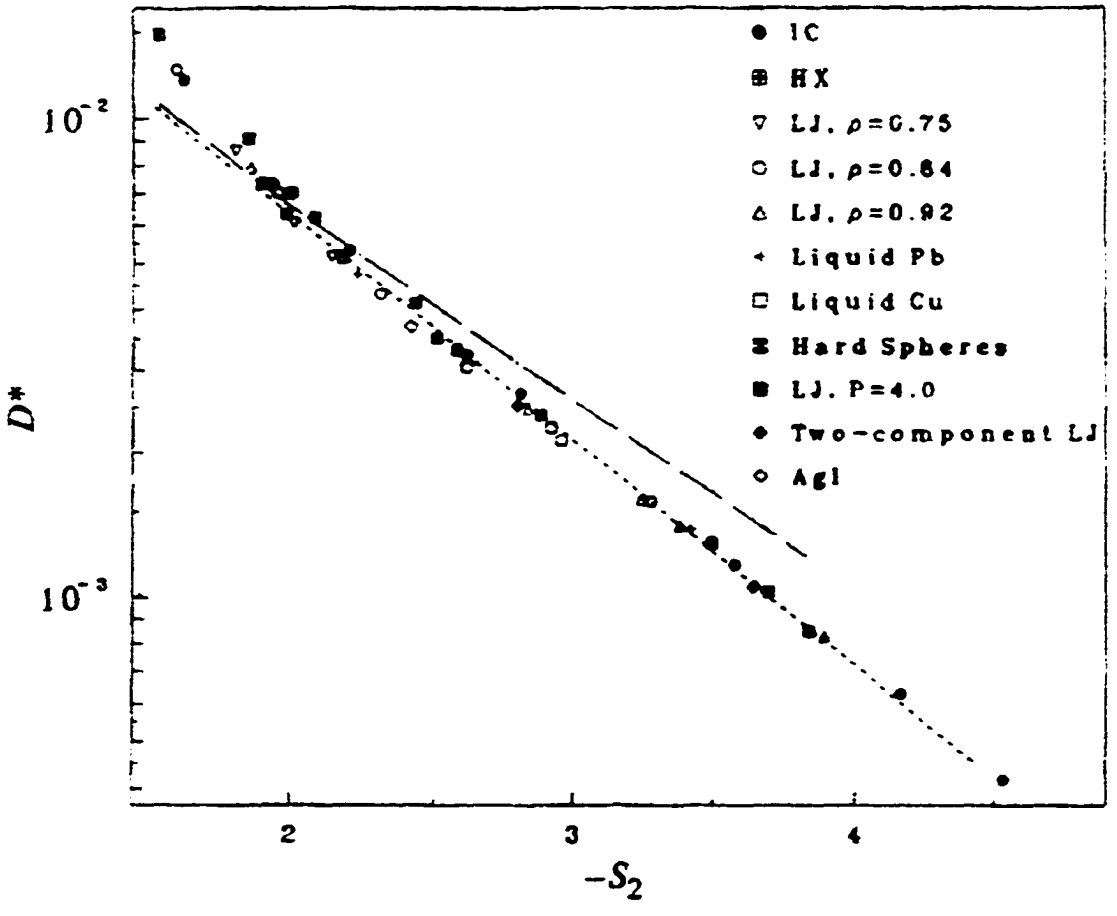

Figure 2.3. Diffusion coefficient D^t for various models, as a function of the excess entropy[27]. *Reproduced from Figure 2a in reference 27.*

By examining viscosities and diffusivities of liquid metals, it is apparent that current models have limitations in their functionality for making accurate predictions. The most significant problem with some of the theories is a general lack of knowledge concerning the pair distribution function and the pair potential for the species. The inadequacy of the theories implies that a deterministic atomistic approach may provide insight in the mechanisms as well as providing data with some certainty. The best atomistic technique available for determining transport properties is molecular dynamics. In fact, molecular dynamics seems to suggest that the mechanism of diffusion transport in non-ionic liquids does not fit either into fluctuation theory or Eyring's activated rate theory[30]. Chapter 4 details the techniques available within molecular dynamics.

CHAPTER 3

EMBEDDED ATOM METHOD

3.1. Background

Since the introduction of the embedded-atom method (EAM) by Daw and Baskes [4, 31-33], the EAM potential has been used extensively for the study of solid systems. Some authors have utilized variations of the embedded-atom potential to study solid-state diffusion processes[34, 35]. Others have studied phase transformations, physical properties, and thermodynamic properties[36-57].

The embedded-atom method (EAM), as first proposed by Daw and Baskes [4, 31-33], is a semi-empirical many-body potential, based on density functional theory. Density functional theory suggests that the energy required to place a small impurity atom in a lattice is determined by the electron density at that site, irrespective of the source of the electron density. The general form for the total energy is given by [58]

$$E_{total} = \sum_i F(\rho_i) + \frac{1}{2}\sum_i \sum_j \phi(r_{ij}) \tag{3.1}$$

where ρ_i is determined by

$$\rho_i = \sum_{j \neq i} f(r_{ij}) \tag{3.2}$$

ρ_i is the charge density at the i^{th} nucleus due to the spherically symmetric atomic charge densities $f(r_{ij})$ of the neighboring atoms, $F(\rho_i)$ is the embedding function, and $\phi(r_{ij})$ is a pair potential term. Both the embedding function and the pair potentials are found empirically, using fits of calculated properties to the lattice constant, cohesive energy,

elastic constants, vacancy formation energy, etc. When applied to binaries, the heats of formation are also fitted [32].

EAM formalism is an improvement over strictly pair potential models for several reasons. EAM is a many-bodied potential. First, most metallic systems show that the Cauchy relation is violated between the elastic constants in cubic crystals. EAM is able to violate the Cauchy relation where a pair potential is not. Second and most significantly, EAM correctly describes the condition of bond strength increasing with decreasing coordination number found in metallic bonding. Compared with *ab initio* or first principle calculations, EAM is not as computationally intensive and maybe only twice as computationally intensive as a simple pair potential.

The EAM is shown to be many-bodied through an expansion of $F(\rho_i)$, as illustrated by Sutton and Ballufi [58], about some reference density $\bar{\rho}$,

$$F(\rho) = F(\bar{\rho}) + (\rho - \bar{\rho})F'(\bar{\rho}) + \frac{(\rho - \bar{\rho})^2 F''(\bar{\rho})}{2} + \ldots \tag{3.3}$$

where ρ is a sum of spherically symmetric charge densities or a sum of pair potentials. The second term $(\rho - \bar{\rho})F'(\bar{\rho})$ is a sum of two-body interactions, and the third term in this series (or the second derivative term) is a sum of three-body interactions. As long as $|\rho - \bar{\rho}|$ is small, this series converges. Another requirement to obtain metallic bonding characteristics is that the second derivative, $F''(\bar{\rho})$, must be positive. $F''(\bar{\rho})$ is always constructed to be positive over a large range of $\bar{\rho}$ but on account of the positive second derivative requirement, a Cauchy relation is violated. For metallic systems, the Cauchy relation needs to be violated. Daw and Baskes [4] showed that for a cubic material

$$c_{12} - c_{44} = positive\ const. \times F''(\overline{\rho}) \tag{3.4}$$

where $\overline{\rho}$ is the value of ρ in the perfect crystal. In addition, the positive second derivative provides the condition for increasing bond strength with decreasing coordination number found in metals.

Another important feature of monoatomic EAM potentials is that are invariant to a linear transformation of the embedding function during a concurrent transformation of the two-body potential term[59]. In other words, it has been shown that the relation

$$G(\rho) = F(\rho) + k\rho \tag{3.5}$$

is invariant when

$$\psi(r) = \phi(r) - 2kf(r) \tag{3.6}$$

where k is an arbitrary constant, $G(\rho)$ is the transformed embedding function, and $\psi(r)$ is the transformed two-body potential. This feature allows a variety of embedding functions that could give comparable results in determining structural and thermodynamic quantities from EAM formalism.

Embedded-atom method potentials have been derived for body-centered cubic[60-62] and hexagonal close packed [36, 63] metals with marginal success. However, the EAM potentials are best suited for face-centered cubic metals because of their general non-directional nature.

Another condition recommended when selecting a potential is that it should obey the universal equation of state for metals derived by Rose *et al.*[64], which is of the form:

$$E(r_{ws}) = \Delta E * E^{*}(a^{*}) \tag{3.7}$$

Where E is the binding energy per atom, r_{ws} is the radius of the Wigner-Seitz sphere containing an average volume per atom, ΔE is the equilibrium binding energy, and a^* is a scaled length factor. $E^*(a^*)$ can be approximated by [64]

$$E^*(a^*) = -E_0(1 + a^*)e^{-a^*} \tag{3.8}$$

where E_0 is a reference binding energy.

Banerjea and Smith [65] expanded upon the work of Rose *et al.*[64] by suggesting that the embedding energy function must follow the form

$$E_{embedding} = -F_0(1 - \ln n^*)n^* \tag{3.9}$$

where n^* is related to the electron density and F_0 is an embedding energy constant. Equations (3.8) and (3.9) should be followed to satisfy the requirements of metals.

According to Cai and Ye [5], a long-range force is needed to evaluate structural stability adequately when angular forces are not considered. Most EAM potentials do not include a long-range force. For instance, Johnson[66] presents an analytical form for face-centered cubic metals and alloys with only a first nearest neighbor interactions. This, according to Cai and Ye[5], means that "the second derivative of the embedding energy will become smaller than zero in the case when the two-body potential changes more rapidly than the equation of state of Rose *et al.* [64]. This behavior may give an incorrect coordination dependence between bond length and energy." Therefore, a long-range potential is needed for structural implications.

In order to utilize effectively an EAM potential in a molecular dynamics simulation, the potential must be computationally feasible. In the early days of the EAM potential, the functional form was derived by complex spline-fit functions.

Computationally these functions are not desirable; it is more convenient to have the EAM potentials in the form of analytical functions for computations.

3.1.1. Binary Models

When dealing with a binary alloy (A-B) in the context of EAM potentials, it is assumed that the embedding function does not rely on the identity of the neighboring atoms, rather only on the local electron density of the location where the atom needs to be embedded. The variables that control the embedding energy function are as follows: $f_a(r)$ and $f_b(r)$, the electron density profile about an "A" and "B" atom, respectively; and two kinds of embedding energy functions $F_a(\rho)$ and $F_b(\rho)$. In addition, one must consider three kinds of pair potential terms $\phi^{aa}(r)$, $\phi^{bb}(r)$, and $\phi^{ab}(r)$. The first six terms are usually assumed to be transferable from the monatomic to the alloy system. The last term, $\phi^{ab}(r)$, has been determined via three principle methods, namely: a geometric mean[32] , a density weighted combination of pair-potentials[59], and a lattice inversion method[67]. The latter, due to its complexity and its principle application to solids, will not be discussed.

In the geometric mean method, it is assumed that the pair-potential is the result of coulombic repulsion between atoms. The pair-potential, according to Foiles, Baskes, and Daw [32], based on the geometric mean is

$$\phi^{ab}(r) = \sqrt{\phi^{aa}(r)\phi^{bb}(r)}. \tag{3.10}$$

The principle problem associated with this method arises where one monatomic pair-potential is negative and the other is positive. In this case, the geometric pair-potential is imaginary.

Because of the preceding problem, Johnson[59] proposed an alternative approach in obtaining a binary pair-potential, called the density weighted combination of pair-potentials. Johnson utilized the property of the invariance of the EAM potential to a linear transformation of the embedding function (equations 3.5 and 3.6). The result of his derivation for the unlike pair-potential, $\phi^{ab}(r)$ is

$$\phi^{ab}(r)=\frac{1}{2}\left[\frac{f^{b}(r)}{f^{a}(r)}\phi^{aa}(r)+\frac{f^{a}(r)}{f^{b}(r)}\phi^{bb}(r)\right]. \tag{3.11}$$

There is no theoretical justification for this form, yet this method has the benefit of not having the possibility of imaginary results as with the geometric mean approach. This model has been applied to both bcc and fcc-based binary alloys [5, 59, 62]. Therefore this study will employ the density weighted combination approach to obtain the dissimilar pair potential term, ϕ^{ab}(r).

3.1.2. Application of EAM to Liquids

When constructing the EAM potential, one typically uses fits to data from properties of the solid material. One may question the applicability of using an EAM potential to simulate a liquid metal using parameters obtained from a solid. However, Foiles[68] showed that the structure of the pure liquid could be reasonably reproduced using parameters obtained from the solid phase. Since Foiles' [68] premiere paper, LeSar *et al.* [37] examined the thermodynamics of liquid transition metals using EAM potentials. Chen *et al.* [38] examined the melting temperature of nickel and obtained good agreement with experimental melting point. Alemany *et al.*[69, 70] utilized the Voter-Chen[39, 40] EAM potential to examine the dynamic, structural, and

thermodynamic properties of liquid nickel and obtained structural data comparable to experiment. Recently, Asta *et al.*[71] examined liquid nickel-aluminum alloys using a variety of EAM potentials. Each of the potentials in their study yielded similar results. Besides these works that directly pertain to nickel or aluminum, there is a host of other papers that utilize EAM potentials in studying liquid metals[41-50, 72-77]. Thus, there is ample evidence that EAM potentials, although having been fitted to solid data, are applicable also to the study of metallic liquids.

3.2. EAM Potentials

Today there is a variety of EAM potentials available, each of which has advantages and disadvantages. This section examines EAM potentials that have been applied to the nickel-aluminum system. By the nickel-aluminum system, we mean the fitting procedure which was applied to both nickel and aluminum monatomics, and in a few cases, the intermetallic compounds. The most notable potentials are due to: a) Johnson [66]; b) Foiles, Baskes, and Daw [4, 31-33]; c) Voter-Chen [39, 40]; and d) Cai and Ye [5]. In the following subsections, each of the embedded-atom methods will be evaluated within the context of the requirements previously described.

3.2.1. Johnson's Analytical Nearest-Neighbor Model

The pair potential term in Johnson's model[66] was based on a Born-Mayer repulsion, namely,

$$\phi(r) = \phi_e \exp\left(-\gamma\left(\frac{r}{r_{1e}} - 1\right)\right), \quad r \le r_c \tag{3.12}$$

where ϕ_e and γ are adjustable parameters, r_c is the cutoff radius, and r_{1e} is the equilibrium electronic radius. The electronic density term is taken as

$$f(r) = f_e \exp\left[-\beta\left(\frac{r}{r_{1e}} - 1\right)\right], \quad r \le r_c \tag{3.13}$$

where β is another adjustable parameter and

$$f_e = \frac{E_c}{\Omega} \tag{3.14}$$

where Ω is the atomic volume, and E_c is the cohesive energy. This electronic density is spherically symmetric. The embedding function is defined as

$$F(\rho) = -E_c\left[1 - \frac{\alpha}{\beta}\ln\left(\frac{\rho}{\rho_e}\right)\right]\left(\frac{\rho}{\rho_e}\right)^{\alpha/\beta} - \Phi_e\left(\frac{\rho}{\rho_e}\right)^{\gamma/\beta} \tag{3.15}$$

where ρ_e=12f_e and $\Phi_e = 6\phi_e$. α is determined by

$$\alpha = 3\left(\frac{\Omega B}{E_c}\right)^{1/2} \tag{3.16}$$

where B is the bulk modulus.

Although the model is analytic, it does suffer from Johnson's selection of r_c. Johnson selects r_c to be between the first and second nearest-neighbor distance, which may prevent its predictions of long-range order. The selection is based upon the fact that the second derivative of the embedding energy becomes negative when the two-body potential changes more rapidly than the equation of state of Rose *et al.*[64]. Furthermore, this short-range potential may give incorrect coordination dependence between energy

and bond length[5]. Because of its short-range EAM potential, this potential is not suitable in our study of nickel, aluminum, and their alloys.

3.2.2. Foiles, Daw, and Baskes Potential

In 1979, Baskes and Melius [31] proposed a semi-empirical method of obtaining functional forms to describe fcc metals. It would later be defined as the embedded atom method [4]. This method of fitting structural and thermodynamic quantities involved a complex method of spline fitting experimental data. With publication of the universal equation of state by Rose[64], Foiles, Baskes and Daw [32] gave a revised potential designed to follow it. The electronic density was given as a tabulated function. In an effort to provide a basis more fundamental than purely empirical relations, Daw [33] showed how first-principle theories (Hartree-Fock Theory and Thomas-Fermi-Dirac-Von Weizsäcker functional) could be used to determine the EAM parameters. Although the EAM potential proposed by Daw [33] has some theoretical basis, it is not based on a simple analytical expression and requires numerical tabulation of the potential.

3.2.3. Voter-Chen EAM Potential

The Voter-Chen potential[39, 40] was fitted to known quantities of the crystalline Ni_3Al system. In this potential, they took the pair-term to be of a Morse style two-body repulsive term,

$$\phi(r) = D_m\left(1-\exp\left(-\alpha_m\left(r-R_m\right)\right)\right)^2 - D_m \tag{3.17}$$

where D_m, R_m and α_m are adjustable parameters that define the depth, distance to the minimum, and a measure of the curvature near the minimum. The density function $\rho(r)$ is given as

$$\rho(r) = r^6\left(e^{-\beta r} + 2^9 e^{-2\beta r}\right) \tag{3.18}$$

where β is another adjustable parameter. Furthermore, they force the function to go smoothly to zero at some cutoff radius, r_{cut}, which varies, based on the fitting parameters. This potential works well for the Ni_3Al system. However, some other authors [51] have found that it does not predict correctly the structure of NiAl. As a result, Ludwig and Gumbsch [78] proposed a modification to the Voter-Chen potential to describe more accurately the NiAl structural behavior. Essentially, Ludwig and Gumbsch[78] fitted the potential of Voter-Chen to more structural parameters in crystalline NiAl.

Each of the potentials has been used to study the transport properties in the liquid nickel-aluminum system by Asta[71]. In his paper, Asta showed that the potentials of both Voter-Chen and Ludwig-Gumbsch do not accurately predict the experimental shear viscosity given by Petrushevskii[3]. Because the Voter-Chen potential and the Ludwig-Gumbsch potential (modified Voter-Chen) do not accurately predict the liquid transport properties, the present study focuses its efforts on another potential.

3.2.4. Other EAM Potentials

There are other potentials describing the pure nickel, pure aluminum, and the intermetallic compounds of nickel and aluminum. Most notable is Baskes' modified EAM [79, 80], which is a short range potential with some angular dependence. Rubini and Ballone [47-49, 51] developed a potential for Ni_xAl_{1-x} within the range of $0.6 \leq x \leq 0.66$ and also applied their potential to metal-silicon systems. Mishin *et al.*[81-83] recently developed a spline-fit and an analytical form for the EAM based on an extensive

list of parameters. The potentials of Mishin *et al.* [81, 82] are primarily directed to the pure substances with an emphasis on fitting a larger number of measurable quantities.

3.2.5. Cai and Ye Potential

The present work utilizes the potential developed by Cai and Ye[5]. The reasons for using it are as follows: a) The second derivative of the embedding function is positive up to a very large electron density. b) The equations obey the universal equation of state by Rose *et al.*[64]. c) The functional form for the embedding function matches that of Banarjea and Smith [65]. d) The potential also describes the nickel-aluminum alloys with the alloying model of Johnson[59], which does not suffer from imaginary heteroatomic pair potentials. e) Finally, the functional form is a simple analytical expression that can be used to describe both alloys and pure substances. Also note that the Cai and Ye potential is defined for solid systems rather than liquids.

The embedding function of Cai and Ye[5] is defined by

$$F(\rho) = -F_0\left[1 - \ln\left(\frac{\rho}{\rho_e}\right)^n\right]\left(\frac{\rho}{\rho_e}\right)^n + F_1\left(\frac{\rho}{\rho_e}\right) \tag{3.19}$$

where ρ_e is the equilibrium electronic density, F_0 is defined as the cohesive energy minus the energy of vacancy formation, F_1 is an adjustable parameter, and ρ is the electronic density given by

$$\rho = \sum_{j \neq i} f(r_{ji}) \tag{3.20}$$

The function $f(r_{ji})$ is a simple exponentially decreasing function given by

$$f(r) = f_e \exp[-\chi(r - r_e)] \tag{3.21}$$

where r_e is the equilibrium nearest neighbor distance, f_e is a scaling constant and χ must be determined through fitting. The scaling constant f_e is determined to be

$$f_e = \left(\frac{E_c}{\Omega}\right)^{\gamma} \tag{3.22}$$

where Ω is the atomic volume, E_c is the cohesive energy, and γ is an adjustable parameter taken as 0.6 and 0.8 for aluminum and nickel, respectively. The pair-potential was taken to be of the form of Rose *et al.*[64], more specifically

$$\phi(r) = -\alpha\left[1+\beta\left(\frac{r}{r_a}-1\right)\right]\exp\left[-\beta\left(\frac{r}{r_a}-1\right)\right] \tag{3.23}$$

where α, β, and r_a are all adjustable parameters. The cutoff distance for the parameterization was set to be 1.65 times the lattice parameter, a_0. This represents a distance between the fifth and sixth nearest neighbor distance.

It was necessary to utilize the expression of 3.20 to obtain the value for the equilibrium electron density, ρ_e. This was evaluated for the perfect face-centered cubic crystal by summing over all the pairs till the equation 3.21 no longer contributed. Expanding the sum in equation 3.20 and allowing the scaling constant in equation 3.21 f_e to be unity (as will be seen, for pure substances f_e can be taken arbitrarily) we obtain the following result for a perfect face-centered cubic crystal for ρ_e:

$$\begin{aligned}\rho_e = {} & 12\exp\left[-\chi\left(\frac{a_0}{\sqrt{2}}-r_e\right)\right]+6\exp\left[-\chi(a_0-r_e)\right]+24\exp\left[-\chi\left(\frac{a_0\sqrt{6}}{2}-r_e\right)\right] \\ & +6\exp\left[-\chi\left(a_0\sqrt{2}-r_e\right)\right]+24\exp\left[-\chi\left(\frac{a_0\sqrt{10}}{2}-r_e\right)\right]+\ldots\end{aligned} \tag{3.23}$$

where a_0 is the lattice constant.

The alloying model of Johnson[59] was used for the calculation of the heteroatomic pair potential. The model of Johnson was given by equation 3.11 and is repeated here for convenience:

$$\phi^{ab}(r) = \frac{1}{2}\left[\frac{f^b(r)}{f^a(r)}\phi^{aa}(r) + \frac{f^a(r)}{f^b(r)}\phi^{bb}(r)\right] \tag{3.24}$$

where f^a(r) and f^b(r) are the electronic density of the a-type and the b-type atoms, ϕ^{aa}(r) and ϕ^{bb}(r) are the monatomic pair potentials of a-type and b-type atoms respectively. Note that for the alloy, f_e cannot be taken arbitrarily anymore.

To fit the parameters for aluminum and nickel alloys, Cai and Ye[5] chose to modify the nickel parameters, thus achieving a better match for the intermetallic thermodynamic quantities. Hereafter these modified nickel parameters will be referred to as the revised nickel parameters. Note that revised nickel parameters will be used only in the discussion of the alloying substances because Cai and Ye[5] designed their potential that way. The parameters used in these calculations are tabulated in Table 3.1.

A graph of the electron density of one atom is shown for aluminum, nickel, and revised nickel in Figure 3.1. The electrons from this Figure are more tightly bound to the nickel atom than to the aluminum atom. As can be seen from equation 3.20, these functions are exponentially decreasing and depend upon the selection of r_e and χ. These functions are also spherically symmetric exponentially decreasing functions to zero at r=∞.

Table 3.1. Parameters used for Cai and Ye potential. Reference [5].

Parameter	Pure Aluminum	Pure Nickel	Revised Nickel
α	0.0834	0.3768	0.1438
β	7.5995	6.5840	8.0235
χ	2.50	3.10	2.50
F_0	2.61	2.85	2.85
F_1	-0.1392	0.8784	-0.6945
r_e	2.8638	2.4890	2.4890
r_a	3.0169	2.3600	2.6759
ρ_e	12.44481	12.33468	12.73285

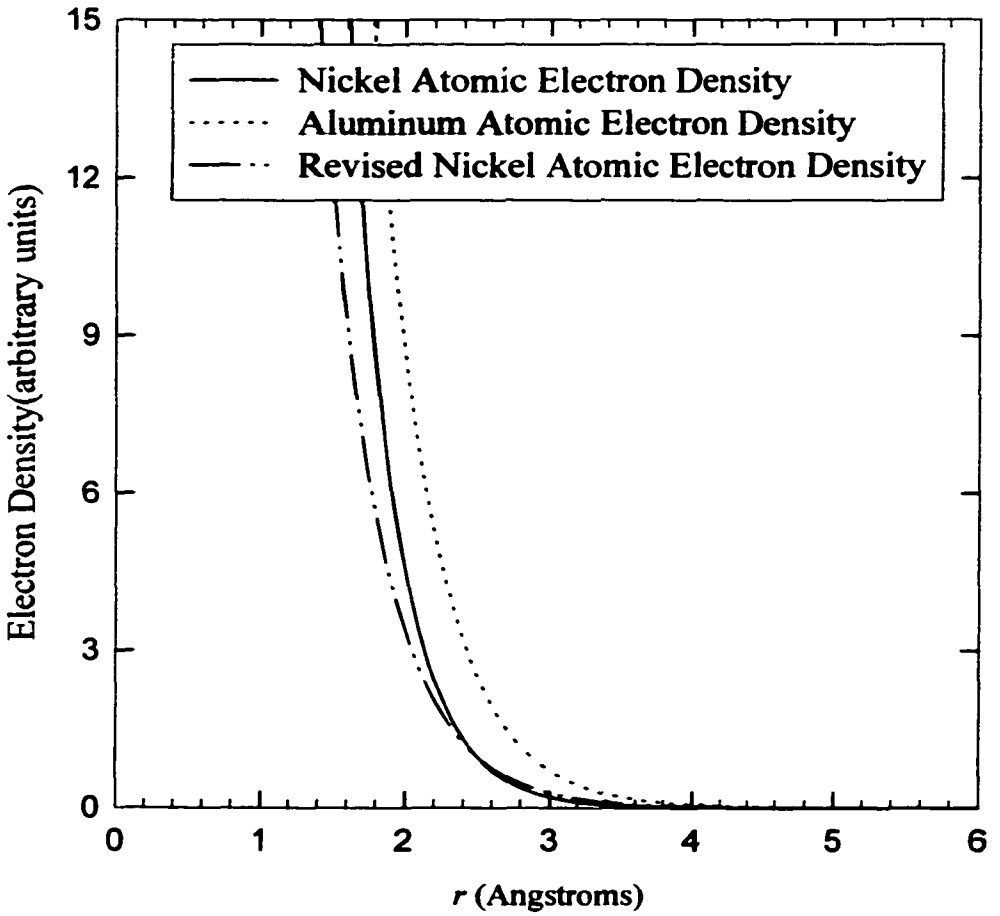

Figure 3.1. Electron density function as a function of distance from the nucleus.

In Figure 3.2, we show the embedding functions of Cai and Ye[5] (equation 3.19) for aluminum, nickel, and revised nickel parameters. Examining the embedding function for aluminum, we note that it is relatively flat. This characteristic of aluminum is consistent with energy calculations for simple metals in which the valence electrons interact weakly with ion-cores. Perturbation theories with pseudopotentials give a total energy as a sum of two contributions--background energy independent of atomic structure and a sum of pair potentials. The embedding energy is nearly independent of ρ_i and, therefore, of the atomic structure [84]. Note that it is difficult to compare the revised nickel potential to that of nickel because, as seen before, the addition of a linear term to the embedding function can be compensated by modifying the pair potential.

Figure 3.3 illustrates the two body potential functions. Notice that each of these functions has a slightly attractive nature to it rather than the purely repulsive potential developed by Daw and Baskes[4]. The pure nickel potentials are the most attractive, whereas the pure aluminum contains the weakest pair-pair potential. The effect of the revised nickel parameters make the nickel-nickel interactions less attractive but again this effect may be compensated by the modified embedding function.

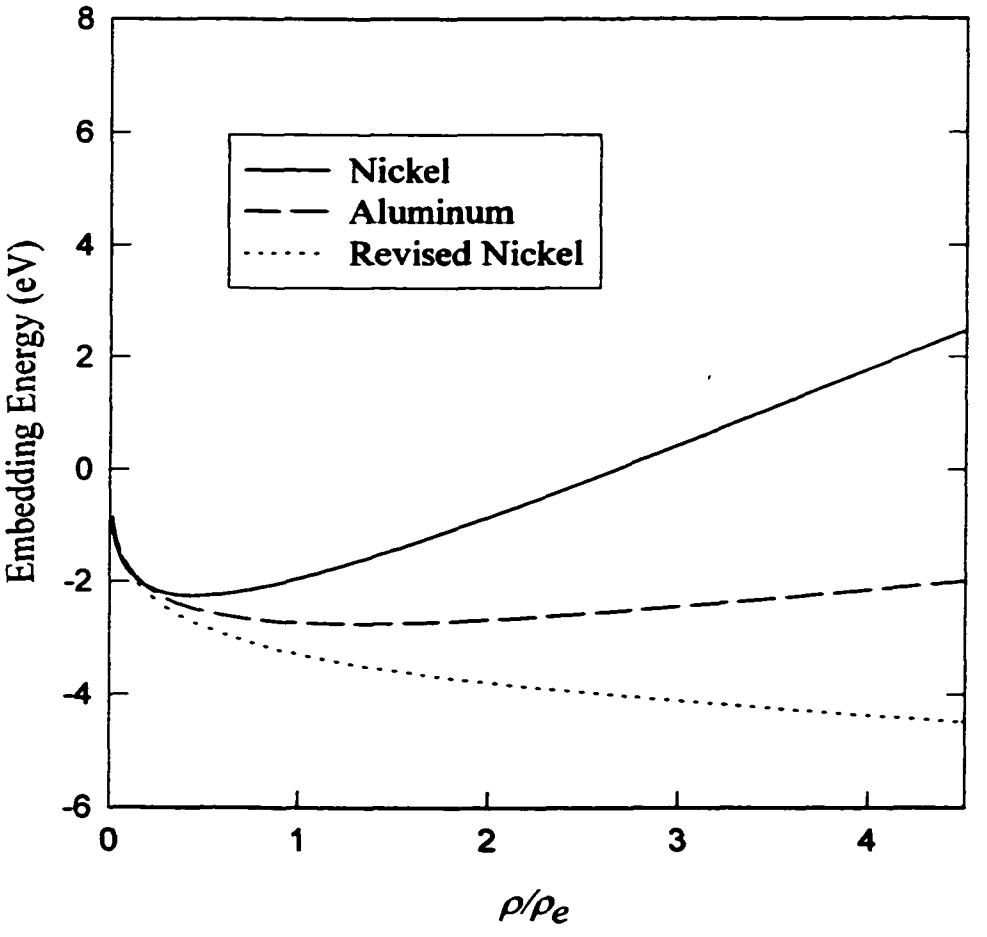

Figure 3.2. Embedding functions of pure aluminum, pure nickel, and the revised nickel parameters.

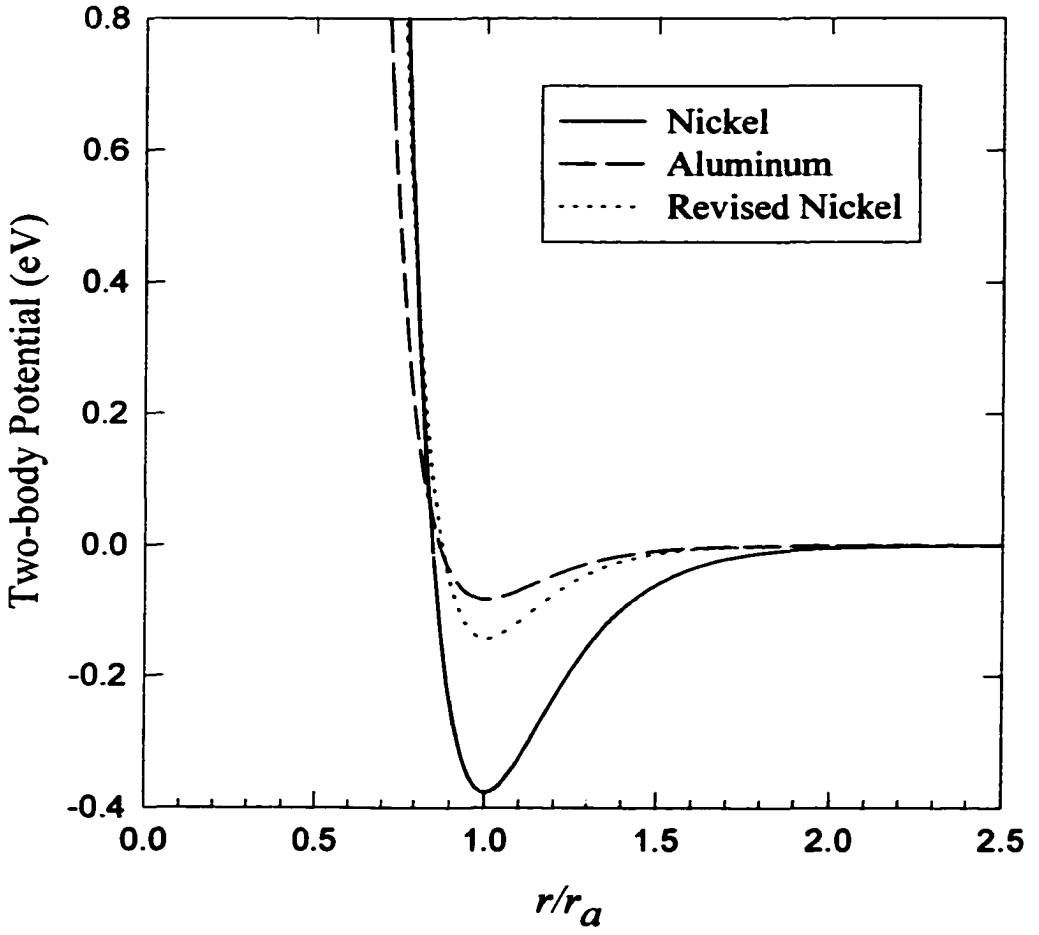

Figure 3.3. Pair potential for the Cai and Ye EAM potential.

The alloyed pair-potential using the pair technique of Johnson[59] is illustrated by Figure 3.4. This graph differs from Figure 3.3 in that it is presented as a function of r rather than r/r_a. Notice also that the attractive nature of the normal nickel parameters is greater than that of the revised nickel parameters. Thus, the revised nickel parameters soften the heteroatomic pair potential. This is consistent with Figure 3.3. The effect of Johnson's alloying function increases the depth of the inter-atomic potential well. Assuming the embedding function weakly affects the interatomic spacing, one would expect the aluminum-nickel pair to have an equilibrium separation of approximately 2.55 Å for the normal nickel and 2.79 Å for the revised nickel parameters. This observation will be discussed with greater detail in Chapter 6.

To conclude this chapter, this work makes use of the potential developed by Cai and Ye [5] to evaluate the structure and properties of pure aluminum, pure nickel, and their alloys in the liquid state. Via non-equilibrium and equilibrium molecular dynamics, the shear viscosity and self-diffusion coefficients of nickel and aluminum are obtained by the methods described in the following chapter. In Chapter 5, the procedure and results for the pure liquid metals are discussed. In Chapter 6, an evaluation of the properties of the binary alloys is made, which includes a proposed modification to the Cai and Ye potential in order to better match the experimentally measured transport properties of the alloys.

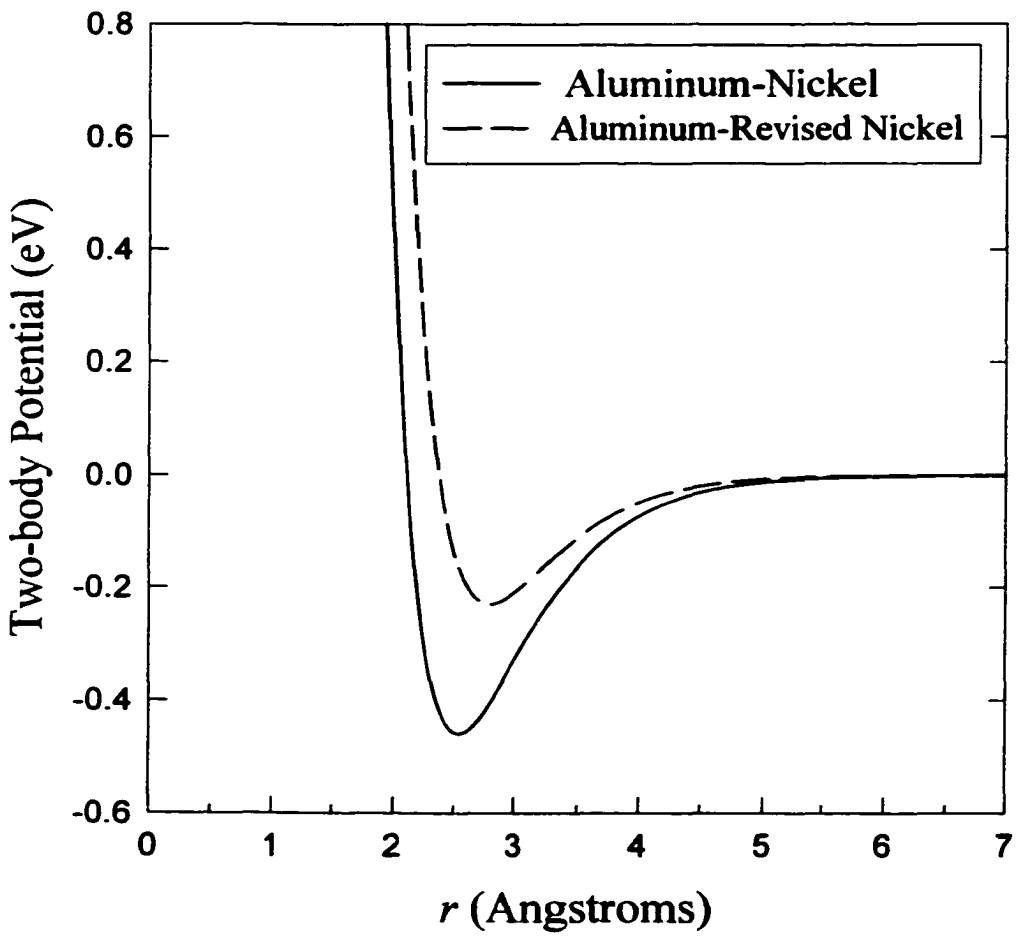

Figure 3.4. Alloying pair potential for aluminum-nickel and aluminum-nickel revised.

CHAPTER 4

TRANSPORT PROPERTIES CALCULATED VIA MOLECULAR DYNAMICS

4.1. Molecular Dynamics (MD) versus Monte Carlo (MC)

Both Monte Carlo (MC) and Molecular Dynamics (MD) are commonly used atomistic computer simulation techniques. The MC method is a stochastic sampling of the configuration space of an assembly of atoms and, therefore, unable to provide any information concerning the true time evolution of the simulated system. The deterministic method of MD solves numerically the classical equations of motion of an assembly of atoms. Thus, MD can measure time-dependent properties of systems both in and out of equilibrium. Transport quantities such as thermal conductivity, diffusion coefficient, shear viscosity, and bulk viscosity can be determined. MD is the only atomistic approach that can be used to study macroscopic transport properties.

Within the framework of MD, there are two well established techniques available whereby one may calculate transport properties of systems, namely equilibrium molecular dynamics (EMD) and non-equilibrium molecular dynamics (NEMD). These methods are discussed in this chapter, along with examples from the literature of these complementary techniques.

4.2. Equilibrium Molecular Dynamics (EMD)

Equilibrium molecular dynamics (EMD) is an extension of the field of statistical mechanics and thermodynamics. Essentially EMD gives computational materials scientists the ability to study properties of materials under equilibrium conditions. Our work focuses on classical mechanics, for example systems of particles which are

describable by Newton's equations of motion. We start with the Lagrangian formulation of classical mechanics that provides the general framework for solving the equations of motions and the positions of the particles. Given a number of particles N with a set of coordinates, $\{\vec{q}_i\}_{i=1,N}$, and momenta, $\{\vec{p}_i\}_{i=1,N}$, one may define the Lagrangian, $L = L(\{\vec{q}_i\}, \{\vec{p}_i\}, t)$. This assumes that all the forces derive from some potential energy function. The Lagrangian from classical mechanics can be written

$$L = \frac{1}{2}\sum_{i}^{N}\left(\frac{\vec{p}_i^{\,2}}{m_i} - U(\{\vec{q}_i\})\right) \tag{4.1}$$

where U is a potential energy function of the coordinates only, and m_i is the mass of the particles. Newton's second law, $\vec{F}_i = m_i\ddot{\vec{q}}_i$, is a direct result of this formalism. The trajectories (time evolution of $\vec{q}_i$ and $\vec{p}_i$) can be obtained from Lagrange equations[31]:

$$\frac{\partial}{\partial t}\left(\frac{\partial L}{\partial \vec{p}_i}\right) - \frac{\partial L}{\partial \vec{q}_i} = 0, \quad i = 1,\ldots,N \tag{4.2}$$

These equations form the starting point for most of the equilibrium properties to be evaluated. Inserting L from equation 4.1 into equation 4.2, and considering a Cartesian coordinate system, we obtain Newton's equation of motion:

$$\vec{F}_i = -\frac{\partial U}{\partial \vec{q}_i} = m_i\ddot{\vec{q}}_i \tag{4.3}$$

By knowing the forces acting on a particle, it is possible to follow in real time the trajectories of the particles. This is the basis of molecular dynamics. Under the condition of ergodicity of the trajectories, Gibbs postulate states that one may calculate the

equilibrium thermodynamic properties of the system simulated as time averages of these trajectories.

Since the equations of motion are solved numerically, and due to current computer limitations, only small numbers of particles may be studied (nowadays in the millions). However, in order to model a macroscopic system (i.e., satisfying the large system limit of thermodynamics), it is often necessary to reduce surface effects on the system by imposing periodic boundary conditions (PBC). These PBC allow the simulation of the system with a finite volume and a finite number of particles. Furthermore, PBC deal with the motion of the atoms or particles near the edge of the finite volume in such a way that the number of particles is conserved. For this, the PBC are such that if the atom leaves one edge of the box then it reappears on the other side of the box. See Figure 4.1 for a two-dimensional representation of this procedure. In addition to the motion of the particles, the particles on the edge of the box are affected by the neighboring atoms within the box as well as by the atoms on the other side of the box, up to the limit of their range of interaction. Therefore, introduction of the periodic boundary conditions onto a system is equivalent to considering an infinite array of identical copies of the simulation cell.

Equations of motion applied to an assembly of particles, conserve the total energy; that is, the trajectories obtained with PBC simulate the behavior of a system at constant energy, constant number of particles, and constant volume. This is considered a microcanonical ensemble, and our equilibrium simulations are evaluated within it.

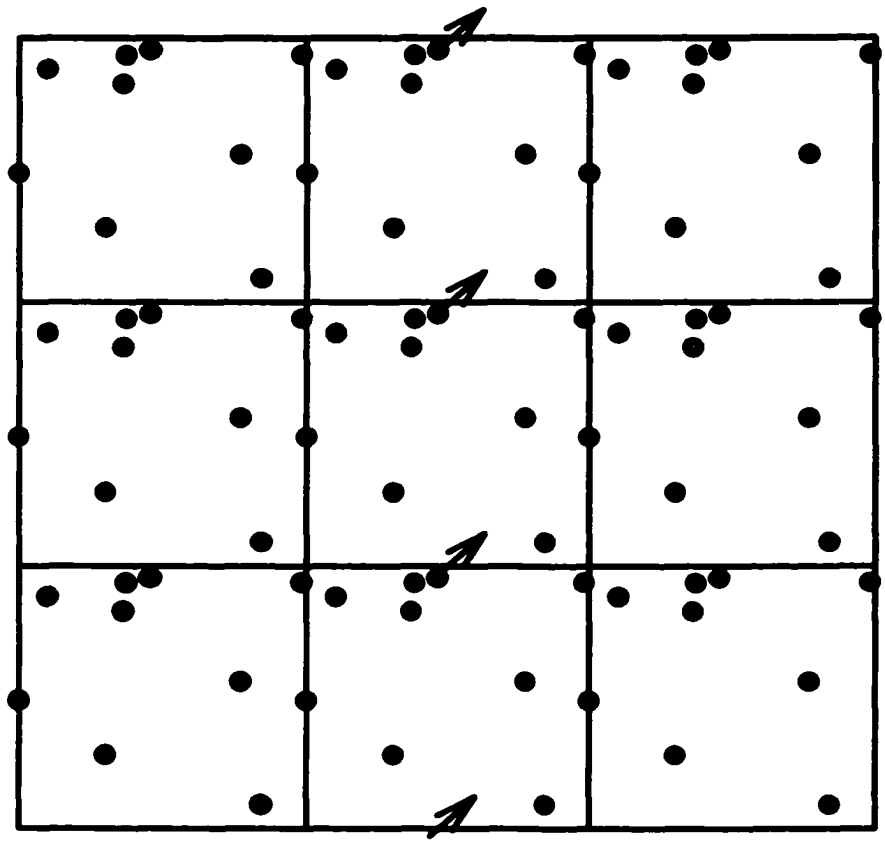

Figure 4.1. Equilibrium Molecular Dynamics periodic boundary conditions.

There are schemes available which allow the solution of the equations of motion. For our equilibrium simulations, we solve Newton's equation of motion with the Leapfrog integrator[85], which conserves very well energy in our system. We see no drift in the energy after 2 ns.

4.2.1. Calculation of Transport Properties from EMD Trajectories: Green-Kubo Formalism

The method of Green-Kubo [87, 88] is a way of obtaining transport properties based on the equilibrium time-evolution of the system. These transport properties can be derived directly from one of the continuum equations of fluid dynamics, such as Navier-Stokes equation for viscosity or Fick's diffusion equation for the diffusion coefficient. The derived result provides a direct relation between the macroscopic transport coefficient and the time integral of the microscopic auto-correlation function (ACF), measured in an equilibrium system.

4.2.1.1. Diffusion Coefficient

Here we follow the method outlined in McQuarrie [86] to obtain an expression for the diffusion coefficient in terms of a velocity ACF. The starting point for the derivation of the diffusion coefficient from statistical mechanics is the diffusion equation or Fick's law. In a continuous system, the diffusion coefficient D through Fick's first law relates mass flow to a density gradient:

$$\rho(\vec{r},t)\cdot v(\vec{r},t) = -D\nabla\rho(\vec{r},t) \qquad (4.8)$$

where $v(\vec{r},t)$ is the local velocity and $\rho(\vec{r},t)$ is the local density or concentration. The time-evolution of $\rho(\vec{r},t)$ comes from Fick's second law, which is described by the equation

$$\frac{\partial \rho}{\partial t} = D\nabla^2 \rho \tag{4.9}$$

The solution to this equation is applicable both to self-diffusion and diffusion of differing species. At the discrete particle level, $\rho(\vec{r},t)$ is given by

$$\rho(\vec{r},t) = \sum_{j=1}^{N} \delta\left[\vec{r} - \vec{r}_j(t)\right] \tag{4.10}$$

where δ is the usual delta function. Then at a large t, it is possible to obtain the Einstein expression [86],

$$D = \lim_{t\to\infty} \frac{1}{6Nt} \left\langle \sum_{j=1}^{N} \left[\vec{r}_j(t) - \vec{r}_j(0)\right]^2 \right\rangle \tag{4.11}$$

where the brackets, $\langle\ \rangle$, denote the time average of the quantity within. This result is essentially the mean square displacement of the particular species we are examining. Following the technique outlined in McQuarrie [86], it is possible to obtain the equation:

$$\vec{r}_j(t) - \vec{r}_j(0) = \int_0^t \vec{v}_j(t')dt' \tag{4.12}$$

and

$$\left[\vec{r}_j(t) - \vec{r}_j(0)\right]^2 = \int_0^t dt' \int_0^t \vec{v}_j(t') \cdot \vec{v}_j(t'')dt'' \tag{4.13}$$

where $\vec{v}_j(t)$ is the velocity of the j^{th} particle. By taking an average of both sides of equation (4.13), the following expression is obtained:

$$\left\langle [\vec{r}_j(t) - \vec{r}_j(0)]^2 \right\rangle = \int_0^t dt' \int_0^t \left\langle \vec{v}_j(t') \cdot \vec{v}_j(t'') \right\rangle dt'' \tag{4.14}$$

Because of the time reversibility of the classical mechanical equations of motion and the stationarity of the equilibrium ensemble average, it can be shown that

$$\left\langle \vec{v}_j(t') \cdot \vec{v}_j(t'') \right\rangle = \left\langle \vec{v}_j(t'' - t') \cdot \vec{v}_j(0) \right\rangle = \left\langle \vec{v}_j(t' - t'') \cdot \vec{v}_j(0) \right\rangle. \tag{4.15}$$

By performing one of the integrations in equation (4.14) and substituting τ for $t'' - t$, the following expression is obtained,

$$\left\langle [\vec{r}_j(t) - \vec{r}_j(0)]^2 \right\rangle = 2t \int_0^t \left(1 - \frac{\tau}{t} \right) \left\langle \vec{v}_j(0) \cdot \vec{v}_j(\tau) \right\rangle d\tau. \tag{4.16}$$

If t is sufficiently greater than τ then equation (4.16) becomes

$$\left\langle [\vec{r}_j(t) - \vec{r}_j(0)]^2 \right\rangle = 2t \int_0^t \left\langle \vec{v}_j(0) \cdot \vec{v}_j(\tau) \right\rangle d\tau \tag{4.17}$$

and recognizing from equation (4.11) that

$$6Dt = \left\langle [\vec{r}_j(t) - \vec{r}_j(0)]^2 \right\rangle \tag{4.18}$$

the diffusion coefficient for one particle is given by

$$D = \frac{1}{3} \int_0^\infty \left\langle \vec{v}_j(0) \cdot \vec{v}_j(\tau) \right\rangle d\tau. \tag{4.19}$$

Now assuming that we have more than one diffusing atom, it is possible to re-write equation (4.19) as

$$D = \frac{1}{3N} \int_0^\infty \left\langle \sum_{j=1}^{N} \vec{v}_j(0) \cdot \vec{v}_j(\tau) \right\rangle d\tau. \tag{4.20}$$

This expression is completely equivalent to the expression for Einstein's equation (4.11). The term within the integral is the velocity auto-correlation function. A sample average

velocity auto-correlation function (averaged over the number of particles and time) for a liquid aluminum simulation is shown in Figure 4.2 and liquid nickel in Figure 4.3. The velocity auto-correlation function is normalized to the τ=0 value. The method for averaging over time is described later. The integral of this function is directly related to the diffusion coefficient from equation (4.20).

When calculating the self-diffusivity with EMD, the velocity auto-correlation function is much more deterministic than the stress ACF, in that the integrated auto-correlation function is less susceptible to large variations in the data. Furthermore the auto-correlation function converges to zero quickly. These principles are illustrated in Figure 4.3, where a pair of normalized velocity auto-correlation functions is presented. From the figure one can see how the integrated velocity auto-correlation function would result in similar values for the diffusion coefficient. This procedure yields diffusion coefficients with ± 2 percent error.

4.2.1.2. Viscosity

Through a similar approach it is possible to calculate shear viscosity. We start with Navier-Stokes equation, from McQuarrie[86]:

$$\rho\left(\frac{\partial}{\partial t}+\vec{v}\cdot\nabla\right)\cdot\vec{v}=\eta\nabla^2\vec{v}+\left(\frac{\eta}{3}+\eta_v\right)\nabla(\nabla\cdot\vec{v})-\nabla P \qquad (4.21)$$

where ρ is the mass density, η is the shear viscosity, η_v is the bulk viscosity, $\vec{v}$ is the local velocity and P is the pressure. Through a series of mathematical steps similar to

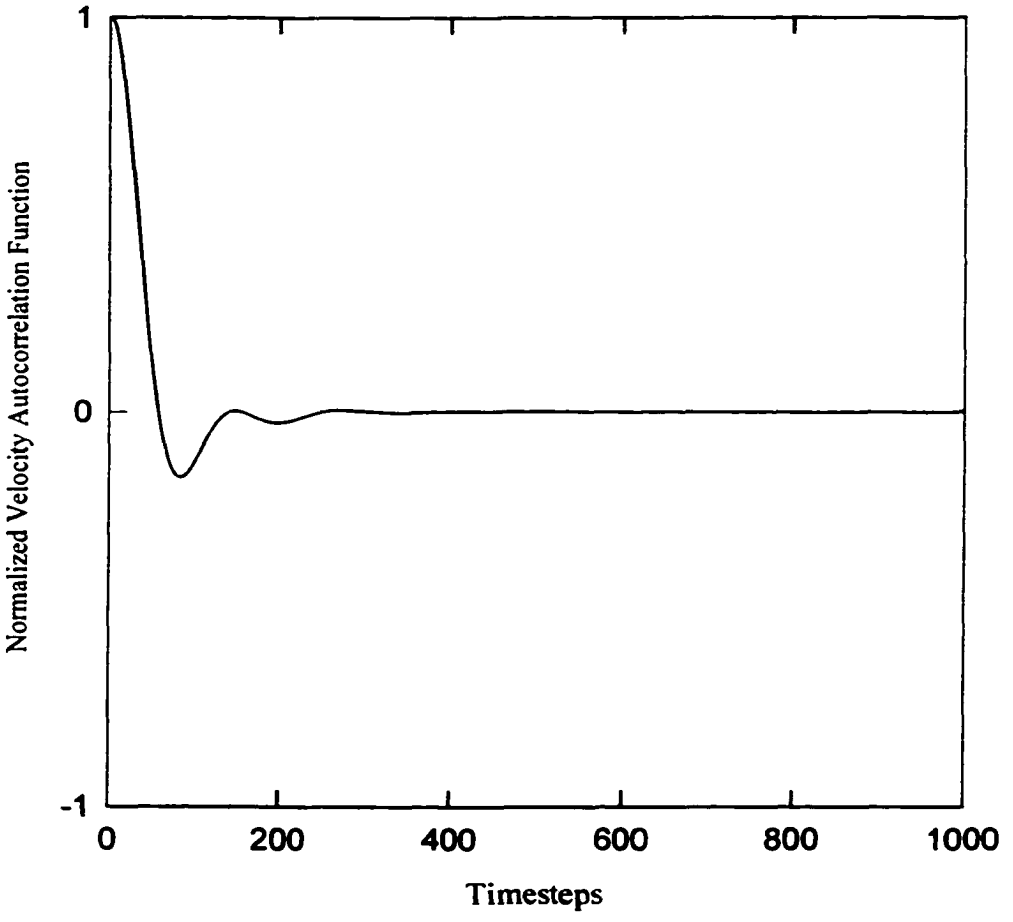

Figure 4.2. Normalized velocity auto-correlation function utilizing an EAM model of liquid aluminum at T=1775K, N=1372 atoms, Δt=10^{-15} s.

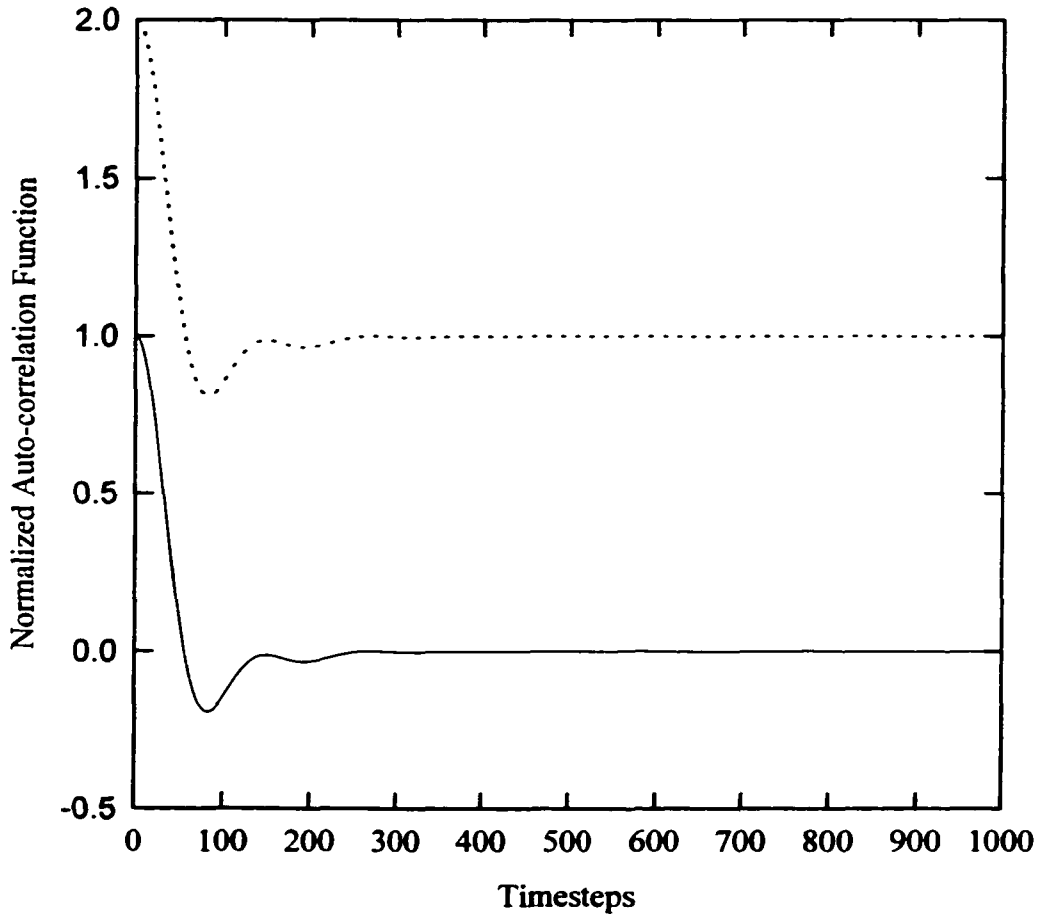

Figure 4.3. Two normalized (τ=0) velocity auto-correlation functions for nickel at T=1775 K, averaged over 500 steps, N=1372, Δt =10^{-15} s. Note the broken curve has been shifted up by one unit to be seen.

the derivation of equation 4.20 for the diffusion coefficient, an expression analogous to equation (4.11) for the shear viscosity, η, is obtained, namely:

$$\eta = \lim_{t\to\infty} \frac{1}{6k_bTVt} \left\langle \sum_{x<y} \left[\sum_j m_j r_{xj}(t) v_{yj}(t) - \sum_j m_j r_{xj}(0) v_{yj}(0) \right]^2 \right\rangle \tag{4.22}$$

where $\sum_{x<y}$ denotes a sum over the three off-diagonal terms to the pressure tensor and m is the mass of the atomic species. Although this equation looks analogous to equation 4.11, it is different. The principle difference is that this equation is a square of the sums rather than a sum of the squares. This suggests that atoms contribute to the sum whereas, with diffusion, each atom contributes individually. According to Allen *et al.* [89], this expression is unusable with the periodic boundary conditions aforementioned because periodic boundaries violate the translational invariance assumed in the derivation.

However, it is possible to construct from the expression a Green-Kubo relation based on the integrated auto-correlation function of the pressure tensor, which does not experience translational invariance. The derived expression is

$$\eta = \frac{1}{Vk_bT} \int_0^\infty \langle J(0)J(t) \rangle dt \tag{4.23}$$

where

$$J = \sum_{j=1}^{N} \left(\frac{p_{xj} p_{zj}}{m_j} + z_j F_{jx} \right) \tag{4.24}$$

and is related to one component of the off-diagonal term within the stress tensor, p_{xj} and p_{zj} are the momenta of particle j in the x and z directions respectively, z_j is the z-component of the j^{th} particles position vector, and F_{jx} is the x-component of the force that

the j^{th} particle experiences. Such average auto-correlation functions are illustrated for aluminum and nickel in Figure 4.4 and 4.5 (technique in averaging described later). It is necessary to have many of these average auto-correlation functions (procedure equivalent to a long simulation) to obtain reasonable values for the viscosity. Holian and Evans[90] also suggested that a large number of atoms are required for consistent values for the viscosity. We examined the effect of system size on the viscosity and found there was no significant difference between N=1372 or N=2048, the smaller systems with N<1372 showed a significant difference.

In Figure 4.5, we present a set of three stress-autocorrelation functions for nickel at 1775 K. The conditions of these stress auto-correlations functions are that they were averaged over 500 individual auto-correlation functions and normalized to the average τ=0 value. Notice the large long-term fluctuations in the normalized stress auto-correlation functions. These fluctuations produce the large standard deviations in the shear viscosity. Standard deviations of between 15 and 30 percent are typical. Longer simulations with a larger number of averaged stress auto-correlation functions are required for the smaller deviations. For instance, we ran a simulation with a 1000 individual auto-correlation functions and obtained smaller standard deviations of about ±15%, yet the same average viscosity was obtained.

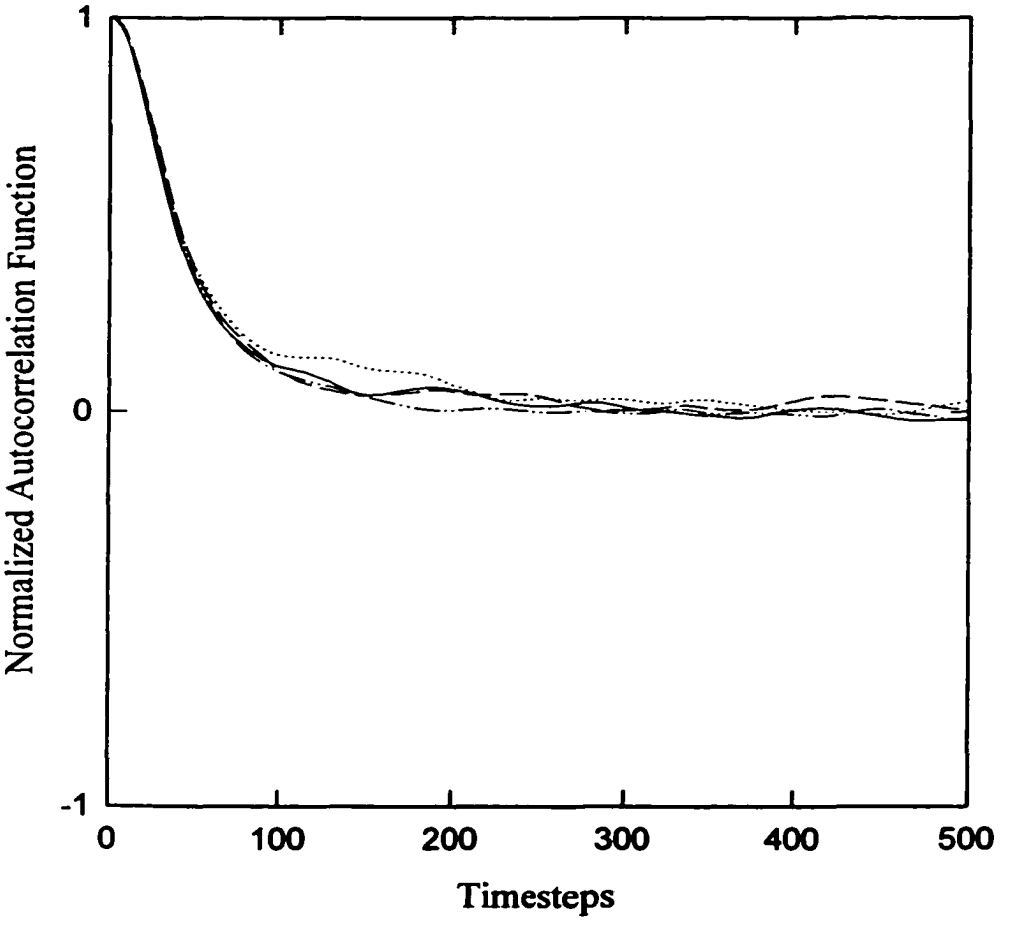

Figure 4.4. Four separate average shear stress auto-correlation functions normalized to τ=0 for the EAM model of aluminum at T=1175K, N=1372, and Δt=10^{-15} s.

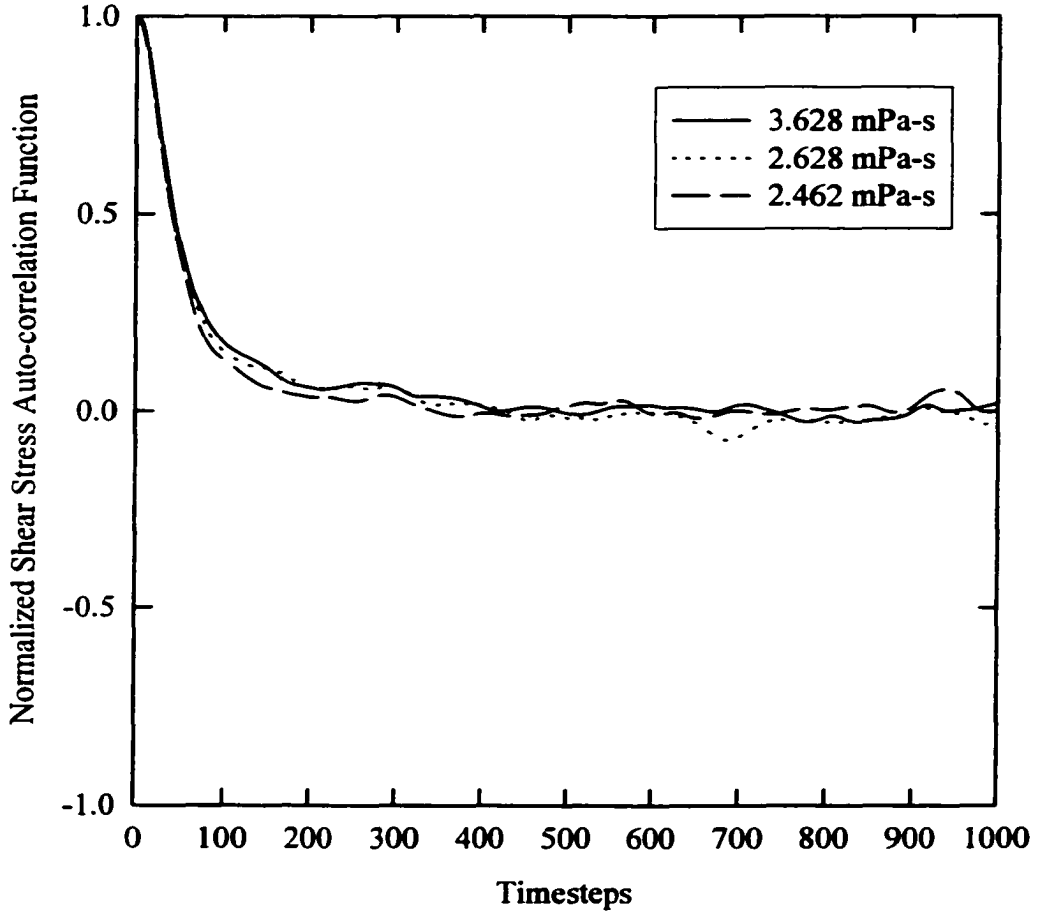

Figure 4.5. Three stress auto-correlation functions determined for nickel at T=1775 K and N=1372.

4.2.1.3. Rapaport Method of Averaging

A method for obtaining more reliable average values for both stress and velocity auto-correlation functions has been reported by Rapaport[85]. We call this method the overlapped time-interval correlation averages. Figure 4.6 illustrates the technique, which allows one to have stored in the memory of the computer a series of auto-correlation functions. These are spaced apart in time determined by the size of a number buffer. The number buffer illustrated in Figure 4.6 would be four. Spacing between the correlation functions should be such that there is no correlation between measurements. The individual correlation functions are averaged to obtain single average auto-correlation function. Although the memory requirements of this method are greater, the computational time is shortened by simultaneously calculating many correlation functions. The correlation functions here utilize this method of overlapping the data for the equilibrium calculations.

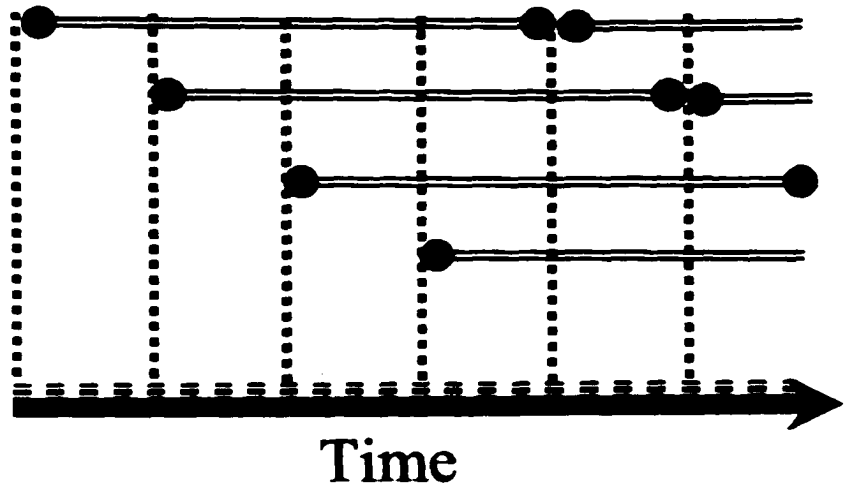

Figure 4.6. Illustration of overlapped data collection. The vertical lines represent the time origin of individual correlation functions. The horizontal lines represent the overall length of the correlation function. Multiple correlation functions are calculated at any given time.

4.3. Calculating Shear Viscosity with Non-Equilibrium Molecular Dynamics (NEMD)

Non-equilibrium molecular dynamics (NEMD) relies on an applied stimulus to the molecular dynamics cell and calculation of its response. The calculated property is the coefficient relating the stimulus to the response. For instance, using equation 2.1, we can apply a velocity gradient, $\frac{\partial v_x}{\partial z}$, and calculate a shear stress τ to obtain a value for viscosity η.

For this study we impose upon the system a linear velocity profile, which establishes a Couette flow, which has a constant strain rate, γ. In NEMD, the simulation cell is maintained at constant temperature. The constraint upon the temperature is required because when we stimulate the molecular dynamics system (a small collection of atoms) we input energy. Without a thermostat, a MD system cannot dissipate its energy. The thermostated equation of motion is given as[85, 91, 92]

$$\ddot{\vec{q}}_i = \frac{\vec{F}_i}{m_i} + \alpha\left(\dot{\vec{q}}_i - \gamma q_{zi}\hat{x}\right) \tag{4.25}$$

where $\hat{x}$ is the unit vector in the x-direction, q_{zi} is the z component of the position vector of particle i, γ is the constant strain rate, $\dot{\vec{q}}_i$ is the velocity of the atom, m_i is the mass of the atom, α is the temperature constraint, and $\vec{F}_i$ is the force on the atom. The temperature constraint arises in the Lagrange multiplier, α, which is given by

$$\alpha = -\frac{\sum_i \left(\dot{\vec{q}}_i \gamma q_{zi}\hat{x}\right)\cdot\left(\frac{\vec{F}_i}{m_i} - \gamma\dot{q}_{zi}\hat{x}\right)}{\sum_i \left(\dot{\vec{q}}_i - \gamma q_{zi}\hat{x}\right)} \tag{4.26}$$

Equation (4.25), assumes there is a linear velocity profile initially imposed on the system. When temperature is maintained constant within the framework of linear response theory, an expression for the shear viscosity develops, which is,

$$\eta = -\lim_{\gamma\to 0}\lim_{t\to\infty}\frac{\langle P_{xz}\rangle}{\gamma} \tag{4.27}$$

where $\langle P_{xz}\rangle$ is the xz-shear component of the stress tensor. Furthermore, it has been observed that η as a function of the strain rate obeys the following relationship[92]

$$\eta = \eta_0 - A\gamma^{1/2} \tag{4.28}$$

where η_0 is the shear viscosity (Newtonian viscosity) when the strain rate is zero, and A is a constant.

For the non-equilibrium simulations, a fundamental work enabling the calculation of shear viscosities, related to the development of a periodic boundary condition (PBC) scheme. Such a scheme was developed by Lees and Edwards [93]. Their scheme

imposed a constant strain rate upon a system of particles. The walls of the boundaries in the z-direction are displaced by the relative velocity of the neighboring cell, and an atom crossing the z-boundary is translated by a distance related to the velocity profile. Atoms crossing the x and y boundaries follow the same periodicity as in EMD. Figure 4.7 illustrates periodic boundary conditions for the NEMD simulations in this work. Say an atom leaves the center simulation cell through its top, as illustrated by the vertical arrow. It is then displaced by a certain distance associated with the strain rate imposed on the system as indicated by the horizontal arrow. The d_x found in the Figure 4.7 is defined by

$$d_x = \left(\gamma L_z t - \frac{L_x}{2}\right) - (\text{int})\left(\frac{\gamma L_z t - \frac{L_x}{2}}{L_x}\right) L_x - \frac{L_x}{2} \tag{4.29}$$

where L_z and L_x are the size of the simulation cell in the x and the z directions, t is the time elapsed, and γ is the shear rate. The velocity change in the x direction whenever a $\pm z$ boundary is crossed is $\mp\gamma L_z$.

To solve the equations of motion for the NEMD simulations, we use a second order predictor-corrector integration scheme. Although this scheme is more computationally intensive than the Leapfrog method, this integration scheme for NEMD simulations is more stable.

Figure 4.8 illustrates how we extrapolate the shear viscosity from NEMD. To do this we run a series of 16 to 24 different shear strain rates ranging from $1.28\text{x}10^{11}$ s^{-1} to $1.89\text{x}10^{13}$ s^{-1}. Each individual strain rate is run for 32 ps or 32,000 timesteps. The average shear component of the stress tensor, P_{xz}, at different values of strain rate, γ, is

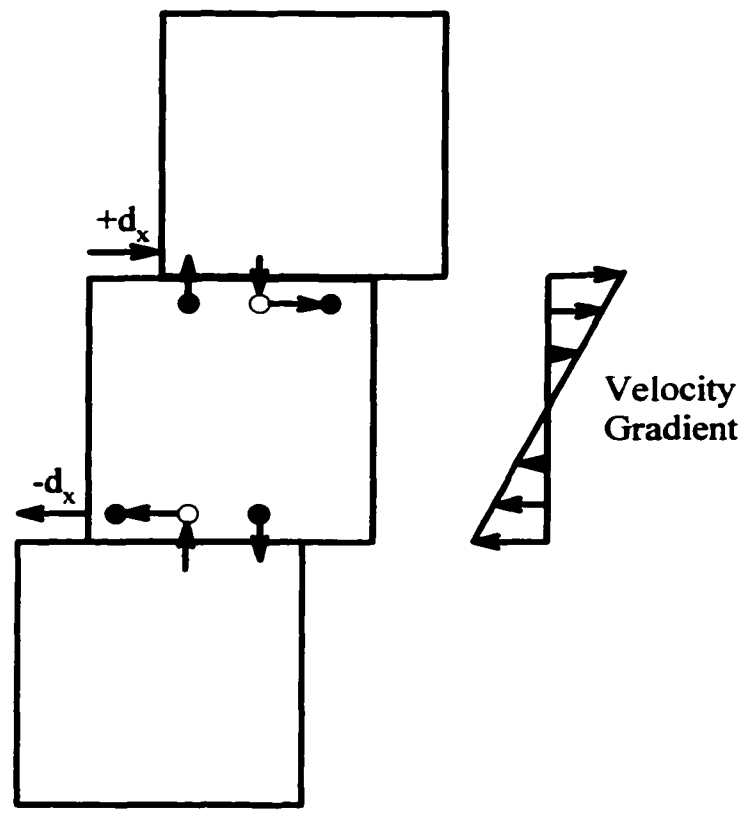

Figure 4.7. Periodic boundary conditions for non-equilibrium simulations.

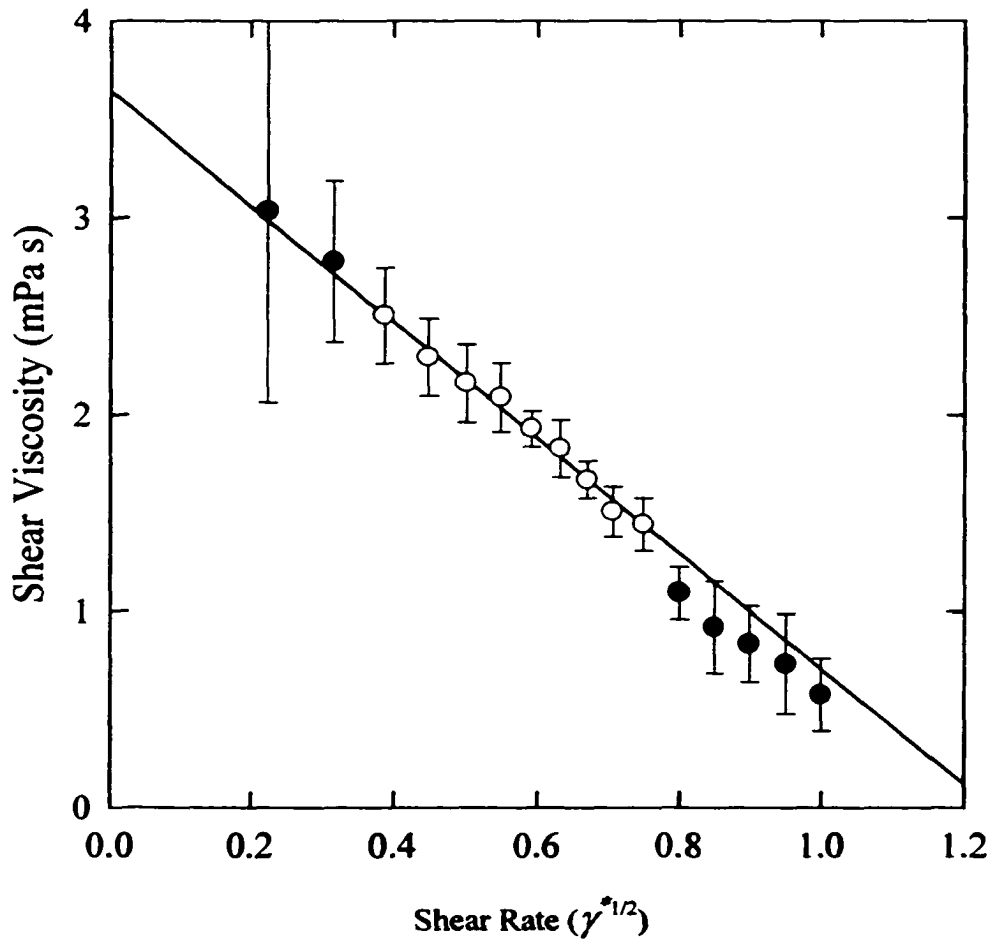

Figure 4.8. Non-equilibrium simulation set for nickel T=1875K with N=256.

calculated. Every 1000 timesteps (1 ps), the average shear viscosity is calculated and recorded for that time segment. These average shear viscosities are then averaged to obtain a cumulative average shear viscosity for the set shear strain rate and its standard deviation. The data from the series are then plotted, as the viscosity versus the square root of the shear rate in reduced units, $\dot{\gamma}^*$ (see Figure 4.8). The unit of time is given by $l\sqrt{\frac{m}{E}}$ where l is the unit of length (Angstroms), m is the unit of mass (the mass of the lightest element in the system), and E is the unit of energy (eV). Our unit of time for the binary and the aluminum systems is 5.29×10^{-14} s and for the nickel is 7.81×10^{-14} s. Utilizing the standard deviation data determined from the average shear viscosity values, those values with a standard deviation of greater than 10 % were discarded. These were typically from low shear strain rates, which had large fluctuations in the shear viscosity. At the high shear strain rates, a kink or discontinuity in the data would typically occur. The discontinuity is evident at $\dot{\gamma}^{*1/2}$ equal to 0.8 and 0.7 for Figures 4.8 and 4.9, respectively. Although the reason for the discontinuity is not known, we believe that it may be related to the constant temperature constraint, the effect of the periodic boundary conditions, and the size of the timestep. In absence of further indications, the data beyond the high shear strain rates are discarded for the purpose of extrapolating the viscosity to the Newtonian regime. By utilizing this technique of data selection, the linear function has a sample index of correlation (R^2) greater than 0.98.

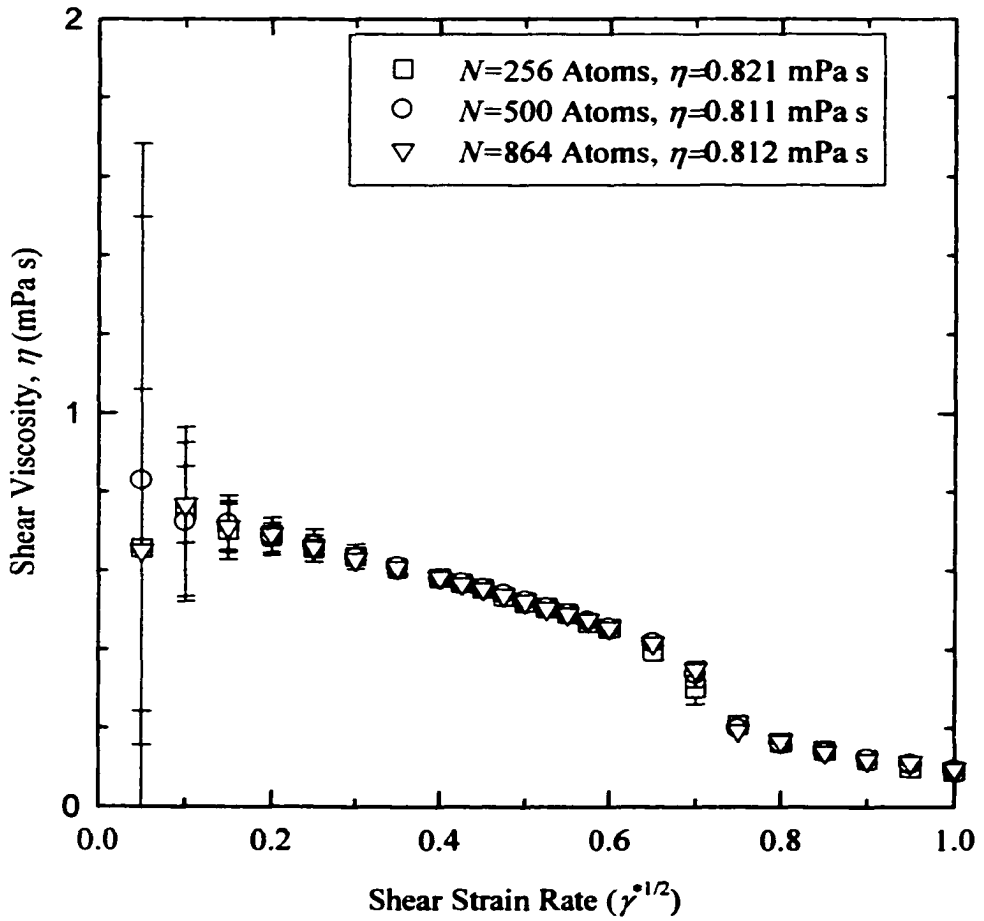

Figure 4.9. Non-equilibrium simulation set for aluminum T=1175K with N=256, 500, and 864.

In order to determine the effect of system size on the calculated NEMD-shear viscosities, a series of three NEMD data sets were run for aluminum at T=1175K utilizing the density corresponding to zero pressure. The simulations studied 256, 500 and 864 atoms (see Figure 4.9). The extrapolated zero shear strain rate viscosity are 0.821, 0.811, and 0.812 mPa s for 256, 500, and 864 atoms respectively. There is only a difference of 1.2 % in the shear viscosity obtained with 256 and 864 atoms; therefore, 256 atoms is suitable for the pure metals. In Figure 4.9, we notice a slight system size effect around the $\gamma^{*1/2} = 0.7$ or $\gamma^{1/2} = 3.04 \times 10^6\ s^{-1/2}$. For computational reasons we employ N=256 although a small percentage error is expected in the viscosity.

4.4. Prior Works Involving NEMD and EMD

Holian and Evans[90] used a Lennard-Jones potential and showed that both equilibrium and non-equilibrium molecular dynamics yield comparable results. They also compared the required size of the simulations to get representative results and found that non-equilibrium simulations required fewer atoms than equilibrium simulations. This work employs both techniques in its analysis of the shear viscosity in liquid nickel, liquid aluminum, and their intermetallic compounds.

EMD techniques have been applied to a variety of systems; however, most of the systems were simple. Transport properties have been predominately calculated using simple pair-type potentials, and most of the studies have focused on the Lennard-Jones fluids [90] or simple metals such as sodium and potassium [94]. Solutions of Lennard-Jones fluids have also been studied by Heyes [95] and Pas [96]. It has been only recently that Stadler *et al.* [97] examined transport coefficients using Green-Kubo relations to

calculate them from an *ab initio* technique. Each of these studies obtained reasonably accurate results.

Viscosities utilizing NEMD have been calculated for glass forming systems [98], simple fluid mixtures [99, 100], simple soft-sphere liquids [92, 101], and liquid sodium using an effective pair potential [102]. These studies also suggest that NEMD techniques are a valid means of obtaining viscosity data for liquids.

Using the EAM potential, very little work has been done for liquid transition metals. To date the transport properties that have been evaluated using a potential based on the Embedded Atom Method are the self diffusion coefficients for the metals of Cu, Ag, Au, Ni, Pd, and Pt by Mei and Davenport [103, 104] using EMD methods with Johnson's analytical embedded atom model[66]. While this work was in progress, a study of liquid nickel was performed by Alemany *et al.* [69]. A study of Nickel impurity diffusion coefficient in liquid Al was also performed [105]. Asta *et al.*[71] examined also the binary alloys of Ni-Al using EMD techniques for three prominent embedded atom potentials. The potentials they use differ from this work, which focuses on the analytical potential of Cai and Ye[5].

In conclusion, in this dissertation both EMD and NEMD techniques are employed to analyze the viscosity of liquid nickel, liquid aluminum, and their liquid solutions. The diffusivity of the pure substances and the alloys are calculated using the EMD method of auto-correlation functions. In order to obtain more accurate values for the diffusivity and viscosity within the framework of EMD, an averaged set of time correlated functions, as described by Rapaport[85], are used.

CHAPTER 5

STRUCTURAL AND TRANSPORT PROPERTIES OF PURE NICKEL AND ALUMINUM

This chapter presents data and its analysis for pure liquid nickel and aluminum, using the EAM potential described in Chapter 3, and the techniques presented in Chapter 4.

5.1. Atomic Number Densities

All of the simulations that follow (NEMD and EMD) are conducted under constant volume conditions; as a result, it is necessary to determine appropriate number densities that provide for an average pressure of zero. These densities were obtained by evaluating a series of four or five constant temperature simulations with different volumes. An average pressure for a given number density was obtained. The average pressures were then plotted as a function of the number densities. Both positive (compressive) and negative (tensile) pressures were necessary to obtain accurate values for the zero pressure density. The zero pressure density was obtained by fitting the average pressure to a quadratic function. The zero of the quadratic expression gives the zero pressure density. Figure 5.1 illustrates this technique for nickel at a temperature of 1975K with 1372 atoms. Data for all the temperatures displayed a similar behavior. This technique was employed for both the pure metals, as well as, nickel-aluminum alloys (See chapter 6).

The errors associated with using the variational density approach are obtained by taking the maximum standard deviation in the pressure, combined with the R^2 value at

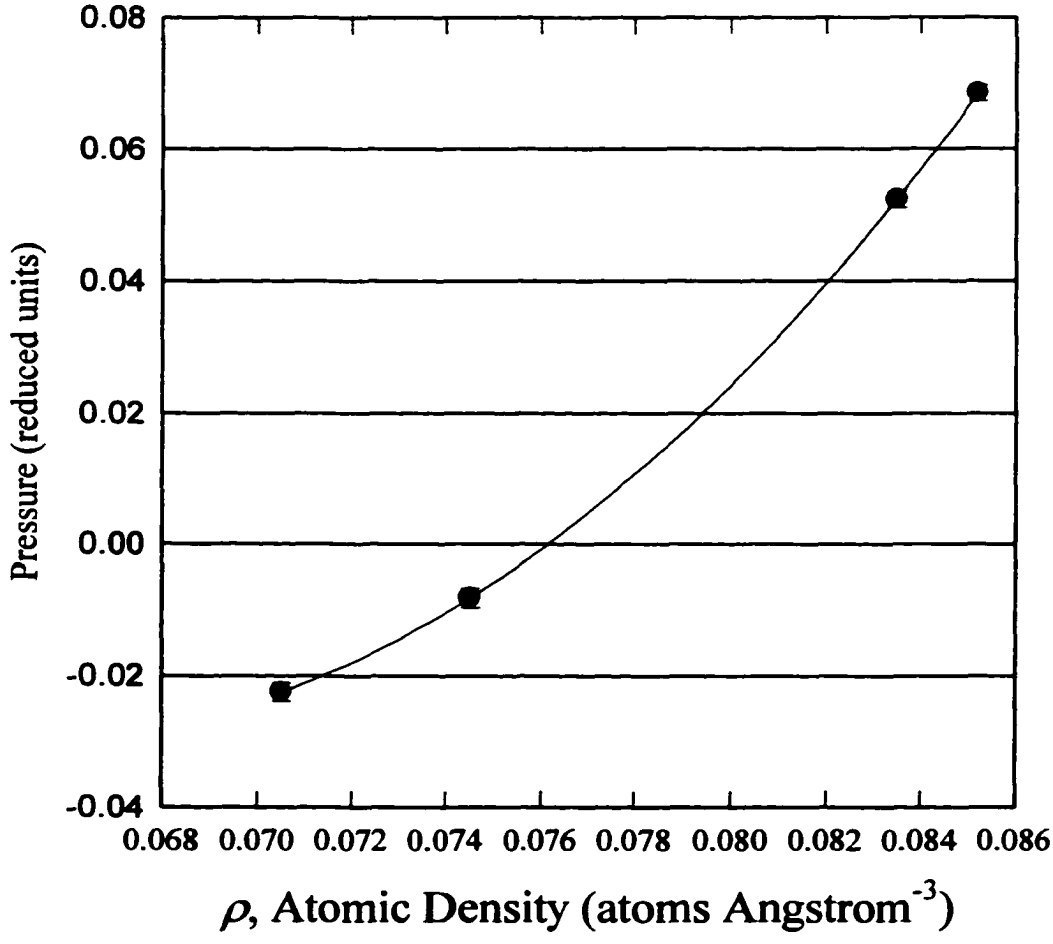

Figure 5.1. Evaluating the number density of nickel at T=1975K, P=244.6ρ^2-31.9ρ+1.0107.

any given density and determining the percent deviation of zero pressure density. This application gives a range of values for the number densities. We estimate the deviation in the number densities for both pure substances and binary alloys to be less than ±2%.

In Table 5.1, we report the resulting number densities and the predicted errors for liquid nickel as a function of temperature, whereas, in Table 5.2, the number densities for liquid aluminum as a function of temperature are reported. Experimental results from Ayushina *et al.*[106] and Smithells[107] are included in Tables 5.1 and 5.2. Also included in Table 5.1 are the experimental results of Waseda [108]. The experimental results of Ayushina and Smithells were found to follow an expression such as

$$\rho = \rho_0 - a\Delta T \tag{5.1}$$

where ρ_0 is the reference density at T_m, ΔT is T-T_m, and a, which is related to the thermal expansion coefficient. Waseda's [108] experimental results were determined from x-ray diffraction. Figure 5.2 shows how zero pressure densities compare to experimental densities of liquid nickel, as a function of temperature. Figure 5.3, similarly, shows the densities of liquid aluminum.

Both Figures 5.2 and 5.3, indicate that the EAM potential of Cai and Ye typically underestimate the experimental atomic densities. The smallest difference is with Waseda's data. It is worth noting that for nickel the EAM densities are at most 1.8% less than Waseda's, which is a reasonable agreement. The EAM density results are 4% lower than the experimental results of Ayushina for liquid nickel, and 5% lower than the liquid aluminum results of Ayushina. For nickel, the EAM potential appears to underestimate

the thermal expansion coefficient *a*. The EAM potential for liquid aluminum, however, overestimates the thermal expansion coefficient.

Table 5.1. Atomic Number Densities for Nickel as a Function of Temperature.

Temp(K)	EAM Densities atoms/Å^3 *(a=7.984x10^{-6} atoms Å^{-3}K^{-1})*	Smithell's [107] atoms/Å^3 *(a= 6.256x10^{-6} atoms Å^{-3}K^{-1})*	Ayushina [106] atoms/Å^3 *(a = 7.15x10^{-6} atoms Å^{-3}K^{-1})*	Waseda [108] atoms/Å^3 (Temp K) *(a= 1.266x10^{-5} atoms Å^{-3}K^{-1})*
1725	0.078163 ±0.8%	0.081136	0.081421	
1775	0.077793 ±0.6%	0.080541	0.080779	0.0792 (1773)
1825	0.077448 ±0.7%	0.079946	0.080138	
1875	0.077002 ±0.3%	0.079351	0.076497	0.0779 (1873)
1925	0.076563 ±0.1%	0.078756	0.078855	0.0773 (1923)
1975	0.076167 ±0.3%	0.078161	0.078214	

Table 5.2. Atomic Number Densities for Aluminum as a Function of Temperature.

Temp (K)	*EAM Densities* atoms/Å^3 *(a = 9.281x10^{-6} atoms Å^{-3}K^{-1})*	*Smithell's[107]* atoms/Å^3 *(a = 6.252x10^{-6} atoms Å^{-3}K^{-1})*	*Ayushina[106]* atoms/Å^3 *(a = 7.144x10^{-6} atoms Å^{-3}K^{-1})*
933	0.051233 ±0.3%	0.053231	0.053317
975	0.050858 ±0.5%	0.052968	0.053017
1025	0.050368 ±0.3%	0.052656	0.053660
1075	0.049925 ±0.4%	0.052343	0.052303
1125	0.049413 ±0.5%	0.052031	0.051945
1175	0.048987 ±0.5%	0.051718	0.051588

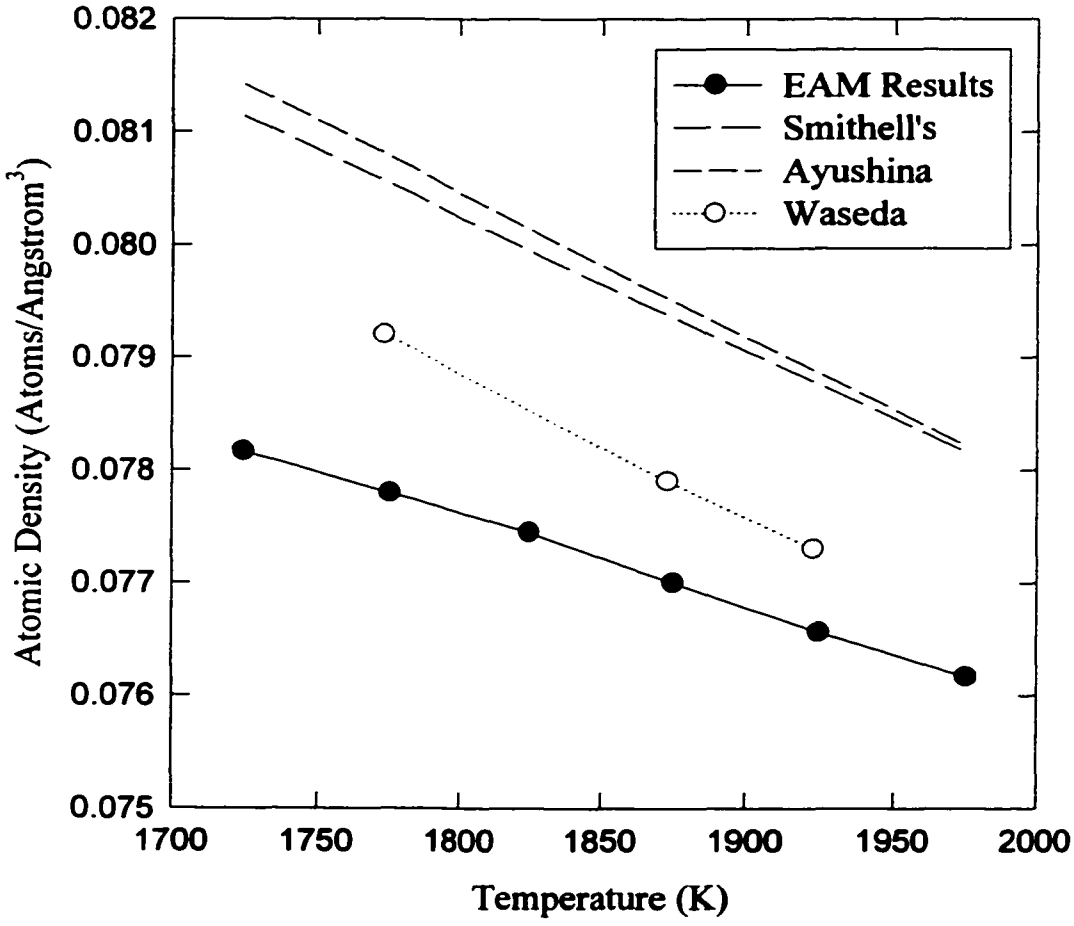

Figure 5.2. Atomic densities of nickel as a function of temperature. References: Ayushina[106]; Smithells[107]; Waseda[108].

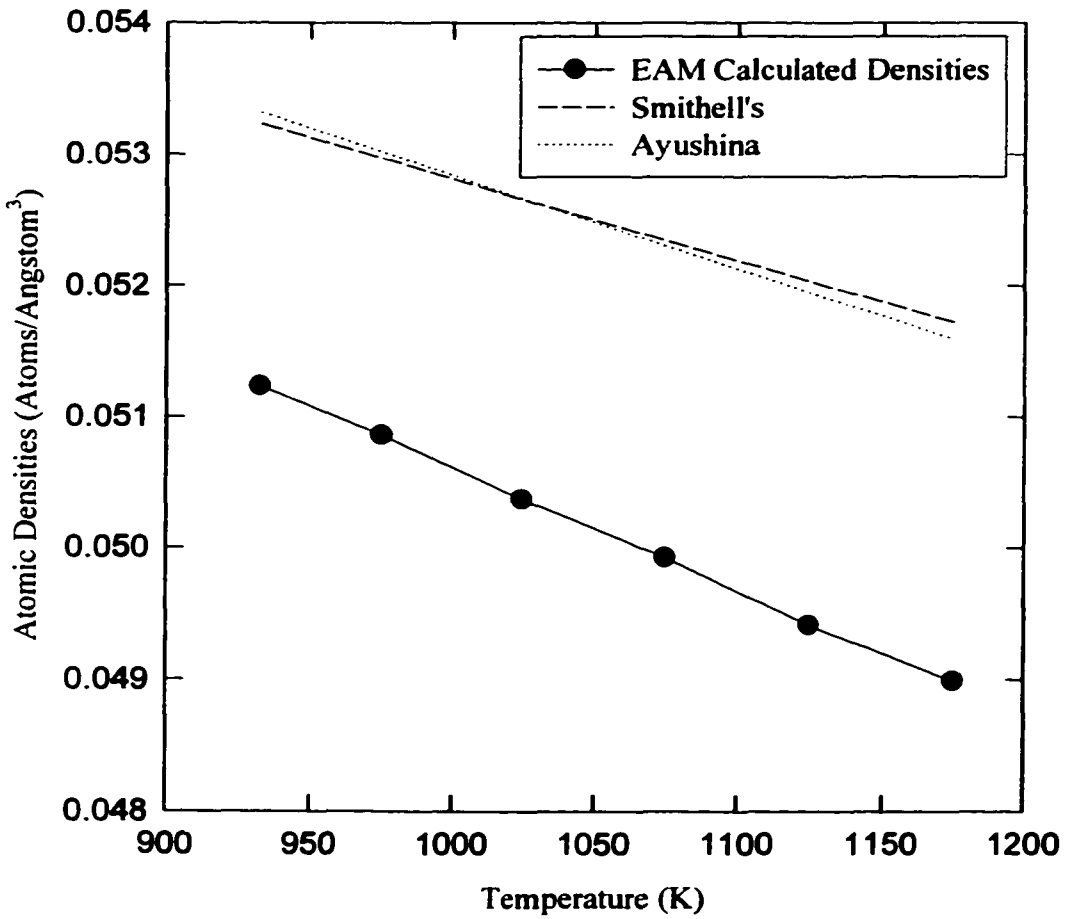

Figure 5.3. Atomic densities of aluminum as a function of temperature. References: Ayushina [106] and Smithells[107].

5.2. Structural Considerations

Most literature reports structural data in terms of a structure factor. Here we opt to examine the structural nature of liquid metals in terms of radial distribution functions (RDF). These two approaches yield similar conclusions, in that the Fourier transformed radial distribution function yields the structure factor *S(Q)* and vice versa. The Fourier transform to obtain the radial distribution function *g(r)* takes the form

$$g(r) = 1 + (2\pi^2 \rho_0 r)^{-1} \int_0^\infty [S(Q) - 1] Q \sin Qr \, dQ \qquad (5.2)$$

where ρ_0 is the average number density of atoms, *g(r)* is the pair correlations function, *S(Q)* is the structure factor, $Q = \frac{4\pi \sin\theta}{\lambda}$, 2θ is the angle between the incident and diffracted beam, and λ is the wavelength. The radial distribution functions calculated from these simulations are obtained through time-averaging the count of atoms at a given distance *r* from any given atom.

The first peak in the radial distribution function corresponds to the first nearest-neighbor distance, which can also be measured experimentally. The first neighbor distances of liquid nickel and aluminum are reported in Tables 5.3 and 5.4; the experimental values were determined by either neutron or x-ray diffraction[108, 109]. The first nearest-neighbor distances for aluminum are in better agreement than those for nickel.

Numerically, the integral in equation 5.2 was evaluated from the available experimental values for *S(Q)* of aluminum[109] and nickel[108]. In Figures 5.4 through 5.6, we report a comparison between radial distribution functions determined from

Table 5.3. First Nearest Neighbor Distances for Nickel (Å).

Temperature	Nearest Neighbor Distance Å	
	EAM MD Results	Experimental Ref 107
1775 K	2.47	2.53
1875 K	2.40	2.53
1925 K	2.39	2.52

Table 5.4. First Nearest Neighbor Distances for Aluminum(Å).

Temperature	Nearest Neighbor Distance Å	
	EAM MD Results	Experimental Ref 108
933 K	2.78	2.8
975 K	2.78	2.8
1075 K	2.79	2.8

experimentally measured *S(Q)* and the molecular dynamics results, for nickel and aluminum at several temperatures. The unfilled symbols and dashed lines, in Figures 5.4 through 5.6, represent the results of the inverse Fourier transformation calculations. The experimental radial distribution functions of aluminum were determined using a neutron diffraction technique[109]. Figures 5.4 and 5.5 compare the EAM radial distribution function to the experimental data for aluminum, at temperatures of 933 K and 1075 K. In addition to a sharp first nearest neighbor peak at 2.8 Å, the experimental RDFs for aluminum exhibits two secondary peaks at 3.35 Å and approximately 3.9 Å. This indicates that the liquid aluminum contains substructure that may be reminiscent of crystalline phases. For instance, the secondary peak at 3.9 Å may correspond to a second nearest neighbor distance in the fcc structure, while the distance of 3.35 Å could possibly be associated with a second nearest-neighbor distance in a bcc structure. The EAM

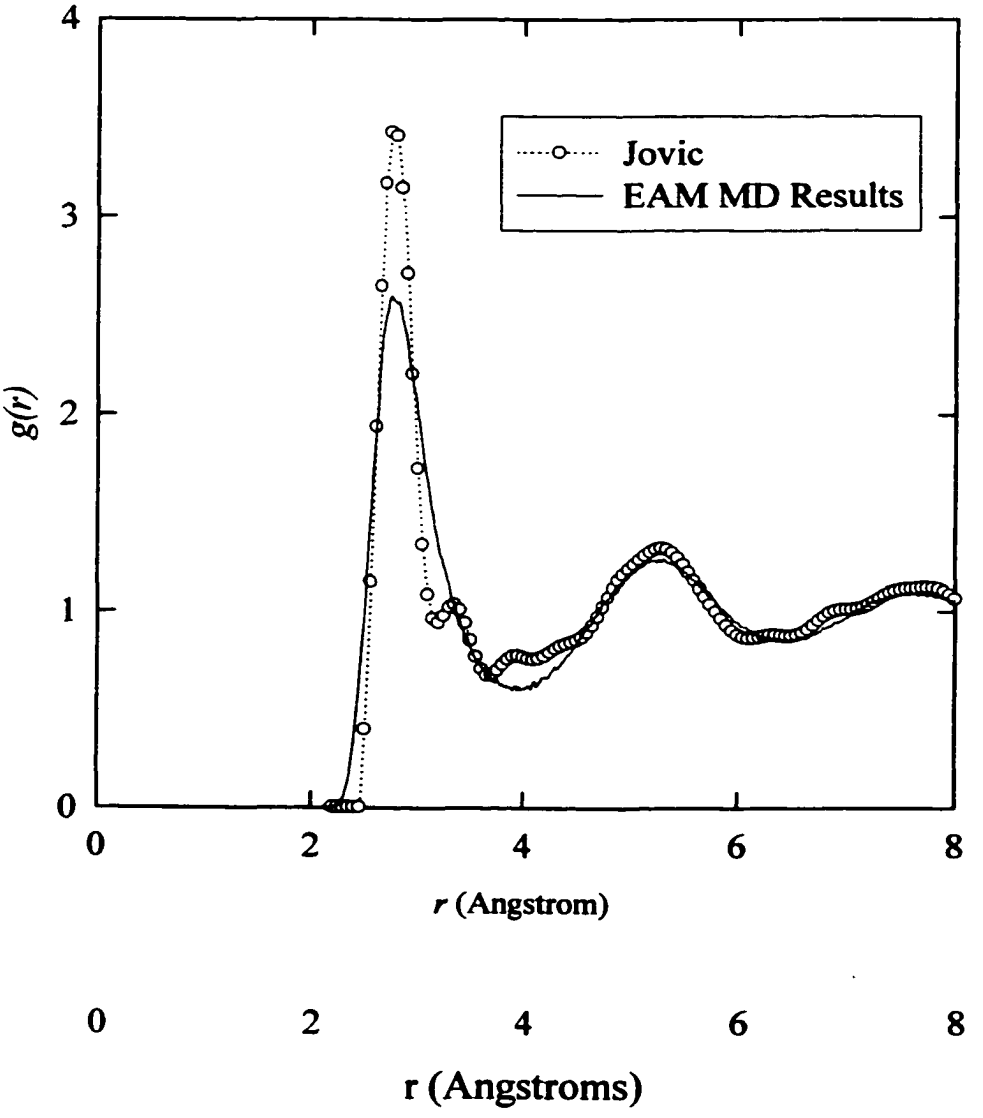

Figure 5.4. Aluminum radial distribution function at 933 K. The solid line is the EAM MD data. The symbols and dashed lines are obtained by Fourier transformation of the experimentally determined structure factor *S(Q)* [109].

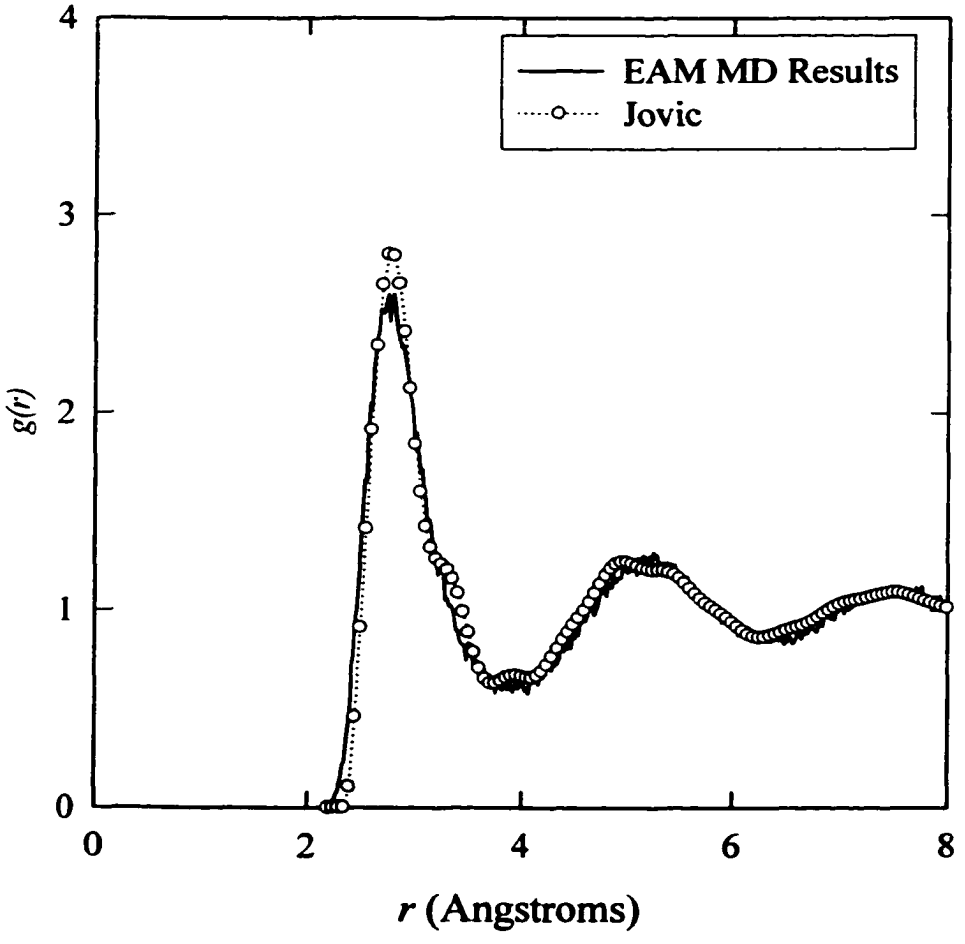

Figure 5.5. Aluminum radial distribution function at 1075K. The solid line is the EAM MD data. The symbols and dashed lines are obtained by Fourier transformation of the experimentally determined structure factor *S(Q)* [109].

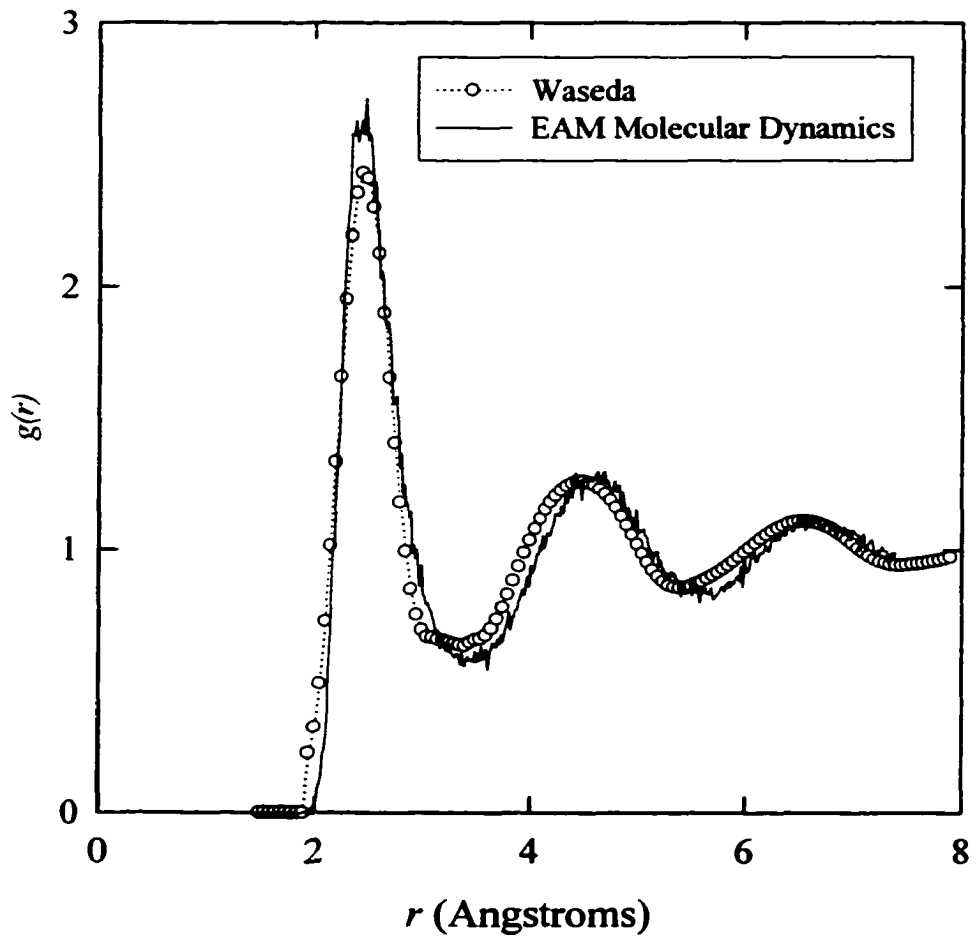

Figure 5.6. Nickel radial distribution function at 1775 K. The solid line is the EAM MD data. The symbols and dashed lines are obtained by Fourier transformation of the experimentally determined structure factor *S(Q)* [108].

potential does resolve such substructures At lower temperatures, T= 933 K, the EAM result underestimates the height of the first nearest neighbor peak and, therefore, the coordination number. The differences between the experimental and the calculated RDF are less pronounced at the higher temperatures.

In Figure 5.6, the radial distribution function of liquid nickel at 1775 K is presented. Unlike the data presented for aluminum, the experimental values for nickel were tabulated up to Q=4.4 $Å^{-1}$, or the main peak, by Waseda and Ohtani[108]. Therefore, data had to be interpreted from the figure they presented for $S(Q)$ which may have introduced errors. Considering this, the radial distribution function for the embedded atom method calculations compares reasonably well with the experimental data, with respect to locations of the peaks.

5.3. Shear Viscosity

To calculate shear viscosity using the NEMD technique(described in Chapter 4), we did a series of simulations, with shear strain rates ranging from $1.89x10^{11}$ s^{-1} to $1.89x10^{13}$ s^{-1} for aluminum, and $1.28x10^{11}$ s^{-1} to $1.28x10^{13}$ s^{-1} for nickel. The total number of atoms was 256. The timestep was 10^{-15} s.

For equilibrium simulations, a timestep of 10^{-15} s and 1372 atoms were used. The simulations started in a liquid state. Random velocities were given to each atom. Constant temperature was maintained for 20 ps. When the energy fluctuations oscillated about a constant value, the liquid reached a state of equilibrium. Thereafter, the energy was held constant. The temperature fluctuations were within ± 15 K. The total length of the simulations was between 2 ns and 4 ns. A total of 500 Green-Kubo relations was

averaged (described in Chapter 4) over a time correlation function corresponding to 5 ps in duration. This provided relatively smooth auto-correlation functions for the determination of both the shear viscosity and the self-diffusion coefficients through the appropriate integrated auto-correlation functions. The standard deviations were between 20 and 30 percent.

The viscosity of liquid nickel, as a function of temperature, obtained with both equilibrium and non-equilibrium techniques, is tabulated in Table 5.5. The temperatures in brackets for the EMD viscosity column result from the fact that in EMD one does not maintain temperature constant but energy, and temperature fluctuates about an average value (value in parenthesis). In the last column, a comparison is made to viscosity calculated with another EAM potential, namely the Voter-Chen[39] potential as reported by Alemany *et al.*[69]. They examined the viscosity of liquid nickel, using equilibrium molecular dynamics techniques. Table 5.6 contains the calculated data for liquid aluminum, where equilibrium and non-equilibrium results are presented.

Table 5.5. Viscosity for Liquid Nickel as a Function of Temperature.

Temperature (K)	NEMD-Viscosity mPa s	EMD-Viscosity mPa s (Temp K)	VC EAM-Viscosity [69] mPa s
1725 K	3.61±0.031	3.13±0.98 (1733 K)	
1775 K	3.56±0.018	3.36±0.95 (1750 K)	4.5±0.32
1825 K	3.38±0.018	3.39±0.72 (1790 K)	
1875 K	3.16±0.026	2.99±0.97 (1889 K)	3.52±0.32
1925 K	2.98±0.040	2.71±0.77 (1906 K)	
1975 K	3.20±0.005	2.66±0.68 (1956 K)	

Table 5.6. Viscosity for Liquid Aluminum as a Function of Temperature.

Temperature (K)	NEMD Viscosity mPa s	EMD Viscosity mPa s (Temp K)
933 K	1.14±0.013	0.972±0.26 (934 K)
975 K	1.05±0.012	0.884±0.29 (978 K)
1025 K	0.974±0.014	0.873±0.27 (1025 K)
1075 K	0.913±0.014	0.754±0.20 (1073 K)
1125 K	0.859±0.009	0.759±0.23 (1134 K)
1175 K	0.821±0.011	0.682±0.24 (1178 K)

In Figure 5.7 our viscosities are reported, as well as the experimental viscosity of liquid nickel determined by various investigators. The solid lines labeled with an "**a**" and a "**p**" in Figure 5.7 are from references [3] and [69]. The viscosity calculated from the equilibrium and non-equilibrium MD simulations is indicated with filled circles and open squares, respectively. The dashed line is a best fit through the NEMD data. Again the temperature uncertainty associated with equilibrium viscosity arises from temperature fluctuations in the constant-energy equilibrium simulations. The standard deviation of the equilibrium viscosity is as much as 30%. In Figure 5.8, we report the same for liquid aluminum. The unlabelled solid curves were reported in Iida and Guthrie [2] from the original sources of the early 1960s. On the other hand, the NEMD simulations give results with much greater certainty. In that case, the error bars amount to less than 2% and are not shown. Although the equilibrium MD data appear to be systematically lower than the NEMD viscosities, we do not believe, in view of the large error bars in the former, that this observation is significant. Therefore, the good agreement between the equilibrium and non-equilibrium viscosity indicates that the simulation data are representative of the EAM model, itself, and is therefore independent of the method used.

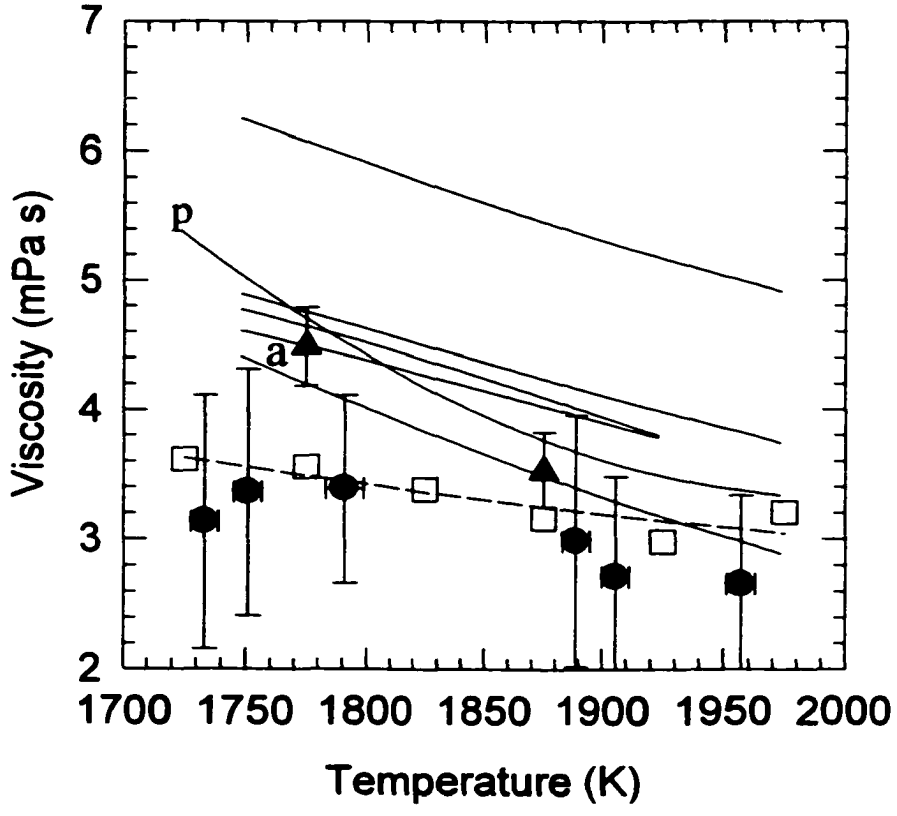

Figure 5.7. Temperature dependence of viscosity for liquid nickel. The solid circles are from EMD; the open squares are from NEMD; the dashed line is a best fit curve to the NEMD; the solid triangles are from reference [69] and the data line from Petrushevskii[3] is indicated by the letter **p**.

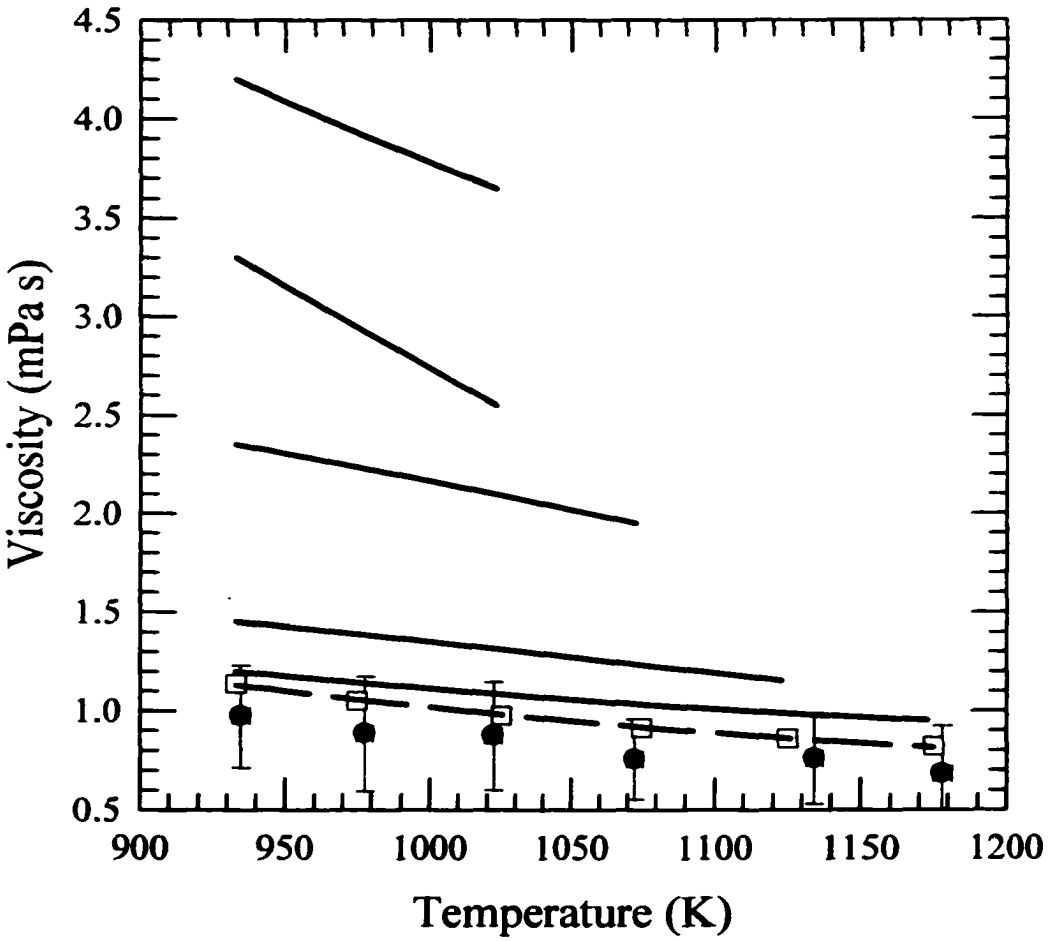

Figure 5.8. Temperature dependence for the viscosity of liquid aluminum. The solid circles are from EMD; the open squares are from NEMD; the dashed line is a best fit curve to the NEMD results; and the solid lines are from Iida and Guthrie[2].

Comparison between calculated and measured viscosity is made difficult by the large discrepancies in the experimental data. The viscosity of high temperature liquid metals is a thermophysical property difficult to measure experimentally. Few experimental methods exist for measuring the viscosity of liquid metals[2]. The oscillating-vessel method is most frequently used in measuring viscosity at elevated temperatures. The determination of viscosity from the damping of the vessel oscillations necessitates an inverse calculation based on an analytical model of the oscillating system. Many secondary effects such as surface tension, slippage at the liquid/vessel interface, etc., need to be accounted for in this model. However, due to the difficulty of solving analytically for the damped oscillations, approximate formulae are often used, resulting in discrepancies as large as 50% between the experimental results of different workers. For example the curve noted with a **p** [3] utilized the Shvidkovskii method in determining the viscosity from the measurements obtained by the oscillating vessel technique, which according to Iida and Guthrie[2] analysis, probably overestimates the viscosity near the melting point.

Although the present calculated viscosity differs from most of the experimental data, it is gratifying to note that it agrees relatively well with some, as seen in Figure 5.7 and 5.8. Furthermore, our data differ with experiments in their temperature dependence. The temperature dependence of viscosity in liquid metals approximates an Arrhenius relationship of the form:

$$\eta = A\exp(E/RT)\,. \qquad (5.3)$$

From the NEMD nickel viscosity, we estimate the apparent activation energy viscous flow, E, to be approximately 19.9 kJ mol^{-1}, with a prefactor of 0.8435 mPa s. From the NEMD aluminum viscosity data, we estimate the apparent activation energy viscous flow, E, to be approximately 12.4 kJ mol^{-1}, with a prefactor of 0.2293 mPa s. The calculated activation energy is lower than the activation energy one can determine from most experimental data by up to a factor 1.5.

Finally, a recent publication [69] reported MD calculations of the viscosity of liquid nickel using a Voter-Chen EAM potential [39, 40]. We present in Figure 5.7 the Green-Kubo equilibrium MD viscosities of their study (solid triangles). These two viscosities differ with our data, in particular at low temperature. Unfortunately, the simulations reported in that paper differ from ours, not only in the EAM potential used, but also in the density. It is, therefore, impossible to separate these effects.

5.3.1. Possible Reasons for Systematic Differences in Viscosities

In an attempt to try to understand the small systematic variations found in the shear viscosity calculated with the NEMD and EMD simulations, we identified the main differences between the NEMD and EMD simulations, namely: NEMD uses a Predictor-Corrector integrator while the EMD uses a Leapfrog integrator; NEMD uses fewer atoms than EMD; and NEMD is a constant temperature simulation while EMD is a constant energy simulation. For the first test, we altered the integration technique of the EMD to use a Predictor-Corrector method and the NEMD to use a Leapfrog method. This alteration yielded a similar systematic difference. As discussed earlier, the viscosity results for the NEMD showed no major system size effect. So it appears that the only

major difference between the results is the fact that in the NEMD the motion of the atoms is constrained to the constant temperature condition. Therefore, it may be necessary in the future to investigate the effect of the thermostat, perhaps by using a Nose'-Hoover thermostat[110] instead of the temperature constraint method.

5.3.2. Effects of Density on Shear Viscosity

We ran several NEMD simulations for liquid nickel, examining the effect of the number density upon the shear viscosity. In Figure 5.9, the effects of the number density upon the shear viscosity are shown. The curves with the solid symbols represent a set of NEMD simulations with the density held at constant value, Waseda's[108] density at 1775 K of 0.0792 atoms $Å^{-3}$, and the other simulations were calculated with zero pressure densities. The zero pressure densities all were lower than the constant value runs and ranged from 0.0766 to 0.0782 atoms $Å^{-3}$. The zero pressure density at the experimental temperature of 1775 K is found to be 1.8% less than the experimental density of 0.0792 atoms $Å^{-3}$. At this temperature, we see a decrease in the viscosity of liquid nickel by nearly 10 percent. From Figure 5.9, it is observed that as the density increases the viscosity also increases for the same temperature, in accord with simple analytical expressions for viscosity(Section 2.1.2).

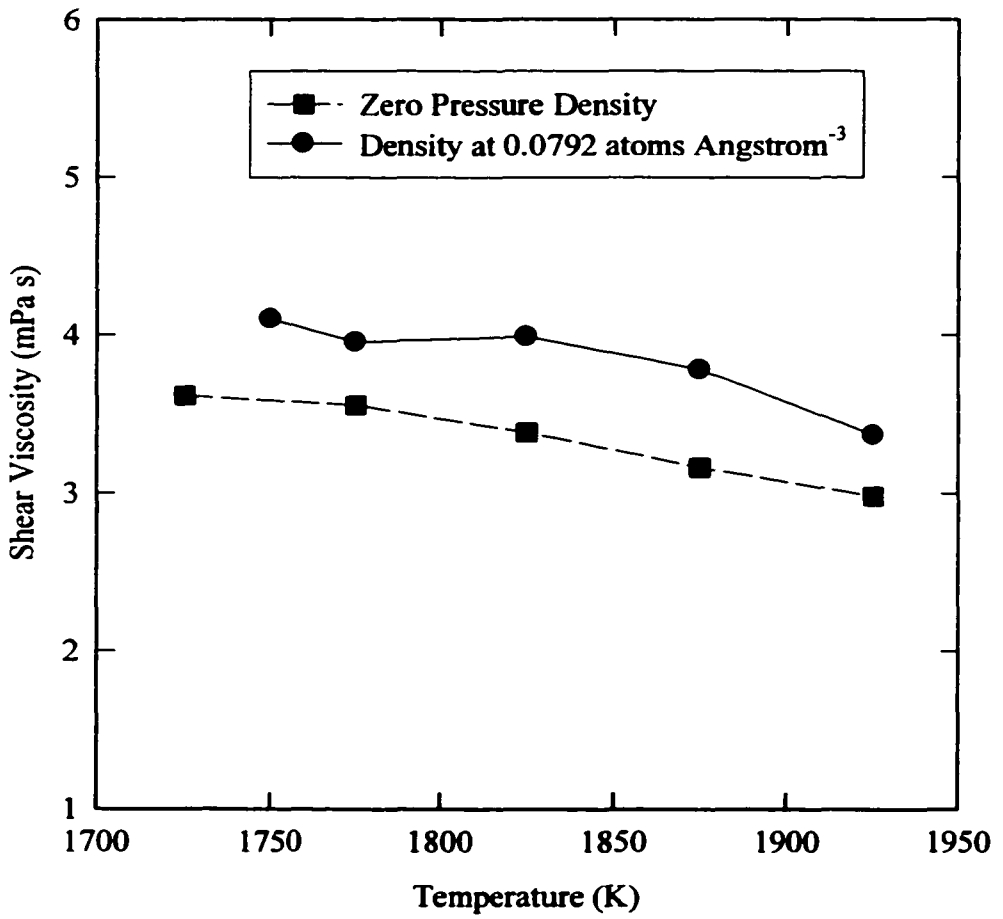

Figure 5.9. Effects of atomic density on the viscosity of liquid nickel. Solid circles represent the NEMD viscosity at a constant density while the solid squares represent the NEMD viscosity at zero pressure. Waseda[108] measured density at 1773 K to be 0.0792 atoms $Å^{-3}$.

5.4. Self-Diffusion

To calculate a diffusion coefficient from the EMD viscosity data, we employ the Stokes-Einstein and Sutherland-Einstein relations. The Stokes-Einstein relationship was given by equation 2.15 or

$$D = \frac{kT}{6\pi R\eta} \tag{5.4}$$

and the Sutherland-Einstein relationship was given by equation 2.16 or

$$D = \frac{kT}{4\pi R\eta} \tag{5.5}$$

where the radius R in the above expressions was determined from the experimental atomic volume, Ω; k is boltzmann's constant; and η is the viscosity. The EMD data for the viscosity was used to obtain the diffusion coefficient from both of these relationships.

Another relationship for the self-diffusion coefficient, found in Chapter 2, was the universal scaling law of Dzugutov [27]. Recall equation 2.22 which stated

$$D^{\dagger} = 0.049e^{S_2} \tag{5.6}$$

where $D^{\dagger}$ is the dimensionless diffusion coefficient and S_2 is the excess entropy of the system (from equation 2.23). $D^{\dagger}$ is related to the diffusivity by the following,

$$D = D^{\dagger}\Gamma_E\sigma^2 \tag{5.7}$$

where Γ_E is the collision frequency determined from Enskog's theory (from equation 2.25) and σ is the hard-sphere diameter or the first nearest neighbor distances.

In Tables 5.7 and 5.8, we report the diffusion coefficients of liquid nickel and aluminum respectively. The values included in the table are the EMD diffusion coefficients calculated using the Green-Kubo technique, and those calculated using equations 5.4 and 5.5 utilizing NEMD viscosity data. The temperature in brackets for the EMD diffusion data again results from the fact that with equilibrium simulations, energy is a constant and temperature fluctuates. Included in Table 5.7 are values for the self-diffusion coefficient calculated by Alemany *et al.* [111] using a tight binding potential and Mei *et al.*[104] using another EAM potential. For the aluminum system, Alemany[111] calculated the diffusion coefficient at 943 K. Figure 5.10 shows the self-diffusion coefficient for nickel, and Figure 5.11 illustrates the self-diffusion coefficient for liquid aluminum. The triangles represent the values for the diffusion coefficient as calculated by the Stokes-Einstein or the Sutherland-Einstein relationships. The data that is often used by the modelers is that predicted by Protopapas[112], which is indicated in the figures by the solid line. The open circles represent the calculations of the self-diffusivity predicted by the universal scaling law or equation 5.6.

Table 5.7. Self-diffusivity of liquid nickel as a function of temperature(10^5 cm^2 s^{-1}).

Temperature (K)	EMD Diffusivity 10^5 cm^2 s^{-1} (Temp)	Stokes-Einstein 10^5 cm^2 s^{-1}	Sutherland-Einstein 10^5 cm^2 s^{-1}	Other Data Reported 10^5 cm^2 s^{-1}
1725 K	4.499±0.057 (1733 K)	2.544	3.816	
1775 K	4.708±0.069 (1750 K)	2.660	3.991	3.85 [104] 2.52 [111]
1825 K	4.851±0.069 (1790 K)	2.875	4.313	
1875 K	5.726±0.072 (1889 K)	3.162	4.743	3.52±0.32 [111]
1925 K	6.026±0.083 (1906 K)	3.442	5.163	
1975 K	6.477±0.084 (1956 K)	3.285	4.927	

Table 5.8. Self-diffusivity of liquid aluminum as a function of temperature(10^5 cm^2 s^{-1}).

Temperature (K)	EMD Diffusivity 10^5 cm^2 s^{-1} (Temp)	Stokes-Einstein 10^5 cm^2 s^{-1}	Sutherland-Einstein 10^5 cm^2 s^{-1}
933 K	7.091±0.12 (934 K)	3.799	5.698
975 K	7.936 ±0.11 (978 K)	4.303	6.455
1025 K	9.244 ±0.097 (1025 K)	4.873	7.310
1075 K	10.10±0.12 (1073 K)	5.453	8.180
1125 K	11.47±0.13 (1134 K)	6.063	9.094
1175 K	12.56±0.14 (1178 K)	6.631	9.946

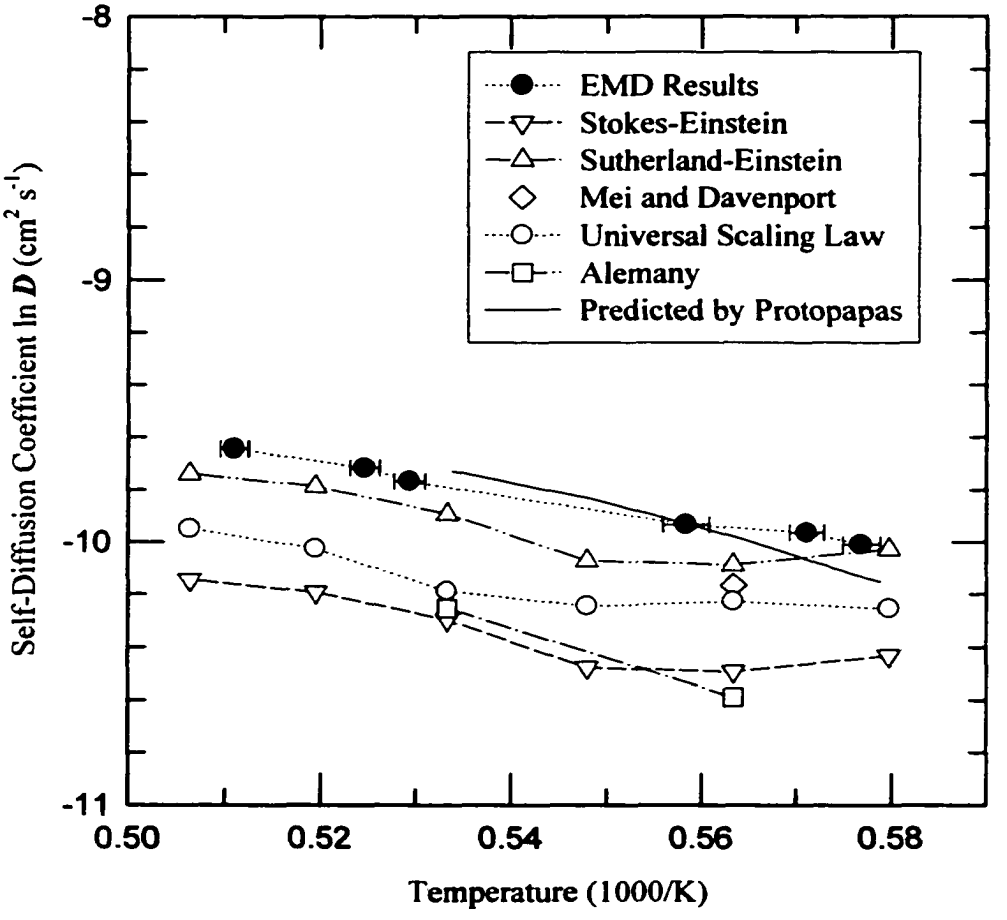

Figure 5.10. Self-diffusivity of liquid nickel. Solid symbols are EMD results; open triangles are computed with Stokes-Einstein and Sutherland-Einstein; square and diamond computed with different potentials utilizing Green-Kubo EMD technique[104][111]; solid line predicted by Protopapas *et al.*[112].

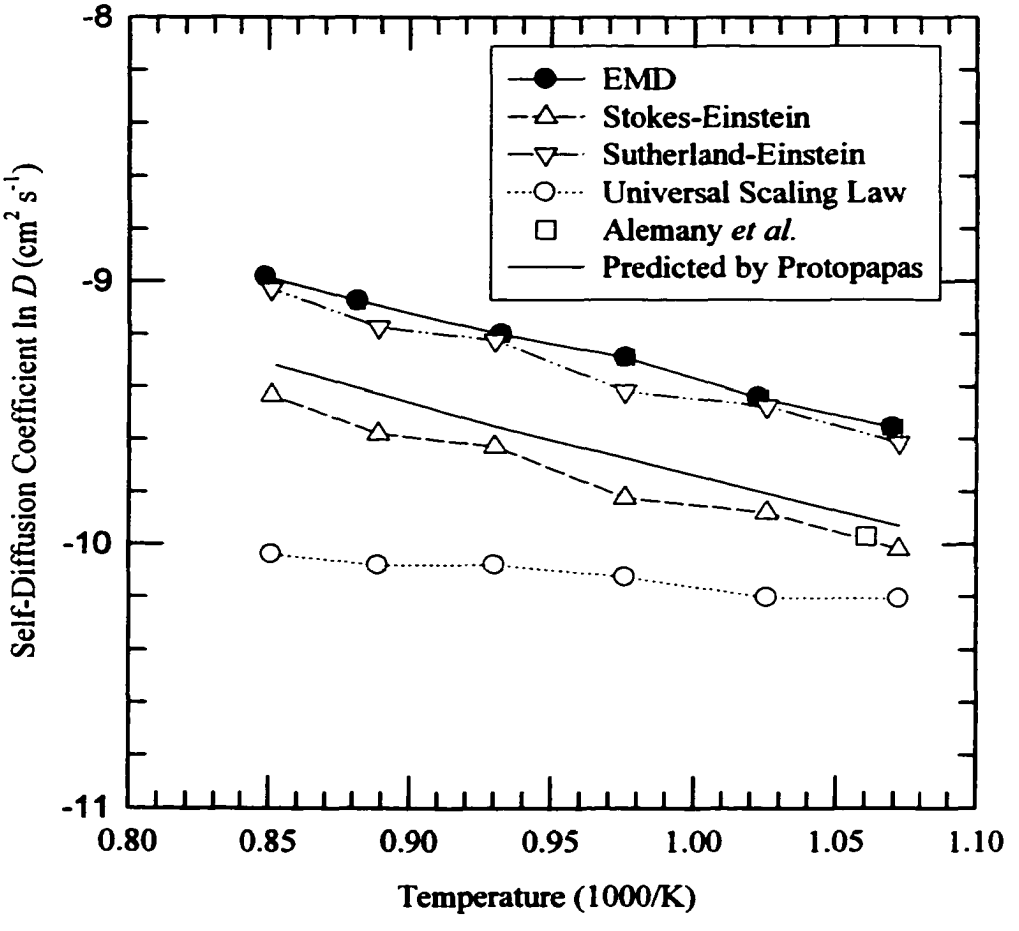

Figure 5.11. Self-diffusivity of liquid aluminum. Solid symbols are EMD results; open triangles are computed with Stokes-Einstein and Sutherland-Einstein; square and diamond computed with different potentials utilizing Green-Kubo EMD technique[111]; solid line predicted by Protopapas *et al.*[112].

The data reported in both Figures 5.10 and Figure 5.11 appear to exhibit Arrhenius behavior similar to equation 5.3. We found the activation energy for the self-diffusivity of liquid nickel was found to be –45.88 kJ/mole with the pre-exponential factor D_0 being 1.08×10^{-3} cm^2/s. Similarly the activation energy for the self-diffusivity of liquid aluminum was found to be –21.33 kJ/mole with the pre-exponential factor D_0 being 1.16×10^{-3} cm^2/s. The values for the activation energy of aluminum as reported by Cahoon[29] are –23.62 kJ/mole with a pre-exponential of 2.5×10^{-4} cm^2/s. This value appears to be calculated from a theory rather than from actual experimental measurements.

Examining Figures 5.10 and 5.11, it is observed that the Sutherland-Einstein relationship seems to fit the Green-Kubo data better than the Stokes-Einstein data. It is suggested by Poirier and Geiger[13], when the radius ratio between the diffusing species and the diffusion medium is approximately equal to one, the Sutherland-Einstein relationship is preferred. The agreement between the Sutherland-Einstein prediction and the EMD results validates this statement. The Sutherland-Einstein diffusivities are at most about 10 % lower than the calculated Green-Kubo diffusivities.

It was hoped that the universal scaling law[27] would provide a means to calculate diffusivities accurately with a representative radial distribution function. It appears that the temperature dependence is not representative of the system, in that the universal scaling law tends to underestimate the diffusivities. Upon closer examination of the paper by Dzutugov[27], it is apparent that the scaling law is valid for $-S_2 > 2.0\ k_b$. With our system, the S_2 is typically less than $2.0\ k_b$ where k_b is Boltzmann's constant.

This means that our system fell into the regime in which the universal scaling law does not apply. Another factor that may play a large role in the usage of this law is its sensitivity to magnitude of $g(\sigma)$ and the selection of σ. As a result of the reasonable estimates that the universal scaling law suggests, a refinement of the universal scaling law should be pursued.

5.5. Closing Remarks

In conclusion, it can be said that the Cai and Ye[5] EAM potential gives comparable results to experimental values for all factors considered. As for the structural characteristics of the liquid, we found both the nickel and the aluminum were in good agreement with the experimental data. With respect to the density, the Cai and Ye potential seems to underestimate the zero pressure density. The values for aluminum are in better agreement with measured viscosities than those of nickel. We found that the diffusion data calculated with the Green-Kubo method agrees very well with Sutherland-Einstein expression. This is in agreement with a statement by Poirier and Geiger[13] regarding the radius ratios of the diffusing atom to the diffusion medium.

CHAPTER 6

LIQUID ALUMINUM-NICKEL BINARY ALLOY

The transport properties of the binary aluminum-nickel system were recently evaluated by Asta *et al.*[71], using equilibrium molecular dynamic techniques and several different EAM potentials. They reported values for the viscosity and the diffusion coefficient as a function of composition. The viscosity for the EAM potentials displayed a monotonic decrease in viscosity from the nickel to the aluminum. Following the same procedures as Asta *et al.*[71] we obtained similar results. Figure 6.1 shows our results and their results compared to the experimental data. Examining the figure it is noticed that our results essentially match those of Asta *et al.*. The experimental values, however, show a peak in the viscosity at approximately the composition of NiAl. The temperature at which we obtained our results (1975 K) was in contrast to the temperature (1925 K) of the experimental and Asta's data(1925 K). Their temperatures are close to the congruent melting point of NiAl at 1923 K. We chose 1975 K to be further away from the congruent melting temperature. Although the temperatures are physically different we do not expect to notice any significant differences in the trends presented.

When one examines the phased diagram for the aluminum-nickel system (Figure 6.2 [113, 114]), qualitatively one would expect a peak in the viscosity as the experimental results show. The aluminum-nickel system would suggest that the viscosity would exhibit a maximum near 50 % composition. In considering the singular behavior, at the equiatomic composition of AlNi, Asta *et al.*[71] suggested that the peak in viscosity at NiAl was due to charge transfer, as previously recognized by Landa *et al.*[115, 116]. The

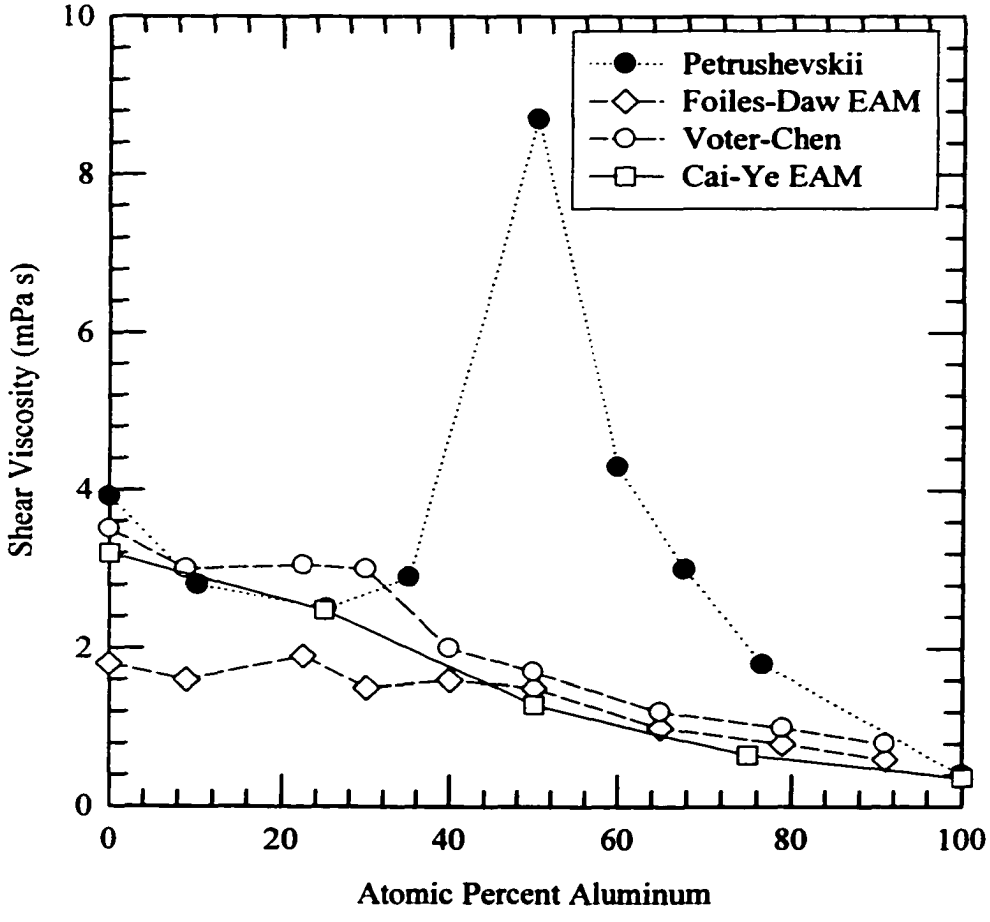

Figure 6.1. Viscosity versus composition. Experimental results are indicated by solid circles reference[3]. The open circles and open diamonds were presented by Asta *et al.*[71] using the EAM potentials of Voter-Chen and Foiles-Daw-Baskes. The open squares are our results for the Cai and Ye potential[5].

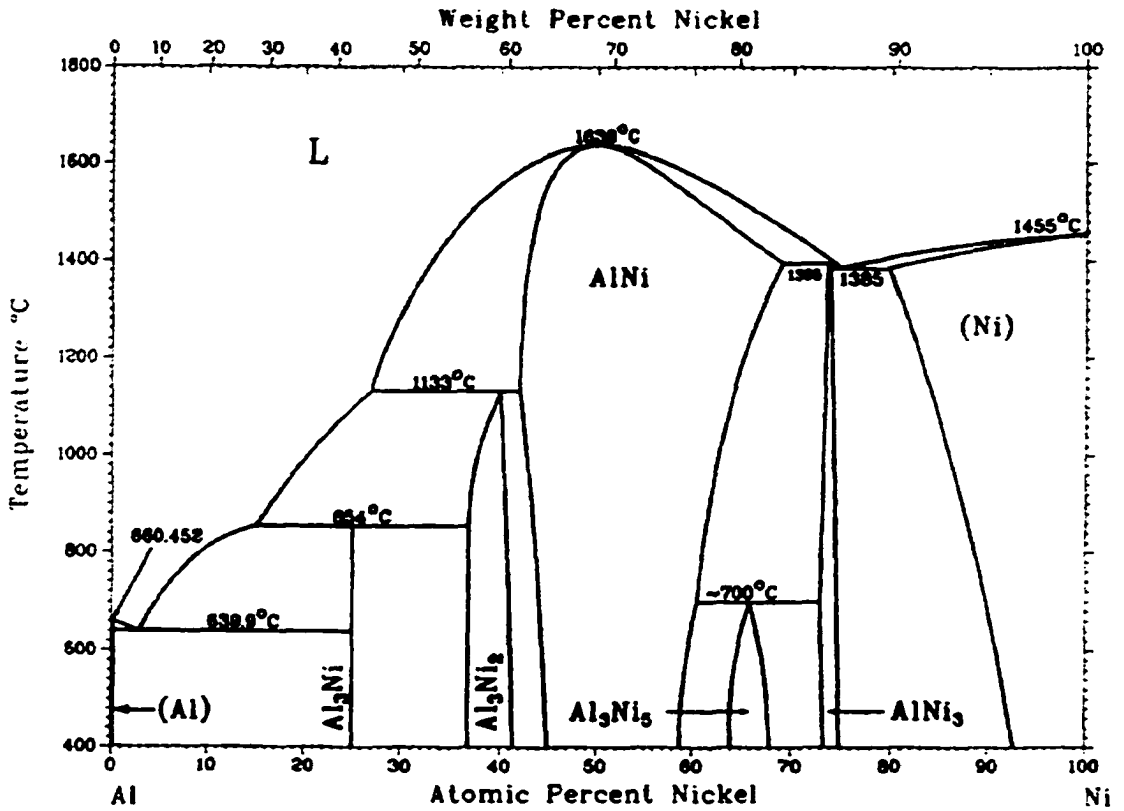

Figure 6.2. Phase diagram for aluminum-nickel binary alloy[113, 114].

following sections detail a way to include charge transfer in the EAM potential and the effects of such a transfer on the viscosity in the aluminum-nickel system.

6.1. Charge Transfer Model

Because the binary alloy viscosity calculated with the embedded-atom method does not reproduce the experimental viscosity data, we sought to include a charge transfer term into our potential. The justification for the charge transfer is rationalized on the basis of soft x-ray spectroscopy measurements showing that there is a filling of the d-band of the transition metal nickel when it is alloyed with the polyvalent metal aluminum[115, 116]. Furthermore, detailed photo-emission studies have ascertained that the density of states near the Fermi level in the equiatomic nickel aluminum alloy is much lower than in pure nickel. This condition is normally found when the d-band is completely filled. Kovneristyi *et al.*[116], utilizing a nonlocal resonant pseudopotential model with charge transfer, calculated the viscosity as a function of composition. They showed a similar increase in the viscosity near the equiatomic alloy as seen in experiment. The values for viscosity, however, were twice the experimental values at the equiatomic alloy composition. This suggests that charge transfer or covalent bonding can have a profound impact upon the viscosity. Within the framework of the EAM potentials, we set out to include a similar charge transfer term into the potential of Cai and Ye[5].

We begin with the condition that the charges must be conserved. In an average sense, the conservation of charge law can be given by

$$X\left(\rho_{Ni}-\rho_{Ni}^{0}\right)+(1-X)\left(\rho_{Al}-\rho_{Al}^{0}\right)=0 \tag{6.1}$$

where X is the concentration of nickel, ρ_{Ni}^{0} and ρ_{Al}^{0} are the electron density of pure nickel and pure aluminum, and ρ_{Ni} and ρ_{Al} are the electron density or charge associated within the binary. In the EAM approach of Cai and Ye[5], the electron density, ρ_i, is given by

$$\rho_i = \sum_{j \neq i} f_{e_j} e^{-\chi_j \left(r_{ji} - r_{e_j} \right)} \tag{6.2}$$

where f_{e_j} is the pre-exponential factor described in Chapter 3, χ_j is a constant, r_{e_j} is the equilibrium separation distance, and r_{ji} is the separation between the atoms. ρ_i could be determined from our alloy as

$$\rho_i = \sum_{\substack{j \neq i \\ j = Ni}} f_{e_{Ni}} e^{-\chi_{Ni} \left(r_{ji} - r_{e_{Ni}} \right)} + \sum_{\substack{j \neq i \\ j = Al}} f_{e_{Al}} e^{-\chi_{Al} \left(r_{ji} - r_{e_{Al}} \right)} \tag{6.3}$$

or

$$\rho_i = f_{e_{Ni}} \sum_{\substack{j \neq i \\ j = Ni}} e^{-\chi_{Ni} \left(r_{ji} - r_{e_{Ni}} \right)} + f_{e_{Al}} \sum_{\substack{j \neq i \\ j = Al}} e^{-\chi_{Al} \left(r_{ji} - r_{e_{Al}} \right)}. \tag{6.4}$$

Now if we assume that in the alloy the r_{ji} is on the average approximately equal to the equilibrium separations ($r_{e_{Ni}}$ and $r_{e_{Al}}$), then we can write a simple relation

$$\rho_i \approx f_{e_{Ni}} N_{Ni} + f_{e_{Al}} N_{Al}. \tag{6.5}$$

At any given composition the total number of atoms in the system is given by

$$N = N_{Ni} + N_{Al}. \tag{6.6}$$

Thus the concentration of nickel atoms is given by

$$X = \frac{N_{Ni}}{N} \tag{6.7}$$

and the concentration of aluminum in terms of the fraction above is given by

$$(1 - X) = \frac{N_{Al}}{N}. \tag{6.8}$$

Inserting equations 6.7 and 6.8 into 6.5, we see that

$$\frac{\rho_i}{N} \approx f_{e_{Ni}} X + f_{e_{Al}} (1 - X) \tag{6.9}$$

In a qualitative sense, ρ_i is independent of the species involved. Substituting the results of equation 6.9 into our conservation equation 6.1, the following expression is valid:

$$X\left(f_{e_{Ni}} - f^0_{e_{Ni}}\right) + (1 - X)\left(f_{e_{Al}} - f^0_{e_{Al}}\right) = 0. \tag{6.10}$$

Equation 6.10 shows that in an average way charge is conserved. We now search for a function for $f_{e_{Al}}$ and $f_{e_{Ni}}$, satisfying the conservation of charges and representing the transfer of charges from aluminum to nickel. In other words, within the alloy the aluminum loses electrons to the nickel. We assume that the functions for $f_{e_{Ni}}$ and $f_{e_{Al}}$ are linear functions of concentration

$$f_{e_{Ni}} = f^0_{e_{Ni}} - (1 - X)B \tag{6.11}$$

and

$$f_{e_{Al}} = f^0_{e_{Al}} + XB \tag{6.12}$$

where B is a constant that needs to be determined. It can be shown that equations 6.11 and 6.12, also satisfy the conservation of charge law given by equation 6.10. In the limit as X approaches the pure nickel case (or X approaches one), there are so many nickel

atoms that their charge is unchanged by the presence of aluminum, but the charge on the aluminum is totally reduced by an amount equal to B. The dimensions of B must be the same as f_e.

In order to determine the constant B, we recall that the alloying pair potential given by the Johnson alloying pair potential[59] for the aluminum-nickel system is

$$\phi^{NiAl}(r)=\frac{1}{2}\left[\frac{f^{Al}(r)}{f^{Ni}(r)}\phi^{NiNi}(r)+\frac{f^{Ni}(r)}{f^{Al}(r)}\phi^{ALAl}(r)\right] \tag{6.13}$$

The heteroatomic pair potential, equation 6.13 suggests that f_e cannot be negative thus

$$f^0_{e_{Al}}-f^0_{e_{Ni}}<B<f^0_{e_{Ni}} \tag{6.14}$$

and with this condition in mind, we are able to choose a value for the constant B. We arbitrarily choose B to have a value to be approximately the ratio of the aluminum valence electrons to the nickel valence electrons multiplied by the average f_e values for aluminum and nickel or

$$B=\frac{1}{3}\left(\frac{f^0_{e_{Ni}}+f^0_{e_{Ni}}}{2}\right) \tag{6.15}$$

Furthermore, to be consistent with Landa *et al.*[115, 116], we choose to define two sets of equations for the composition dependence of f_e. We use the definition of B from equation 6.15, for the concentrations where X is in the interval [0.5, 1]. Under this condition, the first sets of equations essentially are equations 6.11 and 6.12, i.e.

$$f_{e_{Ni}}=f^0_{e_{Ni}}-(1-X)\frac{1}{3}\left(\frac{f^0_{e_{Ni}}+f^0_{e_{Ni}}}{2}\right) \tag{6.16}$$

and

$$f_{e_{Al}} = f^0_{e_{Al}} + X\frac{1}{3}\left(\frac{f^0_{e_{Ni}} + f^0_{e_{Ni}}}{2}\right). \tag{6.17}$$

When $0<X<0.5$, we state that the d-band is completely filled in the nickel and therefore the f_e is considered to be a constant

$$f_{e_{Ni}} = f^0_{e_{Ni}} - \frac{1}{3}\left(\frac{f^0_{e_{Ni}} + f^0_{e_{Ni}}}{4}\right) \tag{6.18}$$

and

$$f_{e_{Al}} = f^0_{e_{Al}} + \frac{1}{3}\left(\frac{f^0_{e_{Ni}} + f^0_{e_{Ni}}}{4}\right). \tag{6.19}$$

In Figure 6.3, we show how this charge transfer modification affects the heteroatomic pair potential. The solid line curve is the heteroatomic pair potential with the charge transfer, and the dashed line corresponds to the case without the heteroatomic charge transfer. The curves suggest that the heteroatomic pair potential with charge transfer will be more attractive than without the charge transfer. Another effect that charge transfer has upon the heteroatomic pair potential, that is not readily apparent, is shift of the radial position of the minimum bringing the Al-Ni pair closer.

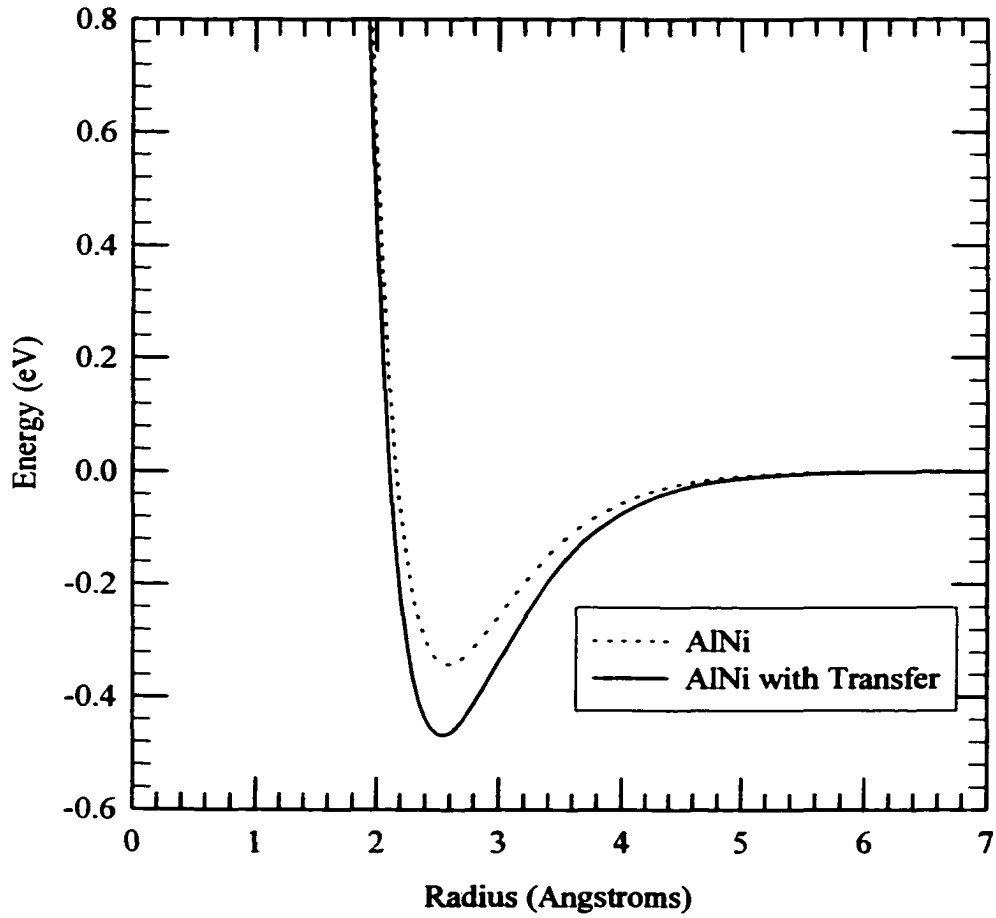

Figure 6.3. Heteroatomic pair potentials. The solid curve is the Al-Ni pair potential for the equiatomic composition with charge transfer. The dashed curve is the Al-Ni pair potential for the equiatomic composition without charge transfer.

6.2. Atomic Density

In this section, we report the charge transfer effect upon the atomic density. We noted in Chapter 3 that the Cai and Ye[5] potential needs a modification to the nickel parameters to get satisfactory heats of solution; these nickel parameters are referred to as revised nickel parameters. To obtain a sense of the structural nature of the aluminum-nickel alloy, we first determined the zero pressure densities for a series of compositions with charge transfer and without, and with revised and normal nickel parameters. The zero pressure densities were obtained in the same fashion described earlier, at 1975 K. We report the densities obtained in Table 6.1.

We illustrate in Figure 6.4, the "charge" transfer effect upon the density for the normal nickel parameter system. The experimental results come from reference[106]. Remember from Chapter 5 that the densities predicted by the Cai and Ye typically underestimate the experimental densities. The same holds true for the densities plotted in Figure 6.4. Notice in Figure 6.4 that the "charge" transfer term tends to follow the experimental results better than the system without the charge transfer. At the equiatomic composition, we see a 3.3% increase in the atomic density for normal nickel with charge transfer compared to without. The charge transfer atomic density for the equiatomic composition is about 7.5% less than the experimental density. The atomic density without charge transfer is 10% less than the experimental density for the same composition.

The aluminum nickel system is a non-ideal solution. Our results suggest the inclusion of charge transfer enhances the non-ideality of mixing behavior. The deviation

from ideal mixing behavior at the equiatomic composition for the non-charge transfer amounts to 4.1% and 4.3% increase from ideal behavior for normal and revised nickel. For charge transfer, the deviation from ideal behavior amounts to 8.5% and 7.3% increase at the equiatomic composition. The experimental deviation from ideal behavior has a 9.8% increase. The inclusion of our charge transfer term accounts for some of the observed deviation from ideality.

Table 6.1. Atomic densities versus composition at 1975 K. Densities reported in atoms-$Å^{-3}$.

Composition (% Al)	Normal Ni	Normal Ni with Charge Transfer	Revised Ni	Revised Ni with Charge Transfer
0	0.0762±0.003	0.0762±0.003	0.0754±0.002	0.0754±0.002
25	0.0708±0.009	0.0726±0.001	0.0690±0.003	0.0708±0.005
50	0.0610±0.002	0.0636±0.010	0.0607±0.005	0.0625±0.007
75	0.0534±0.003	0.0557±0.009	0.0510±0.006	0.0531±0.009
100	0.0410±0.006	0.0410±0.006	0.0410±0.006	0.0410±0.006

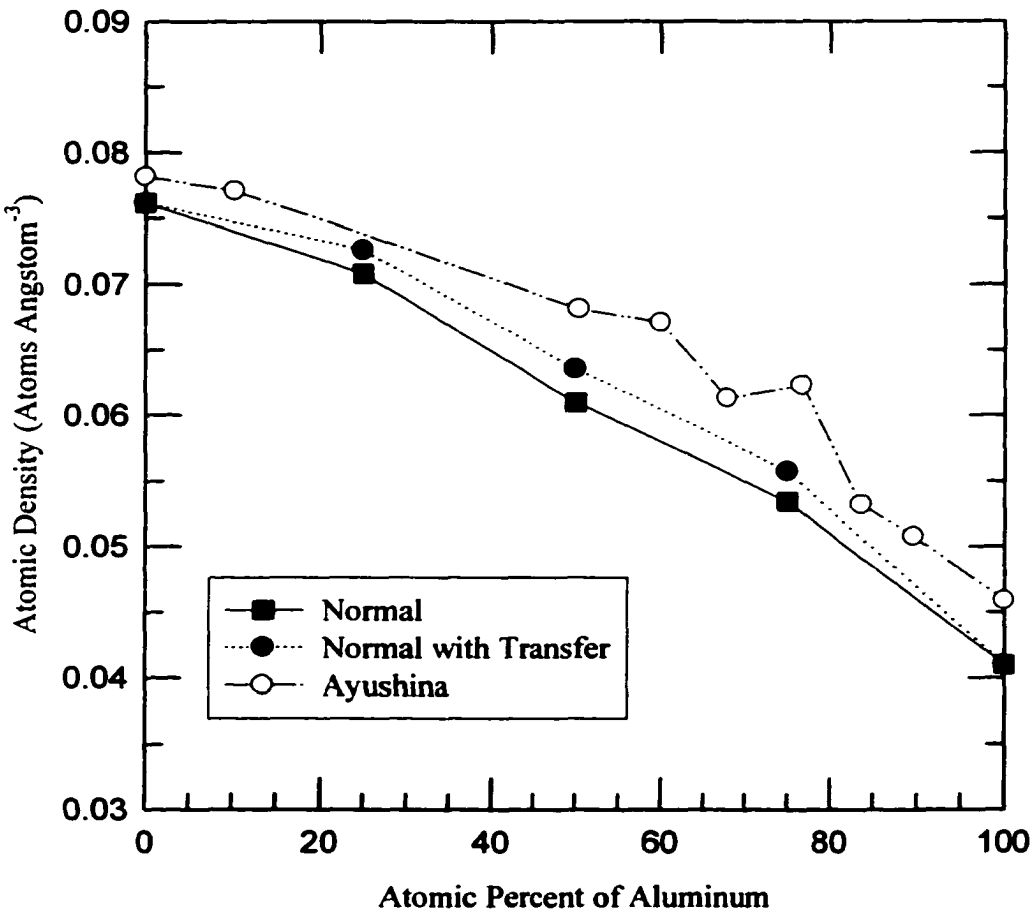

Figure 6.4. Density versus composition at 1975 K. Experimental results are indicated by the open circles, reference [106]. The solid squares are represent the density for the normal nickel parameters. The solid circles represent the density for the normal nickel parameters with charge transfer.

6.3. Structural Parameters

We obtained radial distribution functions averaged over 250 instantaneous radial distribution functions. The radial distribution functions were obtained using equilibrium simulations with 1372 atoms. In Tables 6.2 and 6.3, we report the first nearest-neighbor distances for pairs present in the liquids under consideration, namely, Al-Al, Al-Ni, and Ni-Ni. Table 6.2 is a comparison of the values obtained using the normal nickel parameters. Table 6.3 examines the first nearest-neighbor distances for the revised nickel parameters. Examining the tables, it is noticed that the charge transfer term with normal nickel tends to shorten the aluminum-aluminum separation. The aluminum-nickel separation with the charge transfer term tends to lengthen for the 50% and 75% aluminum concentrations. The nickel-nickel separation distances remain almost unchanged, with the exception at 75% aluminum concentrations, where both the revised and the normal nickel are increased. Other than the notable exception in the nickel-nickel separation distances, the revised nickel parameters seem to be insensitive to presence of charge transfer.

Table 6.2. First nearest neighbor distances for normal nickel parameters. All distances are given in Angstroms.

Composition	Transfer	Al-Al	Al-Ni	Ni-Ni
$AlNi_3$	No	2.6495	2.5665	2.4003
$AlNi_3$	Yes	2.5997	2.5332	2.4336
AlNi	No	2.716	2.5332	2.4502
AlNi	Yes	2.6827	2.7748	2.4668
Al_3Ni	No	2.6993	2.5332	2.4668
Al_3Ni	Yes	2.5332	2.6163	2.6827

Table 6.3. First nearest neighbor distances for revised nickel parameters. All distances are given in Angstroms.

Composition	Transfer	Al-Al	Al-Ni	Ni-Ni
$AlNi_3$	No	2.6661	2.5166	2.4336
$AlNi_3$	Yes	2.6495	2.5332	2.4834
AlNi	No	2.6661	2.5166	2.4668
AlNi	Yes	2.6661	2.5498	2.4502
Al_3Ni	No	2.6993	2.5665	2.4834
Al_3Ni	Yes	2.6661	2.5498	2.5498

6.4. Viscosity

As was aforementioned, the Cai and Ye[5] potential provides comparable results in the viscosity as a function of composition to other EAM potentials. Furthermore, the viscosity calculated with both NEMD and EMD techniques exhibit the same small systematic difference that the pure metals did. In table 6.4, we include all of the viscosities obtained with both techniques. The non-equilibrium runs were conducted with 500 atoms for the 0 %, 25%, 75%, and 100% of aluminum compositions and 432 atoms for the equiatomic composition. The shear rates imposed on the system ranged from 1.89×10^{11} s^{-1} to 1.89×10^{13} s^{-1} for the non-equilibrium compositions, and the NEMD zero shear viscosity was obtained utilizing the fitting procedure described in Chapter 3. The NEMD simulations lasted 42 ps, while the duration of the EMD simulations was 2 ns. The EMD runs were performed with 1372 atoms. We used the densities for each of the four cases found in Table 6.1 for these calculations. It appears from table 6.4, the greatest increase in the viscosity occurs at the equiatomic composition, which amounts to approximately 30%.

We illustrate, in Figure 6.5, the effect of the charge transfer term utilizing non-equilibrium simulations for the normal nickel parameters, while the NEMD results for

Table 6.4. Viscosity of aluminum-nickel binary system at 1975 K, reported in mPa s.

Comp %Al	Normal		Normal with Transfer		Revised		Revised with Transfer	
	EMD (Temp K)	NEMD	EMD (Temp K)	NEMD	EMD (Temp K)	NEMD	EMD (Temp K)	NEMD
0	2.66±0.68 (1957)	3.39	2.66±0.68 (1957)	3.39	3.20±0.72 (1966)	3.33	3.20±0.72 (1966)	3.33
25	2.44±0.66 (1959)	2.53	2.78±0.82 (1995)	3.04	2.48±0.61 (1992)	2.66	3.22±0.77 (1981)	3.09
50	1.33±0.36 (1973)	1.55	1.60±0.53 (1967)	2.04	1.29±0.43 (1959)	1.55	2.05±0.40 (1957)	1.95
75	0.862±0.232 (1958)	0.962	1.05±0.35 (1949)	1.18	0.656±0.240 (1965)	0.821	0.855±0.236 (1969)	1.02
100	0.365±0.093 (2033)	0.373	0.365±0.093 (2033)	0.373	0.365±0.093 (2033)	0.373	0.365±0.093 (2033)	0.373

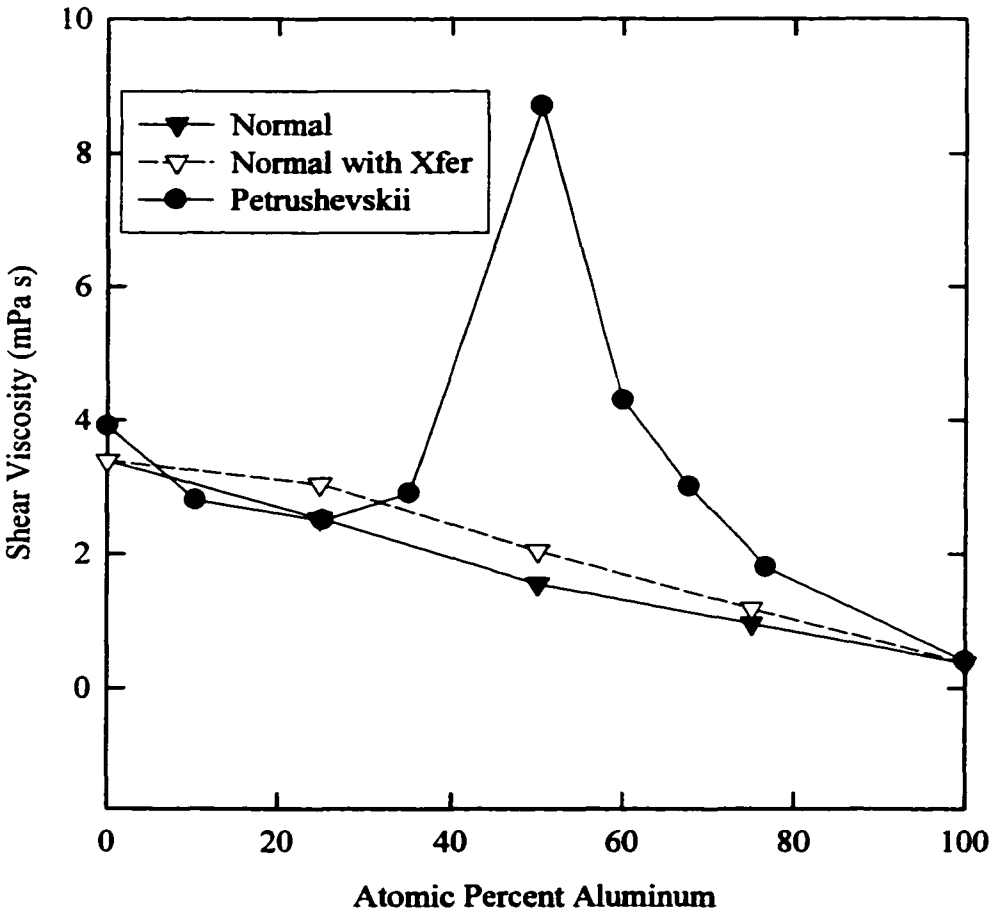

Figure 6.5. Comparison of the viscosity of aluminum-nickel binary for normal nickel parameters with and without charge transfer at 1975 K, N=500.

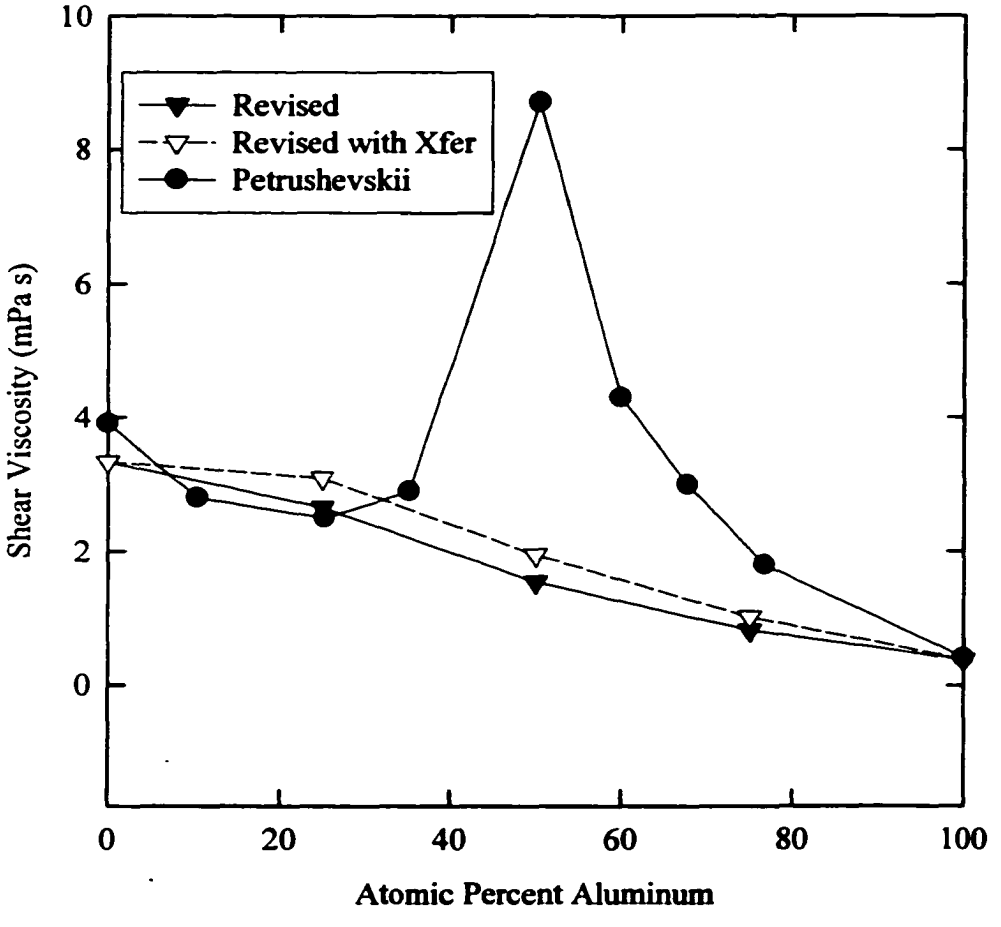

Figure 6.6. Comparison of the viscosity of aluminum-nickel binary for revised nickel parameters with and without charge transfer at 1975 K, N=500.

revised parameters are found in Figure 6.6. From Figures 6.5 and 6.6, it is apparent that the inclusion of charge transfer tends to increase the viscosity which correlates with the increase in the density. The viscosity as a function of composition, however, remains monotonous. This suggests the charge transfer term is not strong enough or binding enough around the equiatomic concentrations. Therefore, the charge transfer concept is valid, however, it needs further refinement.

Although the behavior of the viscosity does not agree well with the experiments, it is necessary to examine the experimental data, as well. The viscosity at the equiatomic concentrations were measured using the oscillating vessel method, which interpreted with the Shvidkovskii's equation is known to overestimate the viscosity near the melting point[2]. Therefore, the dramatic peak exhibited near the equiatomic concentration may be overvalued.

6.5. Diffusion

In Table 6.5, we report the diffusion coefficients obtained from the equilibrium simulations. We graphically illustrate these results for aluminum in Figure 6.7, while Figure 6.8 we do the same for nickel. Within Table 6.5, the temperature in the brackets is the result of calculating the diffusion coefficients under constant energy conditions. The simulation time was on the order of 2 ns or 2 million timesteps, with a time correlation function of 5 ps or 5000 timesteps, and a total of 500 correlations functions averaged. The diffusion data, as in the pure system, had fewer deviations from the average. As such, we estimate the errors to be no more than ±5%.

Although the diffusion coefficients of nickel and aluminum are approximately equal, upon inspecting table 6.5, it is noted that the diffusion coefficient of aluminum is lower than nickel diffusion coefficient at low aluminum concentrations. At the higher aluminum concentrations, the reverse is apparent. Including charge transfer appears to have the greatest impact in lowering the diffusion coefficients at the Al_3Ni composition.

Table 6.5. Diffusivity of aluminum and nickel in the binary system at 1975 K, reported in 10^{-5} cm^2 s^{-1}.

Comp %Al	Normal		Normal with Transfer		Revised		Revised with Transfer	
	Aluminum (Temp K)	Nickel (Temp K)	Aluminum (Temp K)	Nickel (Temp K)	Aluminum (Temp K)	Nickel (Temp K)	Aluminum (Temp K)	Nickel (Temp K)
0	NA	6.48±0.08 (1957)	NA	NA	NA	5.83±0.17 (1966)	NA	NA
25	6.93±0.19 (1959)	7.43±0.16 (1959)	5.88±0.22 (1995)	6.47±0.07 (1995)	7.64±0.23 (1992)	8.12±0.12 (1992)	5.36±0.20 (1981)	6.29±0.16 (1981)
50	11.2±0.24 (1973)	11.4±0.22 (1973)	10.1±0.21 (1967)	10.2±0.13 (1967)	12.2±0.34 (1959)	12.0±0.29 (1959)	9.20±0.17 (1957)	9.21±0.18 (1957)
75	18.6±0.35 (1958)	16.9±0.40 (1958)	14.8±0.27 (1949)	12.9±0.29 (1949)	20.7±1.06 (1965)	18.2±1.08 (1965)	17.8±0.29 (1969)	15.2±0.21 (1969)
100	41.8±0.37 (2033)	NA	NA	NA	NA	NA	NA	NA

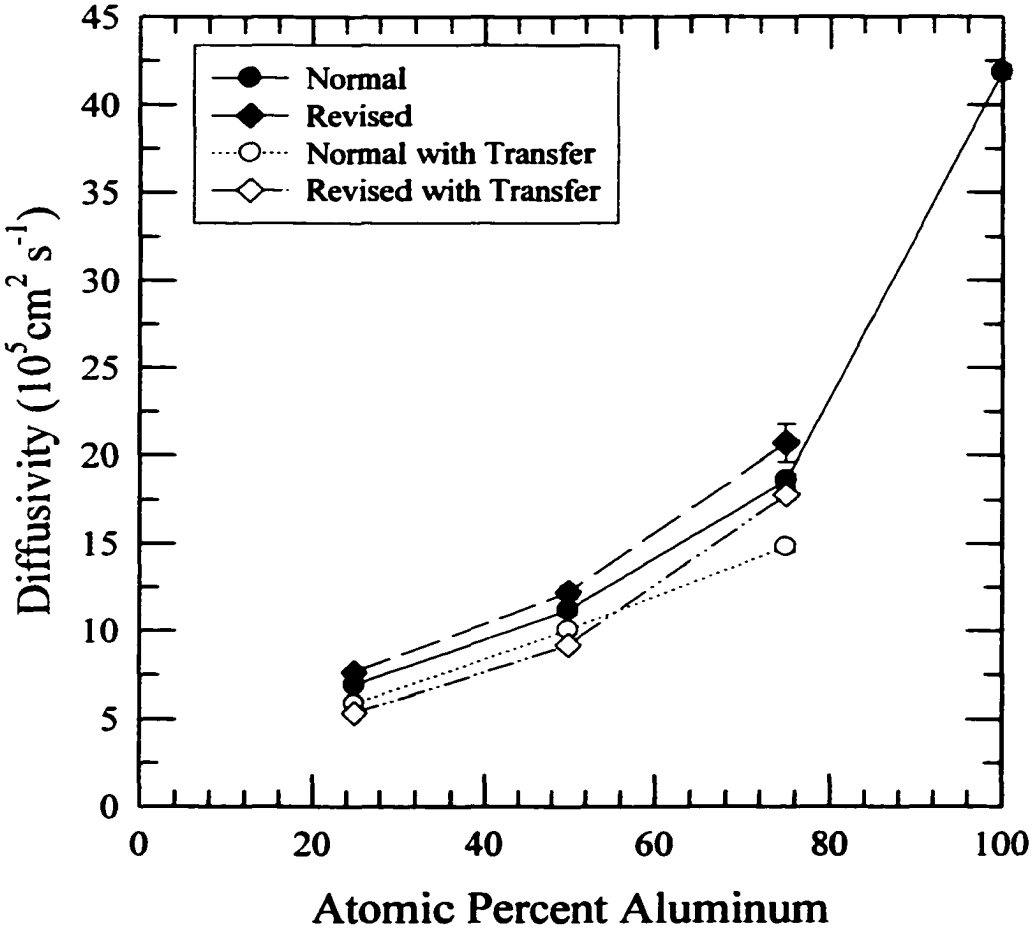

Figure 6.7. Diffusivity of aluminum versus composition at 1975 K. Solid symbols do not include charge transfer and open symbols include the charge transfer term. Diffusivities calculated with Green-Kubo relations for diffusion.

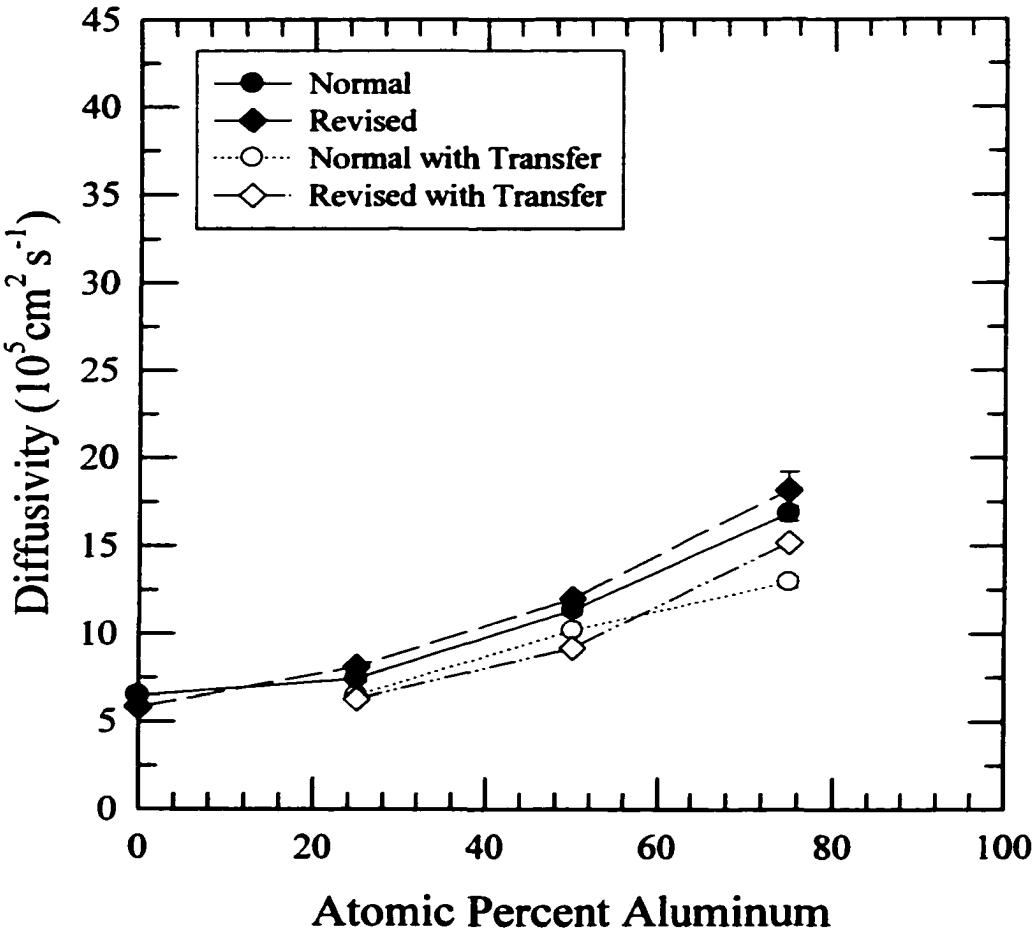

Figure 6.8. Diffusivity of nickel versus composition at 1975 K. Solid symbols do not include charge transfer and open symbols include the charge transfer term. Diffusivities calculated with Green-Kubo relations for diffusion.

6.6. Summary

To summarize this chapter, we note that our approach to include charge transfer in the EAM potential does have a significant effect on the transport and structural properties aluminum-nickel the binary alloy. We note that the largest impact is with the density, and the same trends as the experimental atomic densities are followed. The effect of the charge transfer term, however, was minimal upon the transport properties. We do believe, however, a more in-depth examination of the charge transfer term should be considered. A direction is suggested in the following chapter.

CHAPTER 7

CONCLUSIONS AND FUTURE WORK

The widespread popularity of the embedded-atom method (EAM) potentials results from their simplicity in describing transition metal properties. We undertook the calculations of transport properties for the model aluminum-nickel binary system, in the liquid state, using molecular dynamics (MD) and an EAM potential. In the case of pure aluminum and nickel, we found satisfactory agreement between our calculations and the available experimental data. With respect to the range of available viscosity data, our results matched better the lower experimental values. Based on this success, it appears that MD and EAM models can serve as useful predictive tools in the calculation of transport properties.

When studying the aluminum-nickel binary system, we get comparable results to simulations of other EAM models[54]. However, the experimental viscosity data as a function of composition displays singular behavior near equiatomic composition, which is not reproduced by MD calculations. To alleviate this discrepancy, we introduced a modification into the EAM potential that includes charge transfer between the aluminum and the nickel. This modification yielded improved values for the density compared to the experimental densities[106]. The effect of including charge transfer on calculated transport properties was minimal, however, and did not reproduce the singular behavior observed in the experimental viscosity. To better simulate the binary alloys, we recommend the inclusion of a coulombic force into the EAM potential [117]. The principle behind this recommendation is that intermetallic bonding is slightly ionic in

character, due to charge transfer. By including the ionic character, interatomic bond distance should lengthen for the homonuclear bonding and shorten for the heteronuclear bonding. In the event that including a coulombic force term into the potential can adequately describe a binary alloy, then the principle of charge transfer and coulombic attraction could be extended beneficially to ternary alloys.

On account of the discrepancies with our calculated data to experimental data, it may be necessary to investigate other potentials. One such potential that could be investigated is another modified embedded atom method (MEAM)[79]. The advantage of this model is it accommodates electron densities that are not spherically symmetric. These electron density functions provide directionality to the interatomic bonding.

With the advent of more efficient computer platforms, more fundamental calculations of materials are now possible. These methods are based on a quantum mechanical description of electrons in the system leading to a potential-less model of atomic attraction. One such approach is based on the tight-binding approximation[111,118-124], which allows the simulation of "large" systems. Another approach to calculating viscosity would be to examine the viscosity with a full *ab initio* method[125, 126]. For liquid aluminum, this was recently done with reasonable results[126]. The problem with the full *ab initio* method is that the simulations are limited to small systems. For instance, the liquid aluminum of reference [126] was studied with only 64 atoms, which may have significant size effects in the computation of the Green-Kubo viscosities. As computational performance increases, the *ab initio* approach, however, will become more practical and realistic.

We conducted a systematic comparison between viscosity calculated with NEMD and EMD methods. These proved to provide complementary and comparable viscosity data. Yet there appeared to be a small systematic difference in the numerical data. The difference looks to be smaller for the lower viscosity liquids, such as aluminum. We believe the difference comes from the method of thermostating the NEMD simulations. Future work should include more study on this systematic difference.

In calculating the diffusion coefficient, we found that the Sutherland-Einstein relation better matched the calculated diffusion coefficients from Green-Kubo computations. Calculating the diffusion coefficient from a recently proposed Universal Scaling Law [27] proved to provide relative values for the diffusion coefficient compared to our calculated diffusion coefficient but not exact. A closer examination of simple phenomenological models of diffusion in pure, as well as, alloyed transition elements in the context of MD simulation should be conducted.

APPENDIX A

DERIVATION OF THE FORCE FOR THE PURE METALS USING THE EMBEDDED ATOM METHOD

In order to calculate the properties of the pure metal it is necessary within the framework of molecular dynamics to know or calculate the force on any given particle. From Newtonian mechanics we know that the force on a particle k is

$$\vec{F}_k = -\frac{\partial E}{\partial \vec{r}_k} \tag{A.1}$$

Where $\vec{F}_k$ is the force vector on particle k, E is the potential energy, and $\vec{r}_k$ is the position vector of particle k. In the realm of EAM potentials the energy is defined as:

$$E = \sum_i F_i(\rho_i) + \sum_{i>j} \phi(r_{ij}) \tag{A.2}$$

where the first term in this expression defines the embedding energy associated with the local electronic density and the second term is a pair potential term. Substituting equation (A.2) into equation (A.1) we obtain:

$$\vec{F}_k = -\frac{\partial}{\partial \vec{r}_k}\left[\sum_i F_i(\rho_i) + \sum_{i>j} \phi(r_{ij})\right] = -\left\{\sum_i \frac{\partial}{\partial \vec{r}_k}[F_i(\rho_i)] + \frac{\partial}{\partial \vec{r}_k}\sum_{i>j} \phi(r_{ij})\right\} \tag{A.3}$$

Applying the chain rule the upon the first term and evaluating the derivative effect on the pair potential term the expression for the force becomes:

$$\vec{F}_k = -\left\{\sum \frac{\partial[F_i(\rho_i)]}{\partial \rho_i}\frac{\partial \rho_i}{\partial \vec{r}_k} + \sum_{i \neq k} \frac{\partial \phi(r_{ik})}{\partial \vec{r}_k}\right\} \tag{A.4}$$

Before further derivation of the force it is necessary to define some of the variables present in the standard EAM potential namely ρ_i:

$$\rho_i = \sum_{j \neq i} f(r_{ji}) \tag{A.5}$$

Based on the definition of the electron density it can be seen the ρ_i is a function of r_{ji}. Therefore the force can be written as

$$\vec{F}_k = -\left\{ \sum \frac{\partial [F_i(\rho_i)]}{\partial \rho_i} \sum_l \sum_m \frac{\partial \rho_i}{\partial r_{lm}} \frac{\partial r_{lm}}{\partial \vec{r}_k} + \sum_{i \neq k} \frac{\partial \phi(r_{ik})}{\partial \vec{r}_k} \right\} \tag{A.6}$$

where

$$r_{ij} = \sqrt{(x_i - x_j)^2 + (y_i - y_j)^2 + (z_i - z_j)^2} \tag{A.7}$$

and

$$\frac{\partial r_{lm}}{\partial \vec{r}_k} = \frac{1}{2 r_{lm}} \begin{Bmatrix} [2(x_l - x_m)\delta_{lk} - 2(x_l - x_m)\,\delta_{km}]\hat{x} + \\ [2(y_l - y_m)\delta_{lk} - 2(y_l - y_m)\delta_{km}]\hat{y} + \\ [2(z_l - z_m)\delta_{lk} - 2(z_l - z_m)\,\delta_{km}]\hat{z} \end{Bmatrix} \tag{A.8}$$

Inserting equation A.8 into equation (A.6) and performing some algebra, our equation for the force becomes:

$$\vec{F}_k = -\left\{ \sum \frac{\partial [F_i(\rho_i)]}{\partial \rho_i} \left[\sum_m \left(\frac{\partial \rho_i}{\partial r_{km}} + \frac{\partial \rho_i}{\partial r_{mk}} \right) \frac{1}{r_{km}} \left(\vec{r}_k - \vec{r}_m \right) \right] + \sum \frac{\partial \phi(r_{ik})}{\partial r_{ik}} \frac{\partial r_{ij}}{\partial \vec{r}_k} \right\} \tag{A.9}$$

It is now necessary to evaluate the partial derivative of ρ_i (Equation A.5) with respect to r_{km} and r_{mk}. The partial derivatives become:

$$\frac{\partial \rho_i}{\partial r_{km}} = \frac{\partial\left[\sum_{j\neq k} f(r_{ji})\right]}{\partial r_{km}} = \sum_{j\neq i} \frac{\partial f(r_{ji})}{\partial r_{km}} = \sum_{j\neq i} \frac{\partial f(r_{ji})}{\partial r_{ki}} \delta_{kj}\delta_{im} = \frac{\partial f(r_{ki})}{\partial r_{ki}} \delta_{im} \quad (i \neq k) \quad \text{(A.10)}$$

and

$$\frac{\partial \rho_i}{\partial r_{mk}} = \frac{\partial\left[\sum_{j\neq k} f(r_{ji})\right]}{\partial r_{mk}} = \sum_{j\neq i} \frac{\partial f(r_{ji})}{\partial r_{mk}} = \sum_{j\neq i} \frac{\partial f(r_{ji})}{\partial r_{mk}} \delta_{jm}\delta_{ki} = \frac{\partial f(r_{ki})}{\partial r_{mi}} \delta_{ki} \quad (m \neq i) \quad \text{(A.11)}$$

Substituting the results of equations (A.10) and (A.11) into equation (A.9), the force becomes:

$$\vec{F}_k = -\left\{\sum_i \frac{\partial F_i(\rho_i)}{\partial \rho_i}\left[\sum_m \frac{\vec{r}_{km}}{r_{km}}\left(\frac{\partial f(r_{ki})}{\partial r_{ki}}\delta_{im}\ (i \neq k) + \frac{\partial f(r_{mi})}{\partial r_{mi}}\delta_{ki}\ (m \neq i)\right)\right] + \sum_{i\neq k} \frac{\partial \phi(r_{ij})}{\partial r_{ij}} \frac{\partial r_{ij}}{\partial \vec{r}_k}\right\} \quad \text{(A.12)}$$

or

$$\vec{F}_k = -\left\{\sum_m \sum_i \frac{\partial F_i(\rho_i)}{\partial \rho_i} \frac{\vec{r}_{km}}{r_{km}}\left(\frac{\partial f(r_{ki})}{\partial r_{ki}}\delta_{im}\ (i \neq k) + \frac{\partial f(r_{mi})}{\partial r_{mi}}\delta_{ki}\ (m \neq i)\right) + \sum_{i\neq k} \frac{\partial \phi(r_{ij})}{\partial r_{ij}} \frac{\partial r_{ij}}{\partial \vec{r}_k}\right\} \quad \text{(A.13)}$$

Evaluating the Kroenecker delta function the force becomes

$$\vec{F}_k = -\left\{\sum_{i\neq k} \frac{\partial F_i(\rho_i)}{\partial \rho_i} \frac{\vec{r}_{ki}}{r_{ki}} \frac{\partial f(r_{ki})}{\partial r_{ki}} + \sum_{m\neq k} \frac{\partial F_k(\rho_k)}{\partial \rho_k} \frac{\vec{r}_{km}}{r_{km}} \frac{\partial f(r_{mk})}{\partial r_{mk}} + \sum_{i\neq k} \frac{\partial \phi(r_{ij})}{\partial r_{ij}} \frac{\partial r_{ij}}{\partial \vec{r}_k}\right\} \quad \text{(A.14)}$$

Combining all the sums under a single summation, equation (A.14) becomes

$$\vec{F}_k = -\left\{\sum_{i\neq k}\left(\frac{\partial F_i(\rho_i)}{\partial \rho_i} + \frac{\partial F_k(\rho_k)}{\partial \rho_k}\right) \frac{\vec{r}_{ik}}{r_{ik}} \frac{\partial f(r_{ik})}{\partial r_{ik}} + \frac{\partial \phi(r_{ik})}{\partial r_{ik}} \frac{\partial r_{ki}}{\partial \vec{r}_k}\right\} \quad \text{(A.15)}$$

or the force on particle k can be defined as

$$\vec{F}_k = -\left\{\sum_{i \neq k}\left[\left(\frac{\partial F_i(\rho_i)}{\partial \rho_i} + \frac{\partial F_k(\rho_k)}{\partial \rho_k}\right)\frac{\partial f(r_{ik})}{\partial r_{ik}} + \frac{\partial \phi(r_{ik})}{\partial r_{ik}}\right]\frac{\vec{r}_{ki}}{r_{ik}}\right\} \tag{A.16}$$

With the force on particle k derived in equation A.16, it is necessary to evaluate the functions of Cai and Ye [5] in terms of the above equation namely $F_i(\rho_i)$, $f(r_{ik})$, and $\phi(r_{ik})$. $F_i(\rho_i)$ is defined by the following

$$F_i(\rho_i) = -F_0\left[1 - \ln\left(\frac{\rho_i}{\rho_e}\right)^n\right]\left(\frac{\rho_i}{\rho_e}\right)^n + F_1\left(\frac{\rho_i}{\rho_e}\right) \tag{A.17}$$

where F_0 and F_1 are embedding energy parameters, ρ_e is the equilibrium electronic density, and ρ_i is determined by equation (A.5), and n is defined by Cai and Ye to be 0.5. $f(r_{ik})$ is defined by

$$f(r_{ki}) = f_e \exp[-\chi(r_{ki} - r_e)] \tag{A.18}$$

where r_e is the equilibrium radial separation between atoms, χ is a parameter given by Cai and Ye, r_{ji} is the distance between particles i and j, and f_e is taken as 1 for pure substances. $\phi(r_{ik})$ has the following functional form:

$$\phi(r_{ik}) = -\alpha\left[1 + \beta\left(\frac{r_{ik}}{r_a} - 1\right)\right]\exp\left[-\beta\left(\frac{r_{ik}}{r_a} - 1\right)\right] \tag{A.19}$$

where α, β, and r_a are fitted parameters.

By taking the appropriate derivatives of equations (A.17), (A.18), and (A.19), the remaining elements needed for the calculation of the force can be determined. The first derivative of equation (A.17) becomes the following:

$$\frac{\partial F_i(\rho_i)}{\partial \rho_i} = \frac{1}{\rho_e}\left[n^2 F_0 \left(\frac{\rho_i}{\rho_e}\right)^{n-1} \ln\left(\frac{\rho_i}{\rho_e}\right) + F_1 \right] \tag{A.20}$$

The expression for $\frac{\partial f(r_{ik})}{\partial r_{ik}}$ is

$$\frac{\partial f(r_{ik})}{\partial r_{ik}} = -\chi f_e \exp[-\chi(r_{jk} - r_e)]. \tag{A.21}$$

and the expression for the pair terms is given by

$$\frac{\partial \phi(r_{ik})}{\partial r_{ik}} = \frac{\alpha\beta^2}{r_a}\left(\frac{r_{ik}}{r_a} - 1\right)\exp\left[-\beta\left(\frac{r_{ik}}{r_a} - 1\right)\right]. \tag{A.22}$$

Given these expressions it is now possible to calculate the force on particle *k*.

APPENDIX B

DERIVATION OF THE FORCE FOR A BINARY EAM METAL

In order to calculate the force on particle *k* within a binary it is necessary to identify which type of particle it is. For convenience label each particle either type *a* or type *b*. Therefore in a binary we have two cases of forces to consider. The first case is the force on particle *k* of type *a* or k_a. Before this force can be derived it is necessary to modify by adding superscripts signifying the type of particle the function comes from. It is also necessary to define the electronic density ρ_i^a can be defined as

$$\rho_i^a = \sum_{j^a \neq i^a} f^a\left(r_{j^a i^a}\right) + \sum_{j^b} f^b\left(r_{j^b i^a}\right) \tag{B.1}$$

where the terms from the $f^a\left(r_{j^a i^a}\right)$ is the contribution to the electron density due to particle *j* being of type *a* and $f^b\left(r_{j^b i^a}\right)$ is the contribution to the electronic density due particle *j* of type *b*. These functions can be defined as

$$f^a\left(r_{ji}\right) = f_e^a e^{-\chi^a\left(r_{ji} - r_e^a\right)} \tag{B.2}$$

and

$$f^b\left(r_{ji}\right) = f_e^b e^{-\chi^b\left(r_{ji} - r_e^b\right)} \tag{B.3}$$

The final three functions pertain to the pair potential term in the total energy. When one considers a binary mixture the pair potentials are going to type *a*-*a*, *b*-*b*, and *a*-*b*. Where type *a*-*a* and type *b*-*b* are nothing more than the homonuclear pair potentials. These potentials as defined by Cai and Ye[5] are:

$$\phi^{a-a}(r_{ik}) = -\alpha^a\left[1+\beta^a\left(\frac{r_{ik}}{r_a^a}-1\right)\right]\exp\left[-\beta^a\left(\frac{r_{ik}}{r_a^a}-1\right)\right] \qquad \text{(B.4)}$$

and

$$\phi^{b-b}(r_{ik}) = -\alpha^b\left[1+\beta^b\left(\frac{r_{ik}}{r_a^b}-1\right)\right]\exp\left[-\beta\left(\frac{r_{ik}}{r_a^b}-1\right)\right] \qquad \text{(B.5)}$$

The third pair potential is the potential used to describe the interaction of dissimilar atoms. This function was derived by Johnson[59] and is shown as:

$$\phi^{a-b}(r_{ij}) = \frac{1}{2}\left[\frac{f^b(r_{ij})}{f^a(r_{ij})}\phi^{a-a}(r_{ij}) + \frac{f^a(r_{ij})}{f^b(r_{ij})}\phi^{b-b}(r_{ij})\right]. \qquad \text{(B.6)}$$

The total energy of the binary system is given by

$$E = \sum_{i^a} F^a(\rho_i) + \frac{1}{2}\sum_{i^a,j^a}\phi^{a-a}(r_{ij}) + \sum_{i^b} F^b(\rho_{i^b}) + \frac{1}{2}\sum_{i^b,j^b}\phi^{b-b}(r_{ij}) + \frac{1}{2}\sum_{i^b,j^a}\phi^{b-a}(r_{ij}) \qquad \text{(B.7)}$$

From this expression it is possible to determine the force on particle k of either type a or type b.

Examining the force on particle k_a, where k_a is particle k of type a, is defined as:

$$\vec{F}_{k^a} = -\frac{\partial}{\partial \vec{r}_{ka}}\left[\sum_{i^a} F^a(\rho_i) + \frac{1}{2}\sum_{i^a,j^a}\phi^{a-a}(r_{ij}) + \sum_{i^b} F^b(\rho_{i^b}) + \frac{1}{2}\sum_{i^b,j^b}\phi^{b-b}(r_{ij}) + \frac{1}{2}\sum_{i^b,j^a}\phi^{b-a}(r_{ij})\right] \qquad \text{(B.8)}$$

or

$$\vec{F}_{k^a} = -\left[\begin{array}{l}\displaystyle\sum_{i^a}\frac{\partial F^a(\rho_{ia})}{\partial \rho_{ia}}\frac{\partial \rho_{ia}}{\partial \vec{r}_{ka}} + \frac{1}{2}\sum_{i^a,j^a}\frac{\partial \phi^{a-a}(r_{ij})}{\partial \vec{r}_{ka}} + \sum_{i^b}\frac{\partial F^b(\rho_{ib})}{\partial \rho_{ib}}\frac{\partial \rho_{ib}}{\partial \vec{r}_{ka}} \\ \displaystyle + \frac{1}{2}\sum_{i^b,j^b}\frac{\partial \phi^{b-b}(r_{ij})}{\partial \vec{r}_{ka}} + \frac{1}{2}\sum_{i^b,j^a}\frac{\partial \phi^{b-a}(r_{ij})}{\partial \vec{r}_{ka}}\end{array}\right] \qquad \text{(B.9)}$$

where $\frac{\partial \rho_{ia}}{\partial \vec{r}_{ka}}$ can be found by evaluating the partial derivative of equation (B.1). This partial is defined as

$$\frac{\partial \rho_{i^a}}{\partial \vec{r}_{k^a}} = \frac{\partial}{\partial \vec{r}_{k^a}}\left[\sum_{j^a \neq i^a} f^a\left(r_{j^a i^a}\right) + \sum_{j^b} f^b\left(r_{j^b i^a}\right)\right] \tag{B.10}$$

This partial derivative has two separate solutions for the cases $i_a=k_a$ and $i_a \neq k_a$. For the case where $i_a=k_a$ the derivative is:

$$\frac{\partial \rho_{i^a}}{\partial \vec{r}_{k^a}} = \sum_{j^a \neq k^a} \frac{\partial f^a\left(r_{j^a k^a}\right)}{\partial \vec{r}_{k^a}} + \sum_{j^b} \frac{\partial f^b\left(r_{j^b k^a}\right)}{\partial \vec{r}_{k^a}} \tag{B.11}$$

When $i_a \neq k_a$ the derivative is

$$\frac{\partial \rho_{i^a}}{\partial \vec{r}_{k^a}} = \frac{\partial f^a\left(r_{k^a j^a}\right)}{\partial \vec{r}_{k^a}} \tag{B.12}$$

Evaluating the derivative $\frac{\partial \rho_{i^b}}{\partial \vec{r}_{k^a}}$ only has one case and is given by

$$\frac{\partial \rho_{i^a}}{\partial \vec{r}_{k^a}} = \frac{\partial}{\partial \vec{r}_{k^a}}\left[\sum_{j^b} f^a\left(r_{j^a i^b}\right) + \sum_{j^b \neq i^b} f^b\left(r_{i^b j^b}\right)\right] = \frac{\partial f^a\left(r_{j^a i^b}\right)}{\partial \vec{r}_{k^a}} \tag{B.13}$$

Placing the results of equation B.11, B.12, and B.13 back into the expression for the force on particle k_a the following is obtained

$$\vec{F}_{k^a} = -\left[\begin{array}{l} \sum_{i^a \neq k^a} \frac{\partial F^a\left(\rho_{i^a}\right)}{\partial \rho_{i^a}} \frac{\partial f^a\left(r_{k^a i^a}\right)}{\partial \vec{r}_{k^a}} + \sum_{j^a \neq k^a} \frac{\partial F^a\left(\rho_{k^a}\right)}{\partial \rho_{k^a}} \frac{\partial f^a\left(r_{j^a k^a}\right)}{\partial \vec{r}_{k^a}} + \sum_{j^b} \frac{\partial F^a\left(\rho_{ia}\right)}{\partial \rho_{ia}} \frac{\partial f^b\left(r_{j^b k^a}\right)}{\partial \vec{r}_{k^a}} \\ + \sum_{i^b} \frac{\partial F^b\left(\rho_{i^b}\right)}{\partial \rho_{i^b}} \frac{\partial f^a\left(r_{k^a i^b}\right)}{\partial \vec{r}_{k^a}} + \sum_{i^a \neq k^a} \frac{\partial \phi^{a-a}\left(r_{i^a k^a}\right)}{\partial \vec{r}_{k^a}} + \sum_{j^b} \frac{\partial \phi^{b-a}\left(r_{k^a j^b}\right)}{\partial \vec{r}_{k^a}} \end{array}\right] \tag{B.14}$$

By applying the several algebraic steps one obtains the following expression for the force on a particle k of type a:

$$\vec{F}_{k^a} = -\left\{ \begin{array}{l} \sum\limits_{i^a \neq k^a} \left[\left(\dfrac{\partial F^a(\rho_{i^a})}{\partial \rho_{i^a}} + \dfrac{\partial F^a(\rho_{k^a})}{\partial \rho_{k^a}} \right) \dfrac{\partial f^a(r_{i^a k^a})}{\partial r_{i^a k^a}} + \dfrac{\partial \phi^{a-a}(r_{i^a k^a})}{\partial r_{i^a k^a}} \right] \dfrac{\vec{r}_{k^a i^a}}{r_{i^a k^a}} \\ + \sum\limits_{i^b} \left[\dfrac{\partial F^a(\rho_{k^a})}{\partial \rho_{k^a}} \dfrac{\partial f^b(r_{i^b k^a})}{\partial r_{i^b k^a}} + \dfrac{\partial F^b(\rho_{i^b})}{\partial \rho_{i^b}} \dfrac{\partial f^a(r_{i^b k^a})}{\partial r_{i^b k^a}} + \dfrac{\partial \phi^{a-b}(r_{i^b k^a})}{\partial r_{i^b k^a}} \right] \dfrac{\vec{r}_{k^a i^b}}{r_{i^b k^a}} \end{array} \right\} \qquad \text{(B.15).}$$

If we follow the same procedure as outlined for the force on particle k of type a the following expression for the force action on particle k of type b is obtained:

$$\vec{F}_{k^b} = -\left\{ \begin{array}{l} \sum\limits_{i^b} \left[\dfrac{\partial F^a(\rho_{i^a})}{\partial \rho_{i^a}} \dfrac{\partial f^b(r_{k^b i^a})}{\partial r_{k^b i^a}} + \dfrac{\partial F^b(\rho_{k^b})}{\partial \rho_{k^b}} \dfrac{\partial f^a(r_{k^b i^a})}{\partial r_{k^b i^a}} + \dfrac{\partial \phi^{a-b}(r_{k^b i^a})}{\partial r_{k^b i^a}} \right] \dfrac{\vec{r}_{k^b i^a}}{r_{i^a k^b}} + \\ \sum\limits_{i^b \neq k^b} \left[\left(\dfrac{\partial F^b(\rho_{i^b})}{\partial \rho_{i^b}} + \dfrac{\partial F^b(\rho_{k^b})}{\partial \rho_{k^b}} \right) \dfrac{\partial f^b(r_{k^b i^b})}{\partial r_{k^b i^b}} + \dfrac{\partial \phi^{b-b}(r_{i^b k^b})}{\partial r_{i^b k^b}} \right] \dfrac{\vec{r}_{k^b i^b}}{r_{k^b i^b}} \end{array} \right\} \qquad \text{(B.16)}$$

In order to evaluate either $\vec{F}_{k^a}$ or $\vec{F}_{k^b}$ it is necessary to obtain each of the pertinent derivatives contained within the force expressions. These derivatives for the Cai and Ye[5] potential are as follows:

$$\frac{\partial F^a(\rho_{k^a})}{\partial \rho_{k^a}} = \frac{\partial F^a(\rho_{i^a})}{\partial \rho_{i^a}} = \frac{1}{\rho_{e^a}} \left[n^2 F_0^a \left(\frac{\rho_{i^a}}{\rho_{e^a}} \right)^{n-1} \ln\left(\frac{\rho_{i^a}}{\rho_{e^a}} \right) + F_1^a \right] \qquad \text{(B.17)}$$

$$\frac{\partial F^b(\rho_{k^b})}{\partial \rho_{k^b}} = \frac{\partial F^b(\rho_{i^b})}{\partial \rho_{i^b}} = \frac{1}{\rho_{e^b}} \left[n^2 F_0^b \left(\frac{\rho_{i^b}}{\rho_{e^b}} \right)^{n-1} \ln\left(\frac{\rho_{i^b}}{\rho_{e^b}} \right) + F_1^b \right] \qquad \text{(B.18)}$$

$$\frac{\partial \phi^{a-a}(r_{i^a j^a})}{\partial r_{i^a j^a}} = \frac{\alpha_a \beta_a^2}{r_{a^a}} \left(\frac{r_{i^a j^a}}{r_{a^a}} - 1 \right) \exp\left[-\beta_a \left(\frac{r_{i^a j^a}}{r_{a^a}} - 1 \right) \right] \qquad \text{(B.19)}$$

$$\frac{\partial \phi^{b-b}\left(r_{i^b j^b}\right)}{\partial r_{i^b j^b}} = \frac{\alpha_b \beta_b^2}{r_{a^b}}\left(\frac{r_{i^b j^b}}{r_{a^b}} - 1\right)\exp\left[-\beta_b\left(\frac{r_{i^b j^b}}{r_{a^b}} - 1\right)\right] \tag{B.20}$$

$$\frac{\partial f^a\left(r_{k^a i^a}\right)}{\partial r_{k^a i^a}} = \frac{\partial f^a\left(r_{k^b i^a}\right)}{\partial r_{k^b i^a}} = -\chi_a f_e^a \exp\left[-\chi_a\left(r_{k^a i^a} - r_{e^a}\right)\right] \tag{B.21}$$

$$\frac{\partial f^b\left(r_{k^b i^a}\right)}{\partial r_{k^b i^a}} = \frac{\partial f^b\left(r_{k^b i^b}\right)}{\partial r_{k^b i^b}} = -\chi_b f_e^b \exp\left[-\chi_b\left(r_{k^b i^b} - r_{e^b}\right)\right] \tag{B.22}$$

and

$$\begin{aligned}\frac{\partial \phi^{a-b}\left(r_{k^a i^b}\right)}{\partial r_{k^a i^b}} = \frac{\partial \phi^{a-b}\left(r_{k^b i^a}\right)}{\partial r_{k^b i^a}} &= \frac{\partial}{\partial r_{k^a i^b}}\left\{\frac{1}{2}\left[\frac{f^b\left(r_{k^a i^b}\right)}{f^a\left(r_{k^a i^b}\right)}\phi^{a-a}\left(r_{k^a i^b}\right) + \frac{f^a\left(r_{k^a i^b}\right)}{f^b\left(r_{k^a i^b}\right)}\phi^{b-b}\left(r_{k^a i^b}\right)\right]\right\} \\ &= \frac{1}{2}\left\{\begin{array}{l}\dfrac{\phi^{a-a}\left(r_{k^a i^b}\right)}{f^a\left(r_{k^a i^b}\right)}\left[\dfrac{\partial f^b\left(r_{k^a i^b}\right)}{\partial r_{k^a i^b}} - \dfrac{f^b\left(r_{k^a i^b}\right)}{f^a\left(r_{k^a i^b}\right)}\dfrac{\partial f^a\left(r_{k^a i^b}\right)}{\partial r_{k^a i^b}}\right] + \dfrac{f^b\left(r_{k^a i^b}\right)}{f^a\left(r_{k^a i^b}\right)}\dfrac{\partial \phi^{a-a}\left(r_{k^a i^b}\right)}{\partial r_{k^a i^b}} \\ + \dfrac{\phi^{b-b}\left(r_{k^a i^b}\right)}{f^b\left(r_{k^a i^b}\right)}\left[\dfrac{\partial f^a\left(r_{k^a i^b}\right)}{\partial r_{k^a i^b}} - \dfrac{f^a\left(r_{k^a i^b}\right)}{f^b\left(r_{k^a i^b}\right)}\dfrac{\partial f^b\left(r_{k^a i^b}\right)}{\partial r_{k^a i^b}}\right] + \dfrac{f^a\left(r_{k^a i^b}\right)}{f^b\left(r_{k^a i^b}\right)}\dfrac{\partial \phi^{b-b}\left(r_{k^a i^b}\right)}{\partial r_{k^a i^b}}\end{array}\right\}\end{aligned} \tag{B.23}$$

Given the above expressions the calculation of the force on particle k of either type can be evaluated.

In order to validate the equations for the force on either type of particle it is necessary to examine the limit when particles of type a equal type b. If this examination leads to the monatomic force derived in Appendix A, then our derivation of the force is correct. The proof of this statement is as follows:

$$\lim_{b\to a}\left\{\vec{F}_{k^a}=-\left\{\begin{array}{l}\displaystyle\sum_{i^a\neq k^a}\left[\left(\frac{\partial F^a(\rho_{i^a})}{\partial\rho_{i^a}}+\frac{\partial F^a(\rho_{k^a})}{\partial\rho_{k^a}}\right)\frac{\partial f^a(r_{i^ak^a})}{\partial r_{i^ak^a}}+\frac{\partial\phi^{a-a}(r_{i^ak^a})}{\partial r_{i^ak^a}}\right]\frac{\vec{r}_{k^ai^a}}{r_{i^ak^a}}\\ \displaystyle+\sum_{i^b}\left[\frac{\partial F^a(\rho_{k^a})}{\partial\rho_{k^a}}\frac{\partial f^b(r_{i^bk^a})}{\partial r_{i^bk^a}}+\frac{\partial F^b(\rho_{i^b})}{\partial\rho_{i^b}}\frac{\partial f^a(r_{i^bk^a})}{\partial r_{i^bk^a}}+\frac{\partial\phi^{a-b}(r_{i^bk^a})}{\partial r_{i^bk^a}}\right]\frac{\vec{r}_{k^ai^b}}{r_{i^bk^a}}\end{array}\right\}\right. \quad \text{(B.24)}$$

$$\vec{F}_{k^a}=-\left\{\begin{array}{l}\displaystyle\sum_{i^a\neq k^a}\left[\left(\frac{\partial F^a(\rho_{i^a})}{\partial\rho_{i^a}}+\frac{\partial F^a(\rho_{k^a})}{\partial\rho_{k^a}}\right)\frac{\partial f^a(r_{i^ak^a})}{\partial r_{i^ak^a}}+\frac{\partial\phi^{a-a}(r_{i^ak^a})}{\partial r_{i^ak^a}}\right]\frac{\vec{r}_{k^ai^a}}{r_{i^ak^a}}\\ \displaystyle+\sum_{i^a}\left[\frac{\partial F^a(\rho_{k^a})}{\partial\rho_{k^a}}\frac{\partial f^a(r_{i^ak^a})}{\partial r_{i^ak^a}}+\frac{\partial F^a(\rho_{i^a})}{\partial\rho_{i^a}}\frac{\partial f^a(r_{i^ak^a})}{\partial r_{i^ak^a}}+\frac{\partial\phi^{a-a}(r_{i^ak^a})}{\partial r_{i^ak^a}}\right]\frac{\vec{r}_{k^ai^a}}{r_{i^ak^a}}\end{array}\right\} \quad \text{(B.25)}$$

By realizing that the separate summations can be combined to be over all the particles we have

$$\vec{F}_{k^a}=-\left\{\sum_{i^a\neq k^a}\left[\left(\frac{\partial F^a(\rho_{i^a})}{\partial\rho_{i^a}}+\frac{\partial F^a(\rho_{k^a})}{\partial\rho_{k^a}}\right)\frac{\partial f^a(r_{i^ak^a})}{\partial r_{i^ak^a}}+\frac{\partial\phi^{a-a}(r_{i^ak^a})}{\partial r_{i^ak^a}}\right]\frac{\vec{r}_{k^ai^a}}{r_{i^ak^a}}\right\} \quad \text{(B.26)}$$

Recall from Appendix A equation (A.16):

$$\vec{F}_k=-\left\{\sum_{i\neq k}\left[\left(\frac{\partial F_i(\rho_i)}{\partial\rho_i}+\frac{\partial F_k(\rho_k)}{\partial\rho_k}\right)\frac{\partial f(r_{ik})}{\partial r_{ik}}+\frac{\partial\phi(r_{ik})}{\partial r_{ik}}\right]\frac{\vec{r}_{ki}}{r_{ik}}\right\} \quad \text{(B.27)}$$

Therefore $\vec{F}_k=\lim_{b\to a}\vec{F}_{k^a}$ and because $\vec{F}_{k^b}$ is symmetric with $\vec{F}_{k^a}$, $\vec{F}_k=\lim_{a\to b}\vec{F}_{k^b}$. These results are used to calculate the forces for the binary liquids.

REFERENCES

[1] "Beyond 2000: A Vision for the American Metal Casting Industry," Industry directive from the Department of Energy—Office of Industrial Technologies, http://www.oit.doe.gov/metalcast/mcvision.shtml, September 1995.

[2] Iida, T. and Guthrie R. I. L., *The Physical Properties of Liquid Metals,* Clarendon Press, Oxford, 1988, pp. 147-225.

[3] Petrushevskii, M. S., Levin, E. S., and Gel'd, P. V., "Viscosity and Interaction Energy in Nickel-Aluminum Melts," *Russian Journal of Physical Chemistry,* **45** (1971) 1719-1721.

[4] Daw, M. S. and Baskes, M. I., "Embedded-Atom Method: Derivation and Application to Impurities, Surfaces, and Other Defects in Metals," *Physical Review B,* **29** (1984) 6443-6453.

[5] Cai, J., and Ye, Y.Y., "Simple Analytical Embedded-Atom Potential Model Including a Long-range Force for fcc metals and Their Alloys," *Physical Review B,* **54** (1996) 8398-8410.

[6] Rayleigh, J. W. S., *Theory of Sound,* Dover Publications, New York, 1945, pp. 312-313.

[7] Overfelt, R. A., Matlock, C. A.., and Wells, M. E., "Viscosity of Superalloy 718 by Oscillating Vessel Technique," *Metallurgical and Materials Transactions B,* **27B** (1996) 698-701.

[8] Iida, T., Satoh, A., Ishiura, S., Ishiguro, S., and Morita, Z., "An Investigation on the Viscosity Determination of Liquid-Metals by the Oscillating Vessel Method," *Journal of the Japan Institute of Metals,* **44** (1980) 443-452.

[9] Born, M. and H. S. Green, "A General Kinetic Theory of Liquids: III. Dynamical Properties," *Proceedings of the Royal Society of London, Series A,* **190** (1947) 455-474.

[10] Shimoji, M. and Itami, T., *Atomic Transport in Liquid Metals,* Transtech Publications, Lancaster, PA 1986, pp. 20-21.

[11] Chapman, T, "The Viscosity of Liquid Metals", *A. I. Ch. E. Journal,* **12** (1966) 395-400.

[12] Kirkwood, J. G., "The Statistical Mechanical Theory of Transport Processes," *Journal of Chemical Physics,* **14** (1946) 180-201.

[13] Poirier, D. R. and Geiger, G. H., *Transport Phenomena in Materials Processing,* The Minerals, Metals and Materials Society, Warrendale, PA, 1994, pp. 4-21(viscosity), 444-448(diffusion).

[14] Turkdogan, E. T., *Physical Chemistry of High Temperature Technology,"* Academic Press, Inc, New York, 1980, pp. 108-109.

[15] Ganesan, S., Speiser, R., and Poirier, D. R., "Viscosities of Aluminum-Rich Al-Cu Liquid Alloys," *Metallurgical Transactions B,* **18B** (1987) 421-424.

[16] Chapman, S. and Cowling, T. G., *The Mathematical Theory of Non-Uniform Gases,* Cambridge University Press, London, 1952, pp. 218-234.

[17] Tham, M. K., Gubbins, K. E., "Kinetic Theory of Multicomponent Dense Fluid Mixtures of Dissimilar Rigid Spheres," *Journal of Chemical Physics,* **55** (1971) 268-279.

[18] Van Beijeren, H. and Ernst, M. H., "The Modified Enskog Equation," *Physica,* **68** (1973) 437-456.

[19] Castillo, R. and Casteñada, S., "Correlation Method for the Shear Viscosity of Fluid Mixtures at Moderate Densities," *Journal of Non-Equilibrium Thermodynamics,* **14** (1989) 69-77.

[20] Kucharski, M., "A Model for Predicting the Viscosity of Multicomponent Solutions," *Z. Metallkunde,* **77** (1986) 393-396.

[21] Seetharaman, S. and Du Sichen, "Estimation of the Viscosities of Binary Metallic Melts Using Gibb's Energies of Mixing," *Metallurgical Transactions B,* **25B** (1994) 589-595.

[22] Sutherland, W., "A Dynamical Theory of Diffusion for Non-Electrolytes and the Molecular Mass of Albumin," *Philosophical Magazine,* **9** (1905) 781-785.

[23] Eyring, H., Glasstone, S., and Laidler, K, *Theory of Rate Processes,* McGraw-Hill, New York, 1941, pp. 477-551.

[24] Cohen, M. H. and Turnbull, D., "Molecular Transport in Liquids and Glasses," *Journal of Chemical Physics,* **31** (1959) 1164-1169.

[25] Swalin, R., "On the Theory of Self-Diffusion in Liquid Metals," *Acta Metallurgica* 7 (1959) 736-740.

[26] Reynik, R. J. "A Semiempirical Small Fluctuation Theory of Diffusion in Liquids," *Transactions of the Metallurgical society of AIME,* **245** (1969) 75-81.

[27] Dzugutov, M., "A Universal Scaling Law for Atomic Diffusion in Condensed Matter," *Nature,* **381** (1996) 137-139.

[28] Turkdogan, E. T., *Physical Chemistry of High Temperature Technology,"* Academic Press, Inc, New York, 1980, pp. 115-119.

[29] Cahoon, J. R., "A Modified "Hole" Theory for Solute Impurity Diffusion in Liquid Metals," *Metallurgical and Materials Transactions A,* **28A** (1997) 583-593.

[30] Kirkaldy, J. S. and Young, D. J., *Diffusion in the Condensed State,* The Institute of Metals, London 1987, p. 90.

[31] Baskes, M. I., and Melius, C. F., "Pair Potentials for FCC Metals," *Physical Review B,* **33** (1979) 3197-3204.

[32] Foiles, S. M., Baskes, M. I., and Daw, M. S., "Embedded-atom Method Functions for FCC Metals Cu, Ag, Au, Ni, Pd, Pt, and Their Alloys," *Physical Review B,* **33** (1986) 7983-7991.

[33] Daw, M. S., "Model of Metallic Cohesion: The Embedded-atom Method," *Physical Review B,* **39** (1989) 7441-7452.

[34] Liu, C., and Plimpton, S. J., "Molecular Dynamics Simulations of Grain Boundary Diffusion in Al Using Embedded Atom Method Potentials," *Journal of Materials Research,* **10** (1995) 1589-1592.

[35] Adams, J. B., Foiles, S. M., and Wolfer, W. G., "Self-diffusion of fcc Metals Using the Five-Frequency Model and the Embedded Atom Method," *Journal of Materials Research,* **4** (1989) 102-112.

[36] Bangwei, Z., and Ouyang, Y., "Calculations of the Thermodynamic Properties for Binary hcp Alloys with Simple Embedded Atom Method Model," *Zeitschrift Für Physik B,* **92** (1993) 431-435.

[37] Lesar, R., Najafabadi, R., and Srolovitz, D. J., "Thermodynamics of Solid and Liquid Embedded-atom-method Metals: A Variational Study," *Journal of Chemical Physics,* **94** (1991) 5090-5097.

[38] Chen, E. T., Barnet, R. N., and Landman, U., "Crystal-melt and Melt-vapor Interfaces of Nickel," *Physical Review B,* **40** (1989) 924-932.

[39] Voter, A. F., and Chen, S. P., "Accurate Interatomic Potentials for Ni, Al, and Ni_3Al," *Characterization of Defects in Materials,* edited by R. W. Siegel, J. R. Weertman, and R. Sundan, MRS Symposia Proceedings No. 82 (Materials Research Society, Pittsburgh, PA 1987) 175-180.

[40] Chen, S. P., Srolovitz, D. J., and Voter, A. F., "Computer Simulations on Surfaces and [001] Symmetric Tilt Grain Boundaries in Ni, Al, and Ni_3Al," *Journal of Materials Research,* **4** (1989) 62-77.

[41] Simonelli, G., Pasianot, R., and Savino, E. J., "Phonon Dispersion Curves for Transition Metals within the Embedded-Atom and Embedded-defect methods," *Physical Review B,* **55** (1997) 5570-5573.

[42] Kuiying, C., Hongbo, L., Xiaoping, L., Qiyong, H., and Zhuangqi, H., "Molecular Dynamics Simulation of Local Structure of Aluminum and Copper in Supercooled Liquid and Solid State by Using EAM," *Journal of Physics: Condensed Matter,* **5** (1995) 2379-2394.

[43] Kuiying, C., Xianwei, S., Xiumu, Z., and Yiyi, L., "Rapid Solidification of Cu-25at.% Ni Alloy: Molecular Dynamics Simulations Using Embedded Atom Method," *Materials Science and Engineering A,* **A214** (1996) 139-145.

[44] Aihara, T., Kawazoe, Y., and Masumoto, T., "Molecular Dynamics Simulation for Binary Amorphous Zr-Ni Alloys," *Journal of Non-Crystalline Solids,* **205-207** (1996) 875-878.

[45] Aihara, T., Aoki, K., and Masumoto, T., "Atomistic Computer-simulation for Liquid-glass Transitions in Zr-Ni Alloy," *Materials Science and Engineering A,* **A179/A180** (1994) 256-260.

[46] Shimono, M., and Onodera, H., "Molecular Dynamics Study on Liquid-to-Amorphous Transition in Ti-Al Alloys," *Materials Transactions, JIM,* **39** (1998) 147-153.

[47] Ballone, P., and Rubini, S., "Embedded-Atom Model of Glass-forming Si-metal Alloys," *Physical Review B,* **51** (1995) 14962-14975.

[48] Ballone, P., and Rubini, S., "Roughening Transition of an Amorphous Metal Surface: A Molecular Dynamics Study," *Physical Review Letters,* **77** (1996) 3169-3172.

[49] Ballone, P., and Rubini, S., "An Embedded Atom Study of an Amorphous Metal Surface: $Pd_{80}Si_{20}$," *Surface Science Letters,* **342** (1995) L1116-L1120.

[50] Richardson, C. F., and Clancy, P., "Contribution of Thermal Conductivity to the Crystal-regrowth Velocity of Embedded-atom-method-modeled Metals and Metal Alloys," *Physical Review B,* **45** (1992) 12260-12268.

[51] Rubini, S., and Ballone, P., "Quasiharmonic and Molecular-Dynamics Study of the Martensitic Transformation in Ni-Al Alloys," *Physical Review B,* **48** (1993) 99-111.

[52] Nie, X., Zhong, L., Wang, R., Ye, Y., Zhang, W., Zhou, Y., and Wang, D., "A New Embedded-atom Potential for Metals and Its Applications," *Solid State Communications,* **94** (1995) 359-362.

[53] Ouyang, Y., and Zhang, B., "Analytic Embedded-Atom Potentials for bcc Metals: Application to Calculating the Thermodynamic Data of bcc Alloys," *Physics Letters A,* **192** (1994) 79-86.

[54] Bangwei, Z., and Yifang, O., "Theoretical Calculation of Thermodynamic Data for bcc Binary Alloys with the Embedded-Atom Method," *Physical Review B,* **48** (1993) 3022-3029.

[55] Sabochick, M. J., and Lam, N. Q., "Radiation-Induced Amorphization of Ordered Intermetallic Compounds: CuTi, $CuTi_2$, and Cu_4Ti_3: A Molecular Dyanmics Study," *Physical Review B,* **43** (1991) 5243-5252.

[56] Wolf, R. J., Mansour, K. A., and Lee, M. W., "Temperature Dependence of Elastic Constants of Embedded-atom Models of Palladium," *Physical Review B,* **46** (1992) 8027-8035.

[57] Pavlovic, A. S., Babu, V. S., and Seehra, M. S., "High-temperature Thermal Expansion of Binary Alloys of Ni with Cr, Mo and Re: A Comparison with Molecular Dynamics Simulations," *Journal of Physics: Condensed Matter,* **8** (1996) 3139-3149.

[58] Sutton, A. P. and Ballufi, R. W., *Interfaces in Crystalline Materials,* Clarendon Press, Oxford, 1995, pp. 177-181.

[59] Johnson, R. A., "Alloy Models with the Embedded-Atom Method," *Physical Review B,* **39** (1989) 12554-12559.

[60] Johnson, R. A., and Oh, D. J., "Analytic Embedded Atom Method Model for BCC Metals," *Journal of Materials Research,* **4** (1989) 1195-1201.

[61] Yifang, O., Bangwei, Z., Shuzhi, L., and Zhanpeng, J., "A Simple Analytical EAM Model for BCC Metals Including Cr and Its Application," *Zeitschrift Für Physik B,* **101** (1996) 161-168.

[62] Guellil, A. M., and Adams, J. B., "The Application of the Analytic Embedded Atom Method to bcc Metals and Alloys," *Journal of Materials Research,* **7** (1992) 639-652.

[63] Goldstein, A. S., and Jonsson, H., "An Embedded-atom Method Potential for the H.C.P. Metal Zr," *Philosophical Magazine B,* **71** (1995) 1041-1056.

[64] Rose, J. H., Smith, J. R., Guinea, F., and Ferrante, J., "Universal Features of the Equation of State of Metals," *Physical Review B,* **29** (1994) 2963-2969.

[65] Banerjea, A., and Smith, J. R., "Origins of the Universal Binding-Energy Relation," *Physical Review B,* **37** (1988) 6632-6645.

[66] Johnson, R. A., "Analytic Nearest-neighbor Model for FCC Metals," *Physical Review B,* **37** (1988) 3924-3931.

[67] Xie, Q., and Huang, M., "A Lattice Inversion Method to Construct the Alloy Pair Potential for the Embedded-atom Method," *Journal of Physics: Condensed Matter,* **6** (1994) 11015-11025.

[68] Foiles, S. M., "Application of the Embedded-atom Method to Liquid Transition Metals," *Physical Review B,* **32** (1995) 3409-3415.

[69] Alemany, M. M. G., Rey, C., and Gallego, L. J., "Computer Simulation Study of the Dynamic Properties of Liquid Ni Using the Embedded-atom Model," *Physical Review B,* **58** (1998) 685-693.

[70] Alemany, M. M. G., Calleja, M., Rey, C., Gallego, L. J., Casas, J., and Gonzalez, L. E., "A Theoretical and Computer Simulation Study of the Static Structure and Thermodynamic Properties of Liquid Transition Metals Using the Embedded Atom Model," *Journal of Non-Crystalline Solids,* **250-252** (1999) 53-58.

[71] Asta, M., Morgan, D., Hoyt, J. J., Sadigh, B., Althoff, J. D., de Fontaine, D., and Foiles, S. M., "Embedded-atom-method Study of Structural, Thermodynamic, and Atomic Transport Properties of Liquid Ni-Al Alloys," *Physical Review B,* **59** (1999) 14271-14281.

[72] Bhuiyan, G. M., Silbert, M., and Stott, M. J., "Structure and Thermodynamic Properties of Liquid Transition Metals: An Embedded-Atom-Method Approach," *Physical Review B,* **53** (1996) 636-645.

[73] Bhuiyan, G. M., and Khaleque, M. A., "Structure and Thermodynamic Properties of Liquid Rare Earth Metals: An Embedded Atom Method Approach," *Journal of Non-Crystalline Solids,* **226** (1998) 175-181.

[74] Holtzman, L. M., Adams, J. B., Foiles, S. M., and Hitchon, W. N. G., "Properties of Liquid-Vapor Interface of fcc Metals Calculated Using the Embedded Atom Method," *Journal of Materials Research,* **6** (1991) 298-302.

[75] Maret, M., Pomme, T., and Pasturel, A., "Structure of Liquid $Al_{80}Ni_{20}$ Alloy," *Physical Review B,* **42** (1990) 1598-1604.

[76] Cherne, F. J., and Deymier, P. A., "Calculation of Viscosity of Liquid Nickel by Molecular Dynamics Methods," *Scripta Materialia,* **39** (1998) 1613-1616.

[77] Zahid, F., Bhuiyan, G.M., Khaleque, M. A., and Rashid, R., "Calculations of Structure and Shear Viscosity for Less Simple Liquid Metals," *Journal of Non-Crystalline Solids,* **250-252** (1999) 107-110.

[78] Ludwig, M., and Gumbsch, P., "An Empirical Interatomic Potential for B2 NiAl," *Modeling and Simulation in Materials Science and Engineering,* **3** (1995) 533-542.

[79] Baskes, M. I., "Modified Embedded-atom Potentials for Cubic Materials and Impurities," *Physical Review B,* **46** (1992) 2727-2742.

[80] Baskes, M. I., "Determination of Modified Embedded Atom Method Parameters for Nickel," *Materials Chemistry and Physics,* **50** (1997) 152-158.

[81] Mishin, Y., Farkas, D., Mehl, M. J., and Papaconstantopoulos, D. A., "Interatomic potentials for Al and Ni from Experimental Data and *Ab-initio* Calculations," *Materials Research Society Symposium Proceedings,* **539** (1999) 535-540.

[82] Mishin, Y., Farkas, D., Mehl, M. J., and Papaconstantopoulos, D. A., "Interatomic Potentials for Monatomic Metals from Experimental Data and *Ab Initio* Calculations," *Physical Review B,* **59** (1999) 3393-3407.

[83] Farkas, D., Jones, C., Pete, T., "Interatomic Potentials for Simulations in Multiphase Intermetallics," *Mechanical Properties and Phase Transformations of Multiphase Intermetallic Alloys, Proceedings of a symposium sponsored by the TMS-SMD Physical Metallurgy Committee at '94 TMS Fall Meeting in Rosemont, Illinois, October 2-6, 1994,* edited by Giamei, A. F., Inoue, K., and Mishima, Y., (The Minerals, Metals and Materials Society, Warrendale, PA, 1995) 25-32.

[84] Harrison, W. A., *Pseudopotentials in the Theory of Metals,* W. A. Benjamin, Reading, MA, 1966, pp. 37-59, 289-304.

[85] Rapaport, D. C., *The Art of Molecular Dynamics Simulation,* Cambridge University Press, Cambridge, 1995, pp. 114-145, 181-186.

[86] McQuarrie, D. A., *Statistical Mechanics,* Harper and Row, New York, 1976, pp. 512-522.

[87] Green, M. S., "Markoff Random Processes and the Statistical Mechanics of Time-Dependent Phenomena," *Journal of Chemical Physics*, **20** (1952) 1281.

[88] Green, M. S., "Markoff Random Processes and the Statistical Mechanics of Time-Dependent Phenomena. II. Irreversible Processes in Fluids," *Journal of Chemical Physics,* **22** (1954) 398.

[89] Allen, M. P., and Masters, A. J., "Some Notes on Einstein Relationships," *Molecular Physics,* **79** (1993) 435-443.

[90] Holian, B. L., and Evans, D. J., "Shear Viscosities Away from the Melting Line: A Comparison of Equilibrium and Non-Equilibrium Molecular Dynamics," *Journal of Chemical Physics,* **78** (1983) 5147-5150.

[91] Hoover, W. G., Ladd, A.J.C., and Moran, B., "High Strain-Rate Plastic Flow Studied via Non-equilibrium Molecular Dynamics," *Physical Review Letters,* **48** (1982) 1818-1820.

[92] Hood, L. M., Evans, D. J., and Hanley, D. J. M., "Properties of a Soft Sphere Liquid from Non-Newtonian Molecular Dynamics," *Journal of Statistical Physics,* **57** (1989) 729-743.

[93] Lees, A. W., and Edwards, S. F., "The Computer Study of Transport Processes Under Extreme Conditions," *Journal of Physics C: Solid State Physics,* **5** (1972) 1921-1929.

[94] Berezhkovsky, L. M., Drozdov, A. N., Yu Zizserman, V., Lagar'kov, A. N., and Triger, S. A., "Molecular Dynamics Simulation of the Transport Properties of Liquid Sodium and Potassium," *Journal of Physics F: Metal Physics,* **14** (1984) 2315-2321.

[95] Heyes, D. M., "Molecular Dynamics Simulations of Liquid Binary Mixtures: Partial Properties of Mixing and Transport Coefficients," *Journal of Chemical Physics,* **96** (1992) 2217-2227.

[96] Pas, M. F., and Zwolinski, B. J., "Computation of the Transport Coefficients of Binary Mixtures of Argon-Krypton, Krypton-Xenon, and Argon-Xenon by Molecular Dynamics," *Molecular Physics,* **73** (1991) 483-494.

[97] Stadler, R., Aife, D., Kresse, G., de Wijs, G. A., and Gillan, M. J., "Transport Properties of Liquids from First Principles," *Journal of Non-Crystalline Solids,* **250-252** (1999) 82-90.

[98] Yano, T., Yamane, M., and Inoue, S., "Non-Equilibrium Molecular Dynamics Simulation Study of the Viscosity of Glass Forming Flouride Melts," *Physics and Chemistry of Glasses,* **36** (1995) 228-236.

[99] Evans, D. J., and P. T. Cummings, "Non-Equilibrium Molecular Dynamics Algorithm for the Calculation of Thermal Diffusion in Simple Fluid Mixtures," *Molecular Physics,* **72** (1991) 893-898.

[100] Lee, S. H., and Cummings, P. T., "Shear Viscosity of Model Mixtures by Non-Equilibrium Molecular Dynamics: 1. Argon-Krypton Mixtures," *Journal of Chemical Physics,* **99** (1993) 3919-3925.

[101] Baranyai, A., and Cummings, P. T., "Non-Equilibrium Molecular Dynamics Study of Shear and Shear-free Flows in Simple Fluids," *Journal of Chemical Physics,* **103** (1995) 10217-10225.

[102] Koishi, T., Shirakawa, Y., and Tamaki, S., "Shear Viscosity of Liquid Metals Obtained by Non-Equilibrium Molecular Dynamics," *Journal of Non-Crystalline Solids,* **205-207** (1996) 383-387.

[103] Mei, J., Davenport, J. W., and Fernando, G. W., "Analytic Embedded Atom Potentials for fcc Metals: Application to Liquid and Solid Copper," *Physical Review B,* **43** (1991) 4653-4658.

[104] Mei, J. and Davenport, J. W., "Molecular-Dynamics Study of Self-diffusion in Liquid Transition Metals," *Physical Review B,* **42** (1990) 9682-9684.

[105] Alemany, M. M. G., Rey, C., and Gallego, L. J., "Embedded Atom Model Calculations of the Diffusion Coefficient of Ni Impurity in Liquid Al," *Journal of Chemical Physics,* **111** (1999) 911-9112.

[106] Ayushina, G. D., Levin, E. S., and Gel'd, P. V., "The Density and Surface Energy of Liquid Alloys of Aluminum with Cobalt and Nickel," *Russian Journal of Physical Chemistry,* **43** (1969) 1548-1551.

[107] Smithells, C.J., *Metals Reference Book, 4th Edition, v. 1,* Plenum Press, New York, 1967, pp. 14-6 to 14-8.

[108] Waseda, Y., and Ohtani, M., "Static Structure of Liquid Noble and Transition Metals by X-ray Diffraction," *Physica Status Solidi B,* **62** (1974) 535-546.

[109] Jovic, D., Padureanu, I., and Rapeanu, S., "Structure Factor and Radial Distribution Function in Liquid Aluminum," *Liquid Metals, 1976, Conference Series Number 30,* edited by R. Evans and D. A. Greenwood, The Institute of Physics, Bristol, 1977, 120-125.

[110] Nosé, S., "Constant Temperature Molecular Dynamics Methods," *Progress of Theoretical Physics Supplement,* **103** (1991) 1-46.

[111] Alemany, M. M. G., Dieguez, O., Rey, C., and Gallego, L. J., "Molecular-Dynamics Study of the Dynamic Properties of fcc Transition and Simple Metals in the Liquid Phase Using the Second-Moment Approximation to the Tight-Binding Method," *Physical Review B.,* **60** (1999) 9208-9211.

[112] Protopapas, P., Andersen, H. C., and Parlee, N. A. D., "Theory of Transport in Liquid-Metals: 1. Calculation of Self-diffusion Coefficients," *Journal of Chemical Physics,* **59** (1973) 15-25.

[113] *Phase Diagrams of Binary Nickel Alloys, Monograph Series on Alloy Phase Diagrams, v. 6,* edited by P. Nash, ASM International, Metals Park, OH, 1991, pp. 3-11.

[114] *Binary Alloy Phase Diagrams, 2nd Edition*, edited by T.P. Massalski, ASM International, Materials Park, OH, 1990, pp. 183-184.

[115] Landa, A. I., Yuryev, A. A., Ruban, A.V., Gurskaya, E. G., Kovneristyi, Yu K., and Vatolin, N. A., "Psuedopotential Calculation of Thermodynamic Properties and Glass Transition Temperatures of Binary Ni-Al Alloys," *Journal of Physics: Condensed Matter*, **3** (1991) 9229-9243.

[116] Kovneristyi, Yu K., Vatolin, N. A., Landa, A. I., Romankevitch, and Yuryev, A. A., "*Ab-initio* Calculation of the Thermodynamic Properties of Liquid Alloys with the Application to Ni-Al: A Non-local Psuedopotential Approach," *Journal of Non-Crystalline Solids,* **117/118** (1990) 589-592.

[117] Streitz, F. H. and Mintmire, J. W., "Electrostatic Potentials for Metal-Oxide Surfaces and Interfaces," *Physical Review B.,* **50** (1994) 11996-12003.

[118] Liu, H. B., Hu, Z. Q., and An, G. Y., "Thermodynamic Properties of Ni_3Al and Cu_3Al as Calculated with the Tight-Binding Potential," *Philosophical Magazine B,* **79** (1999) 981-991.

[119] Shinoda, T., Mishima, Y., Masuda-Jindo, K., and Sluiter, M. H. F., "Tight-Binding Calculations of Cohesive Properties and Phase Diagram of Ni-Al-X Alloy Systems," *Journal of Phase Equilibria,* **18** (1997) 624-627.

[120] Lathiotakis, N. N., Andriotis, A. N., Menon, M., and Connolly, J., "Tight Binding Molecular Dynamics Study of Ni Clusters," *Journal of Chemical Physics,* **104** (1996) 992-1003.

[121] Colombo, L., "Tight-Binding Molecular Dynamics Simulations," *Computational Materials Science,* **12** (1998) 278-287.

[122] Mehl, M. J., and Papaconstantopoulos, D. A., "Tight-Binding Parametrization of First-Principles Results," *Computational Materials Science,* C. Fong editor, (World Scientific Publishing, Singapore, 1998), pp. 1-45.

[123] Cohen, R. E., Mehl, M. J., and Papaconstantopoulos, D. A., "A New Tight-Binding Total Energy Method for Transition and Noble Metals," *Physical Review B: Rapid Communications*, **50** (1994) 14694-14697.

[124] Liu, F., Khanna, S. N., and Jena, P., "Ab-Initio Tight-Binding Theory for the Electronic Structure," *Journal of Non-Crystalline Solids,* **117/118** (1990) 297-299.

[125] Colinet, C. and Pasturel, A., "Ab-Initio Calculation of Thermodynamic Data and Phase Diagram of Binary Transition Metal Based Alloys," *Journal of Phase Equilibria,* **15** (1994) 330-338.

[126] Alfè, D. and Gillan, M. J., "First-Principles Calculation of Transport Coefficients," *Physical Review Letters,* **81** (1998) 5161-5164.